CHALMERS
UNIVERSITY OF TECHNOLOGY

Load distribution in instrumented cohesion piles

A case study of E45 Gullbergstunneln

Master's thesis in Master Program Infrastructure and Environmental engineering

YLVA STAFSTRÖM
ELON STAXÄNG

Department of Architecture and Civil Engineering
CHALMERS UNIVERSITY OF TECHNOLOGY
Master's thesis ACEX30
Gothenburg, Sweden 2023

Master's thesis ACEX30

Load distribution in instrumented cohesion piles

A case study of E45 Gullbergstunneln

YLVA STAFSTRÖM
ELON STAXÄNG

CHALMERS
UNIVERSITY OF TECHNOLOGY

Department of Architecture and Civil Engineering
Division of Geology and Geotechnics
Chalmers University of Technology
Gothenburg, Sweden 2023

Load distribution in instrumented cohesion piles
A case study of E45 Gullbergstunneln

YLVA STAFSTRÖM

ELON STAXÄNG

Supervisors: Marcus Högberg, Peab Anläggning AB; Johannes Pettersson, Peab Anläggning AB; Jonatan Isaksson, NCC AB/Department of Architecture and Civil Engineering
Examiner: Mats Karlsson, Department of Architecture and Civil Engineering

Department of Architecture and Civil Engineering
Division of Geology and Geotechnics
Chalmers University of Technology
SE-412 96 Gothenburg
Telephone +46 31 772 1000

Cover: Installation of instrumented piles.

Department of Architecture and Civil Engineering
Gothenburg, Sweden 2023

Load distribution in instrumented cohesion piles
A case study of E45 Gullbergstunneln
YLVA STAFSTRÖM
ELON STAXÄNG
Department of Architecture and Civil Engineering
Chalmers University of Technology

Abstract

This thesis investigates the load distribution in three instrumented precast concrete cohesion piles installed in a tunnel project in Gothenburg, Sweden. The piles are supporting a tunnel and will furthermore support 10-14 story buildings planned on top of the tunnel. The piles are instrumented with Sister Bar strain gauges, which were used to estimate the load distribution in the piles. The results show that the piles have been subject to tension forces after driving, but the load distribution shows a tendency towards compression over time.

To compare the findings from the data analysis, hand calculations using the α- and β-methods were used to estimate the theoretical load distribution in the case study piles. This was done for both a heaving and a settling soil matrix. Additionally, a numerical analysis was used to investigate the load distribution for a pile subject to unloading and mass displacement from nearby piling.

The results show that development of significant tension forces is possible due to nearby piling. Comparison between data analysis, hand calculations and the numerical model show a resemblance in the shape of the load distribution.

Keywords: Instrumented piles, Sister Bars, strain gauges, load distribution, heave, drag load, negative, positive, skin friction.

Load distribution in instrumented cohesion piles
A case study of E45 Gullbergstunneln
YLVA STAFSTRÖM
ELON STAXÄNG
Department of Architecture and Civil Engineering
Chalmers University of Technology

Sammanfattning

Detta examensarbete undersöker lastfördelningen i tre instrumenterade prefabricerade kohesionspålar i betong installerade i ett tunnelprojekt i Göteborg, Sverige. Pålarna utgör grundläggningen för tunneln samt framtida 10-14 våningshus planerade ovanpå tunneln. Pålarna är instrumenterade med Sister Bar-töjningsgivare, som användes för att uppskatta lastfördelningen i pålarna. Resultaten visar att pålarna har utsatts för draglaster efter installation, men med tiden visar lastfördelningen en tendens mot trycklaster.

För att jämföra resultaten från dataanalysen utfördes handberäkningar med α- och β-metoderna för att uppskatta den teoretiska lastfördelningen hos pålarna. Detta gjordes både för en jordprofil i hävning och i sättning. Dessutom användes en numerisk modell för att undersöka lastfördelningen för en påle som utsätts för avlastning och massundanträngning från närliggande pålning.

Resultaten visar att utvecklingen av betydande draglaster är möjlig till följd av närliggande pålning. Jämförelse mellan dataanalys, handberäkningar och den numeriska modellen visar en överrensstämmelse i formen hos lastfördelningskurvan.

Nyckelord: Instrumenterade pålar, Sister Bars, töjningsgivare, lastfördelning, hävning, påhängslast, negativ, positiv, mantelfriktion.

Contents

Acknowledgements

We would like to express our gratitude towards our supervisors Mats Karlsson at Chalmers and Jonatan Isaksson at Chalmers/NCC AB. They have shown great interest in our work, and provided us with wise observations and guidance during the process. We would also like to thank our supervisors at Peab Anläggning AB, Johannes Pettersson and Marcus Högberg. Beyond valuable time and feedback, they have also provided us with relevant documents, data and contacts needed for the report.

In addition, we would also like to express our appreciation to

- Johnny Wallgren and Michael Sabattini at Peab Anläggning AB for initiating the project and for providing us with interesting discussions and literature during the learning process.
- Magnus Eliasson at Peab Anläggning AB for his help with accessing the tunnel and gathering data.
- Johannes Tornborg at Skanska AB, for feedback on the report and technical support in the calculations.
- Anders Engström at Peab Anläggning AB for providing time and giving insight into the construction process of the case study.

Göteborg June 2023

Ylva Stafström

Elon Staxäng

Important notations

Greek		Latin	
α	Adhesion factor	c_u	Undrained shear strength
β	β factor	$c_{u,0}$	In situ undrained shear strength
γ	Unit weigh	E	Young's modulus
ε	Strain	F	Load
σ_0	In situ total stress	k_v	Vertical hydraulic conductivity
σ'_0	In situ effective stress	k_h	Horizontal hydraulic conductivity
σ_{UL}	Total stress after unloading	M_0	Compression modulus below σ'_c
σ'_{UL}	Effective stress after unloading	M_L	Compression modulus above σ'_c
σ'_c	Pre consolidation pressure	Q_b	Toe or base resistance
ϕ	Friction angle	Q_∞ or Q_d	Dead load
		Q_m	Shaft resistance
		Q_n	Drag load
		Q_s	Heave load
		R	Resistance
		u	Pore water pressure
		u_0	In situ pore water pressure
		Δu	Excess pore water pressure

1 Introduction

A common problem when constructing houses, bridges or other types of infrastructure is ground settlements. Both historically and today, piles have been used to limit the settlements of structures. In Sweden, around 60 % of the total number of installed piles are precast driven concrete piles (Pålkommissionen, 2022). These are either carrying load through cohesion with the soil surrounding the pile, or by carrying the load in the pile toe and transferring it to strong soil layers or bedrock.

Piles are mainly used to transfer loads to more competent soil layers. As a foundation, piles are subject to a dead load, i.e. the load that is applied to the pile head. This is however not the only load as piles are also subject to forces induced from surrounding soils. This additional load is caused by the relative movement between the pile and the soil - effectively an effect of friction between the pile surface and the soil. These two types of loads determine the load distribution within the pile. When structural loads are small, the loads due to relative movements between soil and pile are of greater importance for the load distribution.

To obtain a better understanding of the load distribution within cohesion piles, and changes in distribution due to excavation and loading, this master's thesis studies a set of instrumented piles situated in Gothenburg clay. The project studied is the lowering of E45 and the construction of Gullbergstunneln.

The lowering of E45 was executed by Peab Anläggning (turnkey contractor) with the Swedish Transport Administration (*Swedish:* Trafikverket) as client. The construction started in 2016 with acceptance and final inspections carried out during mid-2021. During and after the construction of the tunnel, major changes in earth pressure distribution occurred. This is mainly since approximately 300 000 meters of displacement piles have been installed in the area, along with large excavations. The piles supporting the tunnel are designed for an additional load of 10-14 story houses on top of the tunnel. The displacement piles reach a depth of approximately 65 meters below the tunnel. Three of the approximately 4 500 piles have been equipped with instruments to measure strain along the pile lengths. The instruments are Sister Bar Strain Gauges, and the measured strain can be used to estimate the load in the pile.

What has not been studied to a large extent is the potential effect from the surrounding piling, excavation, and how induced stresses and movements in the soil impacts the load distribution in the piles. During construction time, the pore pressure in the vicinity of the project is estimated to have increased by a maximum of

$\Delta u \approx 80$ kPa at a depth of 45 m, due to driving of the large number of surrounding displacement piles. There have also been extensive excavations for the tunnel, resulting in unloading of the clay wherein the piles are driven.

This study investigates the evolving load distribution in the instrumented piles, from the time of installation. A literature study is provided to introduce relevant concepts of pile design, down drag, drag loads, soil heave and strain gauges. For calculations, firstly a data evaluation of the strain gauges is used to estimate the load distribution. A simplified investigation is conducted using the α- & β-methods as hand calculations. Finally, a numerical model of the soil-pile behaviour during unloading and nearby mass displacement is analysed.

1.1 Aim

The aim of this master's thesis is to study the development and distribution of forces in three instrumented piles installed in a deep clay deposit under a tunnel at E45. Furthermore, the aim is to explain the results and provide plausible reasons for the load distributions in the instrumented piles.

1.2 Objectives

- To conduct a literature study on cohesion piles, load transfer, Sister Bar strain gauges and the concepts of skin friction.
- To conduct a data evaluation of forces in instrumented piles under E45.
- To use analytical hand calculations to determine the load distribution for a simplified version of the case study piles.
- To build a numerical model in order to analyse of load distribution for a simplified version of the case study piles.
- To compare the pile-soil interactions between the empiricism, analytical calculations and the numerical model.

1.3 Demarcations & limitations

The analytical and numerical calculations will not take into consideration that the case studied piles are driven at an angle and a bearing. In fact, this implies that the skin friction is not parallel to the pile, and thus would induce moments in the piles. The piles are driven at a 4:1 angle but will be assumed vertical. Additionally, the analytical and numerical calculations are performed assuming that no nearby piles are present, and subsequently group effects are not considered.

1.4 Thesis outline

This report is structured by a first providing a literature study on load-carrying mechanisms for cohesion piles, pile design, forces in piles and equipment for load monitoring. This is followed by a more detailed description of the case study site - the lowering of E45.

Thereafter the methods used and results for each estimation of load distribution is presented, i.e. data analysis, hand calculations and numerical modelling. Following the results, discussions are provided with plausible explanations of the projects findings together with potential errors and uncertainties associated with the results. Lastly, relevant conclusions are summarized, followed by the authors suggestions for future research.

2 Displacement piles in clay

In this chapter relevant background theory from a literature study is presented, both regarding important mechanisms and pile design for cohesion piles in clay, as well as a description of the instrumentation used in the case study piles.

2.1 Cohesion piles

In the topic of deep foundations, floating pile foundations have proven to be an effective and competent method to transfer load between a given superstructure and the soil matrix. The concept of utilizing long, slender piles suspended in the soil is to transfer loads to typically stiffer and stronger soil layers situated deeper in the soil strata. While many pile types exists and are in use (e.g. steel piles, bored piles, timber piles), driven concrete piles is undoubtedly the most common method in Sweden (Pålkommissionen, 2022). For driven concrete piles, the load is transferred through resistance at the pile toe, resistance along the pile shaft or a combination of both. Among driven concrete piles, long pre-cast cohesion piles are commonly used in deep clay deposits.

2.1.1 Development of bearing capacity and load bearing mechanisms

The term bearing capacity of a pile can be considered as ambiguous. It is important to make the distinction between the piles' geotechnical bearing capacity and structural strength. The geotechnical bearing capacity is determined by both the soil properties and the interface between pile and soil. More specifically, the shear strength of the soil around the pile toe and at the soil surrounding the pile shaft, together with the circumferential and base area of the pile. The structural capacity for an axially loaded pile is determined by the pile material, e.g., the compression or tension strength of the pile (Alén, 2012).

The geotechnical bearing capacity of a pile is mobilised when there is a relative displacement between a pile and the soil it is situated in. This relative displacement, and the following adhesion or friction between pile and soil, is what governs the load transfer mechanism between soil and pile, see figure 2.1.1. The friction between pile and soil, which is generally referred to as **skin friction**, can act both in an upward and downward direction, i.e., as positive or negative skin friction.

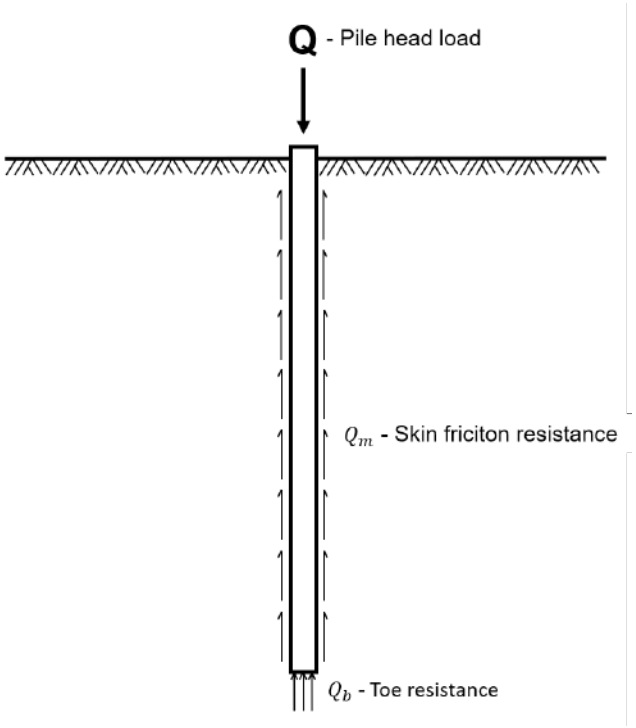

Figure 2.1.1: Load transfer of cohesion pile.

2.1.2 Action, action effects and resistance effects

The concepts action, action effect and resistance need to be distinguished when further discussing pile design. Actions are defined as the applied forces to the pile head (Alén, 2012). These include the known dead loads e.g., the weight of the superstructure and live loads e.g., wind- & snow-loads, traffic-loads, among others. The action effects are the subsequent consequences in the foundation, as a result of the above-mentioned actions. Among others, these include the structural forces in the foundation, potentially induced bending moments & displacements. In principle, all potential actions effects must be less than or equal to the resistance:

$$E \leq R \tag{2.1.1}$$

The resistance R, the geotechnical bearing, of the pile can be quantified as

$$R = Q_m + Q_b \tag{2.1.2}$$

in which Q_m is the resistance from the pile shaft, and Q_b is the resistance at the pile toe (Alén, 2012). In other words, the resistance of a floating pile is a combination of the shaft and pile toe resistance. The shaft resistance is a product of the positive skin friction that develops when there is upwards relative movement between soil and pile. The toe resistance is a product of the pile toe resting on the soil.
The sum of the resistance contributions can be calculated as

$$Q_m + Q_b = f_m \cdot A_m + f_b \cdot A_b \tag{2.1.3}$$

in which

f_m is the mean friction strength between the soil and pile shaft
A_m is the surface area of the shaft
f_b is the compression strength of the soil at the location of the pile toe
A_b is the cross-sectional area of the pile toe

It should be noted that for cohesion piles in clay the toe resistance contribution is often disregarded due to being negligible in size (Alén, 2012), and thus $Q_b = f_b \cdot A_b = 0$.

Two of the most established methods to estimate the geotechnical bearing capacity of a pile is the α-method and the β-method (Wrana, 2015). The main difference between the two methods is that the α-method is a **total stress** method while the β-method is based on **effective stresses**. The two terms total and effective stresses was first presented by Terzhagi (1943) who described the relationship between the following stresses:

- **Total normal stress,** σ - force per unit area transmitted in the normal direction when the soil is imagined as one solid material
- **Pore water pressure,** u - the pressure created by water filling the void space between soil particles
- **Effective normal stress,** σ**'** - force per unit area transmitted in a plane through the soil skeleton only

Their internal relationship is:

$$\sigma = \sigma' + u \tag{2.1.4}$$

While the α-method is exclusively used for cohesion soils (clays), the β-method is used for both cohesion and friction soils.

2.1.3 Total stress method

The α-method is used for determining the bearing capacity of a cohesion pile installed in clay. Design of cohesion piles with this method is based on a total stress approach, and the undrained end-bearing capacity of a cohesion pile can be evaluated as (Alén, 2012):

$$f_b = N \cdot c_u \tag{2.1.5}$$

where

N is a bearing capacity factor
c_u is the undrained shear strength at the end of the pile

Regarding the end bearing capacity factor N, this factor is normally chosen as 6-9 (Alén, 2012). A value of 9 indicates that the pile end is penetrating the underlying soil layer by three pile diameters of more, whereas 6 indicates that the pile end is just reaching the underlying bearing layer (Flemming et al., 2008). Furthermore, Flemming et al. (2008) points out that the value of N should be set as 9 *"for depths relevant to piles"*.

The shaft resistance can be evaluated as (Alén, 2012):

$$f_m = \alpha \cdot c_u \tag{2.1.6}$$

where,

α is an emipirical adhesion factor

c_u is the undrained shear strength

The adhesion factor is based on several pile tests. The factor is site dependent and varies due to a number of factors such as pile material and installation methods (Flemming et al., 2008). Normally values between 0.7 and 1.0 are recommended for α (Alén, 2012). Based on empirical studies, a relationship between the adhesion and the ratio of average shear strength in relation to average overburden effective stresses, has been established. Figure 2.1.2 below presents a graph originally from Norsk Peleveiledning (1987).

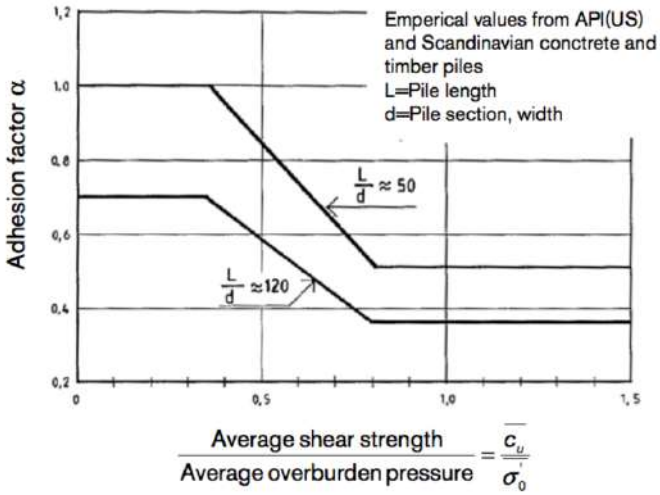

Figure 2.1.2: Adhesion factor for driven piles installed in clay, obtained from Alén (2012).

2.1.4 Effective stress method

A β-factor is often used when determining the bearing capacity for a pile installed in friction material, or to estimate the long-term bearing capacity for a pile installed in clay. The use of this factor has given name to the method, which is often called the β-method. Unlike the α-method, the β-method is based on effective stresses. The bearing capacity of a pile is divided into an end resistance and a shaft resistance. The toe resistance is often expressed using a bearing capacity factor N_q (Alén, 2012):

$$f_b = N_q \cdot \sigma'_v \tag{2.1.7}$$

where

N_q is the bearing capacity factor

σ'_v is the effective vertical stresses in the soil at the pile toe

The bearing capacity factor, N_q, can be evaluated from relationships based on the friction angle ϕ', as per suggested in figures 2.1.3a and 2.1.3b.

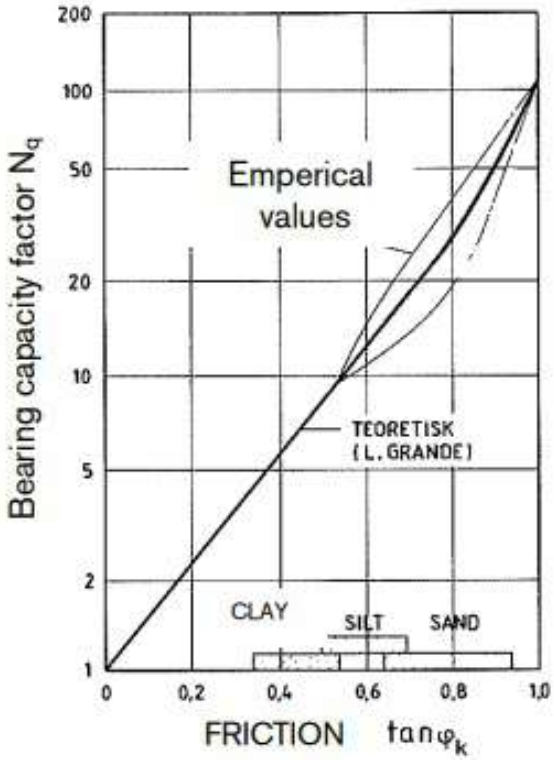

(a) Figure obtained from Alén (2012).

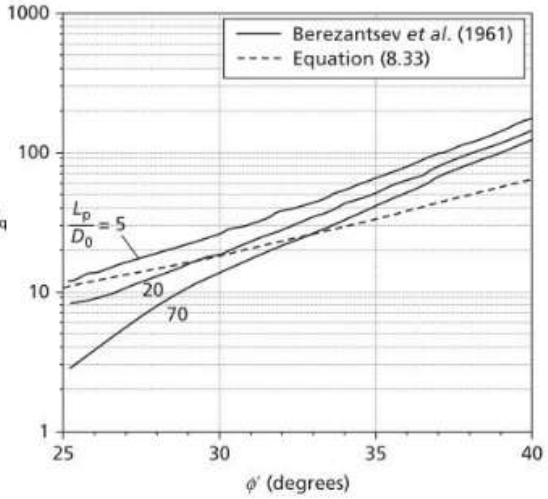

(b) Figure obtained from Knappet & Craig (2012).

Figure 2.1.3: Two different published graphs on how to interpret bearing capacity factor N_q from friction angle ϕ'.

To estimate the bearing capacity from shaft resistance in friction material the following equation can be used (Flemming et al., 2008):

$$f_m = \sigma'_h \cdot tan(\delta) = K \cdot \sigma'_v \cdot tan(\delta) \tag{2.1.8}$$

where

σ'_h is the horizontal effective stress around the pile
δ is the angle of friction between soil and pile
K is the coefficient of lateral earth pressure
σ'_v is the vertical effective stress

Usually, the terms K and $tan(\delta)$ are put together into the term β as $K \cdot tan(\delta) = \beta$. Like the α-method, literature proposes different ways to interpret or evaluate the value for β. Two examples can be seen in figure 2.1.4b and 2.1.4a below.

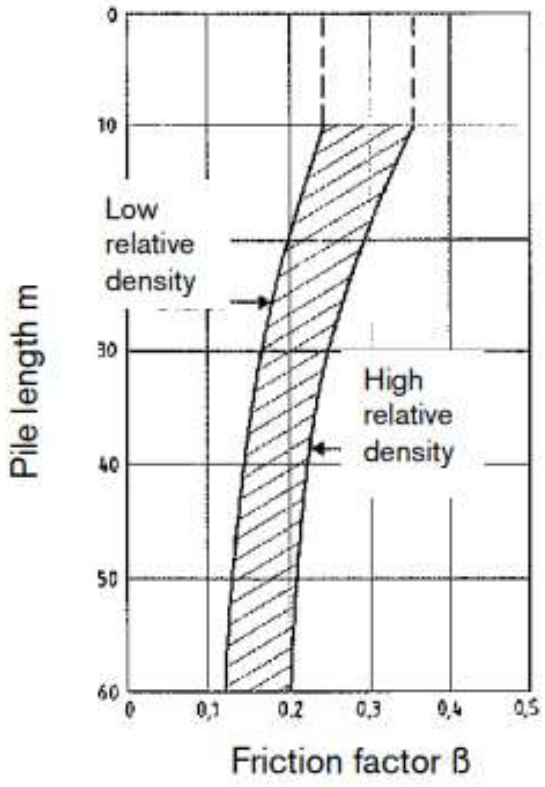

(a) Figure obtained from Alén (2012).

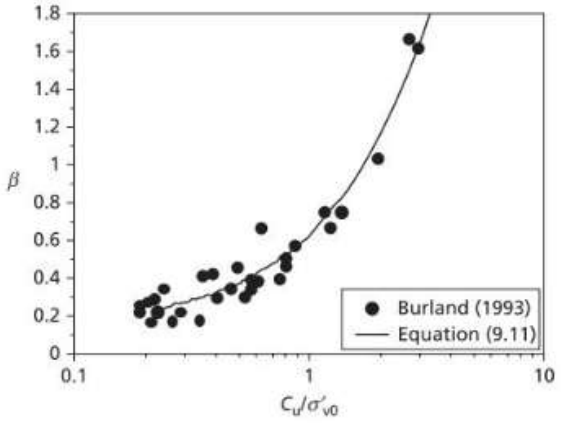

(b) Figure obtained from Knappet & Craig (2012).

Figure 2.1.4: Two different published graphs on how to interpret the β-factor.

2.1.5 Negative skin friction and downdrag

When a pile is situated in an area with ongoing settlements where the soil along the top of the pile settles more than the pile itself, negative skin friction is induced, contributing to the action effect (B. H. Fellenius, 1984). The concept of positive skin friction contributing to the resistance, and induced negative skin friction contributing to action effect can be seen in figure 2.1.5.

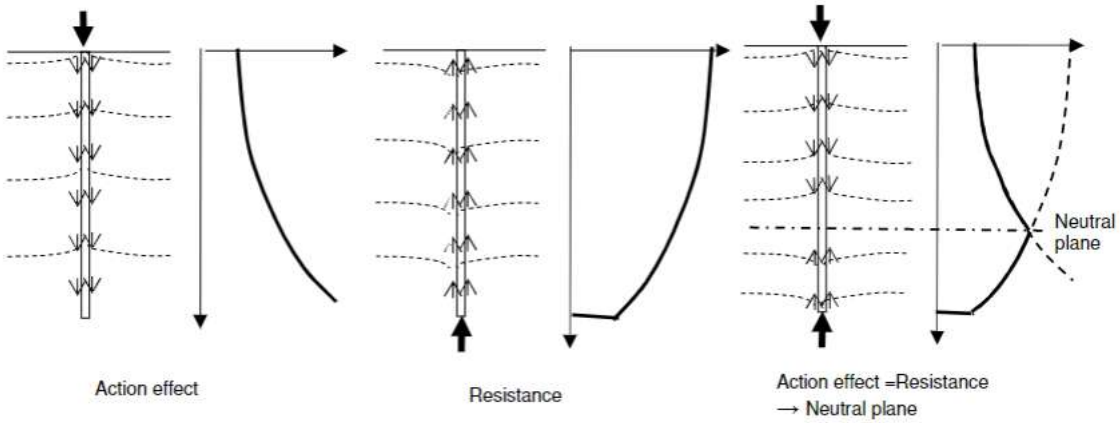

Figure 2.1.5: Illustration on the development of negative and positive skin friction from action effect and resistance (Alén, 2012).

The maximum structural load in a pile caused by the dead load and the drag load (due to negative skin friction) develops where no relative movement occurs between pile and soil. This position is known as the **neutral plane** (NP), and is defined as the point of equilibrium, where the pile and the soil settles at the same rate (B. H. Fellenius, 2006a). The neutral plane is however not necessarily a specific point, as there can be an extended zone where the soil and pile settle at the same rate, thus the pile will experience less drag load (and more down drag) than estimated with analytical calculation of a neutral plane (Alén, 2012). Subsequently, the estimated action effect calculated is an upper limit, and the load distribution can be considered a limiting load profile.

The total magnitude of the soil settlement does not affect the total magnitude of the drag force (B. H. Fellenius, 2006a). In fact, very small relative movements between pile and soil will induce the ultimate shaft shear forces (B. H. Fellenius, 2006b) and the magnitude of the drag force is dependent on the position of the neutral plane along with the soil and pile properties at their interface.

To estimate the location of the neutral plane, the subsequent maximum force in the pile and the magnitude of drag load, a common method is to plot action and resistance curves, assuming a fully mobilised skin friction, along the pile length:

$$E = Q_{\infty} + \int_0^z f_m dA \tag{2.1.9}$$

$$R = R_{toe} + \int_z^L f_m dA \tag{2.1.10}$$

in which

Q_{∞} is the long term load on the pile, i.e. the dead load
L is the length of the pile
f_m is the shaft resistance
z is the depth of interest
R_{toe} is the toe resistance, often assumed to be 0 for soft clays
A is shaft area of the pile

In figure 2.1.6 the location of the neutral plane is illustrated as the point where the action and resistance effects intersect. The magnitude of the drag load, maximum force, geotechnical bearing capacity, toe resistance and dead load can also be seen.

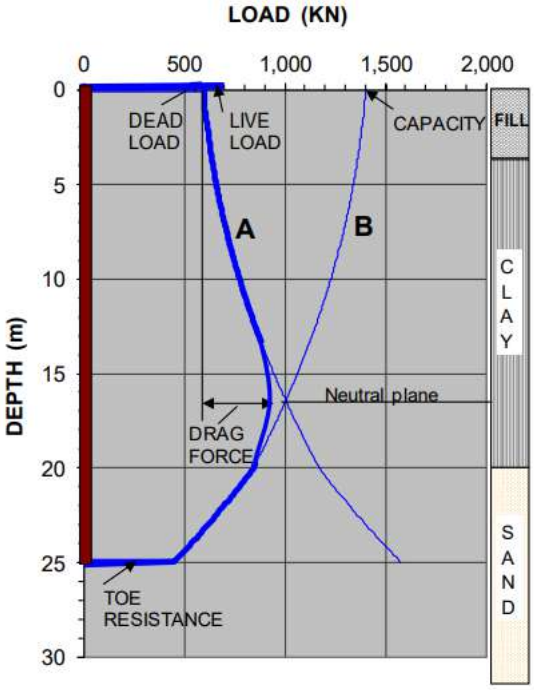

Figure 2.1.6: Illustrated example on finding the neutral plane via equation 2.1.9 and 2.1.10 (B. H. Fellenius, 2006a).

The sum of the dead load (Q_∞) and drag force (Q_n) must be equal to the sum of the total resistance, i.e.

$$Q_\infty + Q_n = R_{toe} + R_{shaft} \tag{2.1.11}$$

If the dead load is increased, the position of the neutral plane will move upwards, thus changing negative skin friction into positive friction, and alleviate the drag force experienced by the pile. In figure 2.1.7 the concept of how the position of the neutral plane changes with different magnitude of loads is shown.

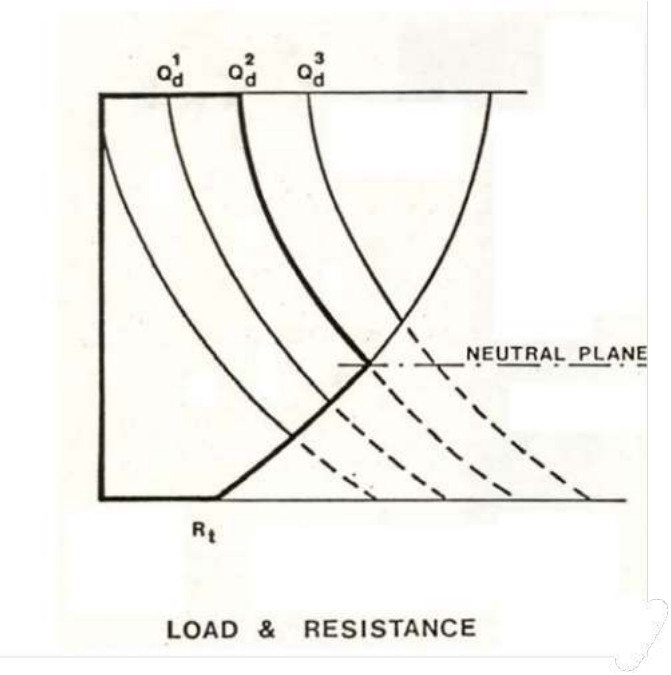

Figure 2.1.7: Illustrated example on how the position of the neutral plane changes with varying dead loads (B. H. Fellenius, 1984).

When designing for geotechnical bearing capacity, it is important to not consider negative skin friction as the drag load by definition decreases with increased pile head loads. Thus, no negative friction can exist close to or at geotechnical failure of the pile. The down drag on the pile and the chosen factor of safety for the design are interconnected. The less load that is allowed on the pile head, the more negative skin friction will be induced as the pile will settle less in relation to the adjacent soil (Flemming et al., 2008, B. H. Fellenius, 2006a).

It is important to emphasize that negative skin friction and its associated drag load is not necessarily unwanted. B. H. Fellenius, 1999 describes in a discussion paper that as long as the pile has sufficient structural integrity to accommodate for the dead load and the drag load, a large drag load indicates a stiff and competent foundation. A large down drag is on the other hand generally undesirable and means that the pile is being dragged down by the soil so that the foundation settles along with the soil surface (B. H. Fellenius, 1997).

2.1.6 Soil heaving and tension forces in piles

Previous descriptions of negative skin friction and resulting drag loads in cohesion piles emanates from a situation where the piles are installed in a settling soil profile. If the soil instead is heaving, the friction between pile and soil can cause unloading of the piles. The mechanisms behind induced tension in piles originates from that in a heaving soil, the soil surrounding the top part of the pile is moving up relative to the pile, and the soil around the lower part has a smaller movement than the pile itself (O'Reilly and Al-Tabbaa, 1990). Positive skin friction is induced in the

upper part of the pile shaft, and negative skin friction is induced in the lower part of the pile shaft. Much like the shaft resistance can be used to estimate a maximum theoretical compressive force in a pile, a maximum theoretical tension force can be calculated. Like a pile experiencing compression, the point of maximum tension can also be defined as a neutral plane along the piles' length, i.e., the plane where no shear forces are present.

The mechanisms pointed out by O'Reilly and Al-Tabba are also emphasized by Fellenius in his book on foundation design (2023). He describes that for a pile without a dead load, the load distribution remains identical for settling and heaving soils, but the signs are reversed. However, no load is transferred at the toe for a pile in a heaving soil. In other words, the concept of a neutral plane and a maximum force remains the same, but the graph is mirrored. If a dead load is applied to a pile in a heaving soil, the location of the neutral plane moves downwards along the pile and the magnitude of the maximum tension force decreases. In figure 2.1.8 the concepts are illustrated.

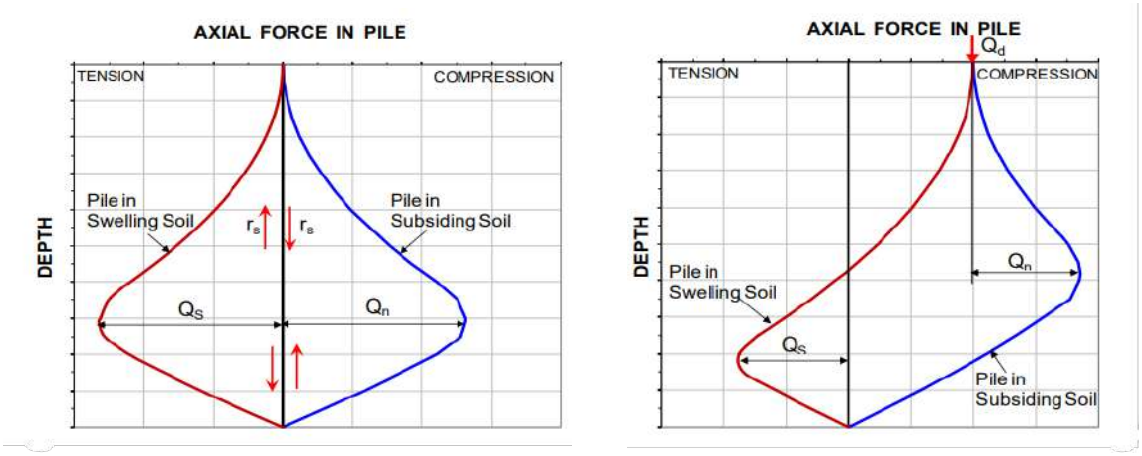

(a) Load distribution without a dead load for a pile in swelling and settling soils (B. Fellenius, 2023).

(b) Load distribution with a dead load for a pile in swelling and settling soils (B. Fellenius, 2023).

Figure 2.1.8: Illustration on the load distribution in a pile in both swelling and settling soils.

When multiple displacement piles are driven with close proximity to one another, there lies a risk of *pile heave* (Klohn, 1963). In situations where many displacement piles are used in a dense distribution, the displaced soil favour moving upwards. In figure 2.1.9 the concept is illustrated, including the displacement distribution in the soil.

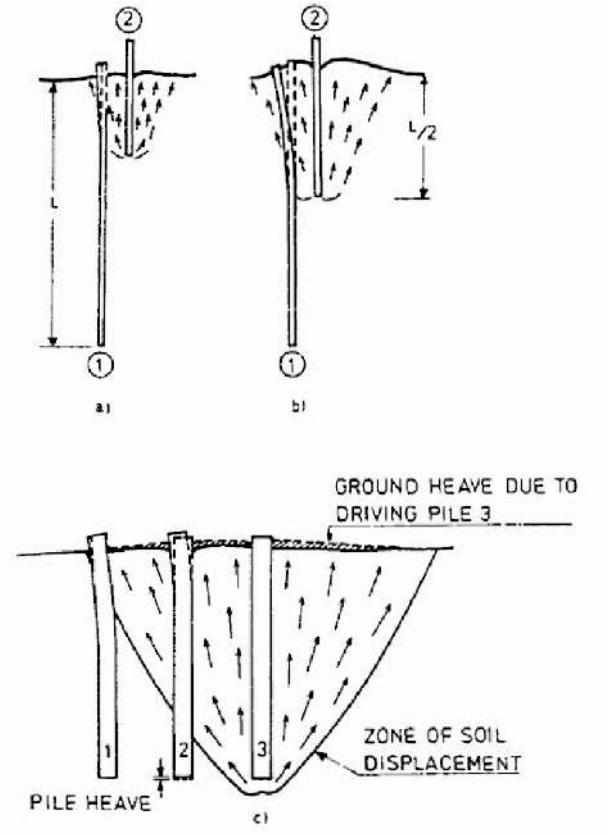

Figure 2.1.9: Illustration of how heaving due to adjacent piling emerge and its distribution (Wersäll and Massarsch, 2013).

As described by Dugan and Freed (1984), the heave effects are greatest close to the driven pile, but studies have also shown that the effect can be seen at larger distances (Edstam, 2011). Additionally, FE modelling has shown that a longer pile length gives heaving further from the driven pile than a short pile (Wersäll and Massarsch, 2013), however the maximum displacements remain the same.

Pile driving of displacement piles also causes displacements in the horizontal direction. When a displacement pile is installed in soil, the distribution of resulting soil displacement follows a triangular pattern, with its origin at the pile toe. The amount of displacement can be analysed using a method called SSPM (Shallow Strain Path Method), first developed by Sagaseta et al., 1997. Research has found that this method is very well suited for the type of clay found in the Gothenburg region (Trafikkontoret, 2021).

Tornborg, 2017 outlines in a report the risks of tension forming in piled foundations, where heaving of the soil occurs due to unloading and/or excavation. The size of soil heaving and the subsequent pressure on the ground concrete slab is an effect of multiple factors Tornborg, 2017:

- The depth of excavation
- The time between foundation construction and the excavation
- Dead loads and foundation stiffness

- Effects from pile foundations (e.g. c-t-c distance, geometry etc.)
- Geotechnical and hydrogeological properties of the stratigraphy

When piles are installed in clay prior to excavation, the resulting heaving of the soil pre-stresses the piles in drag (Tornborg, 2017), which can be particularly problematic when the ground concrete slab is not designed for high contact pressure and tension due to heaving of the soil.

2.1.7 Installation effects for driven cohesion piles in clay

As described in the previous section, installation of displacement piles can cause soil movements in proximity to the driven pile. Pile installation also causes a remoulded zone to form around the pile, where the soil's physical and mechanical parameters are altered (Konkol and Balachowski, 2017). Initially, there is a loss of strength in the soil for piles installed in clay, but as the built-up pore pressures during pile driving dissipates, the soil structure is reorganized. When the driving is completed, the stress state in the soil will be complex and widely different from the initial stress state in the soil.

Depending on the pile driving conditions, the pile may be affected in different ways. If the pile driving is easy, the compressive stresses used to drive the pile can be reflected as a tensile wave and cause tensile stresses in the pile (Flemming et al., 2008). This can be damaging for pre-cast concrete piles as the tensile stresses caused through pile driving can result in small transverse cracks through the pile. The cracks can in turn result in a reduction of concrete modulus (Flemming et al., 2008).

2.1.8 Pile group effects

A structure on soft soil is supported not by a single pile but of piles formed in pile groups or pile rows. The degree of interaction between piles in a row or group depends on the centre-to-centre distance in relation to their diameter. Thus, the negative skin friction that a pile in a pile group will experience differs from that of a single pile. For a pile group, research has shown that piles located near the perimeter or corners of a pile group experience more negative skin friction than piles at the centre (Huang et al., 2015). The gradient effect of interior piles experiencing less drag force than perimeter piles is not evident when a sufficient centre to centre distance is chosen ($\approx$ 5 pile diameters).

One way to estimate the maximum negative drag load for a pile in a pile group is to calculate the soil weight within the pile group, which is shared among the piles within the group (B. H. Fellenius, 1971). The maximum drag load is also influenced by the pile spacing, if pile spacing is large the interaction effects are lower, and thus the piles acts more like single piles (Altahrany and Elshehawy, 2022). Differential settlements within a pile group will also influence the drag loads experienced within the pile group (B. H. Fellenius, 1971).

2.2 Sister Bar strain gauges

The case study piles under the lowering of the E45 are instrumented with Sister Bar strain gauges (Geokon model 4911). These strain gauges are installed to measure strains in the driven piles. The use of Sister Bar strain gauges to monitor strains, and subsequently forces, in piles has been utilized in several studies (Chen et al., 2014; Haque et al., 2017; Brown and Hyde, 2008). Brown et al. (2008) and Chen et al. (2014) used the installed strain gauges to monitor pile resistance during both dynamic and static load tests, while Haque et al. (2017) used the strain gauges for static load tests. The exact same model of strain gauges as in the case study piles are also used by both Chen et al. (2014) and by Haque et al. (2017). More recently, Fiber Optic Sensing has also been used (Kania et al., 2020), which can measure continuous strain as opposed to Sister Bars, that only measure strain in specific levels along the pile's length. A high conformity between measurements using fibre optic sensors and vibrating wire strain gauges has been shown in studies (Kania and Sorensen, 2018).

2.2.1 Operating principle & installation

The strain gauge model 4911, is installed by tying the strain meter to the rebar cage during the fabrication of the pile (Geokon, 2011). In figure 2.2.1 a schematic of the strain gauge can be seen.

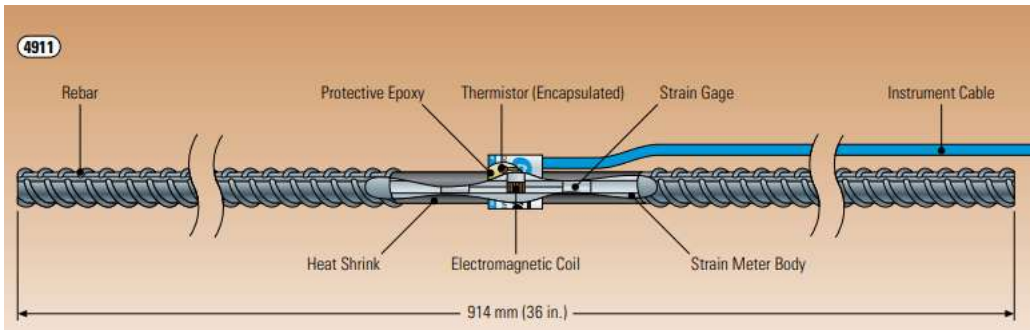

Figure 2.2.1: Visualization of the strain gauge model 4911 (Geokon, 2011).

The strain gauge measures a vibration frequency that can be converted into a strain. The Sister Bars also contain a thermistor, which allows for corrections due to thermally induced strains. It is advised to install Sister Bars on both sides of the pile, so that bending moments and axial loads can be measured individually (e.g. axial loads can be measured by simply taking the average strain of both strain gauges).

The instruments at the centre of the Sister Bar are coated in a plastic film which prevents adhesion to the concrete. The instruments in turn are attached to a ϕ12 mm rebar that is tied to the rebar cage in the pile. Each strain gauge has a signal cable that runs along the outside of the pile and is connected to readout box. In figure 2.2.2a, the installation of the specific Sister Bars used in the E45 project can be seen. The signal cables run along the pile in a custom build cable duct, as seen in figure 2.2.2b.

(a) Strain gauge installation. **(b)** Cable management.

Figure 2.2.2: Installation of the Sister Bar strain gauges, and the signal cables. Photos courtesy of Johnny Wallgren, Peab Anläggning AB

In the piles at E45 the strain gauges are installed at depths of 2, 19.5, 32.5, 45.5 and 63 meters. For every depth, four (4) separate Sister Bars were installed - one in each corner of the rebar cage. This gives a significant improvement in redundancy (Sinnreich, 2020), along with the possibility to isolate only the axial loads experienced by the pile.

2.2.2 Specification and limitations of Sister Bars

According the supplier of the strain gauges (Geokon, 2011), they inhabit an accuracy of $\pm 0.25\%$, over their full range, in a lab setting. The resolution is limited to 0.4 $\mu\varepsilon$. Vibrating wire strain gauges are, according to Lam and Jefferis, not instruments with high precision (2011). Furthermore, the authors explain that when piles are casted, the installed strain gauges can become subject to high temperatures as the concrete generates heat during hydration, and then subsequent cooling. As the concrete and steel have different expansion reactions to heating, this causes the Sister Bars to experience some strains during the casting process. This phenomenon can cause residual loads to be built up in the pile, which can affect readings from installed vibrating wire strain gauges. Other than this, there is the issue of once installed, the strain gauges cannot be repaired or repositioned.

2.2.3 Strain evaluation

The measurements from the Sister Bars are reported as 4 separate frequencies for each depth, one for each installed strain gauge. The base unit for the calculation of strain is digits, D (Geokon, 2013), which defines as

$$D = \frac{F^2}{1000} \tag{2.2.1}$$

where F is the registered frequency in Hz. From the digits an initial apparent strain can be calculated with equation 2.2.2. Negative strain indicates compression whereas positive strain indicates tension.

$$\varepsilon_{apparent} = (R_1 - R_0) \times C \tag{2.2.2}$$

in which

R_0 is the initial recording in digits
R_1 is the contemporary recording in digits
C is a calibration factor

In order to separate the load related strain, i.e. the strain that is uniquely caused by the dead load and the drag load, the strain has to be corrected for temperature induced strain in the pile. This can be done via equation 2.2.3.

$$\varepsilon_{load-related} = ((R_1 - R_0) \times C) + ((T_1 - T_0) \times K) \tag{2.2.3}$$

in which

T_0 is the initial temperature recording
T_1 is the contemporary temperature recording
K is a thermal coefficient, based on the different expansion rates of concrete and steel due to temperature variation

The actual strain of the Sister Bar can be expressed as seen in equation 2.2.4.

$$\varepsilon_{actual} = ((R_1 - R_0) \times C) + ((T_1 - T_0) \times K_{steel}) \tag{2.2.4}$$

K_{steel} is the thermal expansion coefficient for steel

The load in the pile can then be calculated with Hooke's law, see equation 2.2.5.

$$F = E \cdot \varepsilon \cdot A \tag{2.2.5}$$

in which

F is the calculated load
E is the Young's modulus for the entire pile
ε is the strain expressed as microstrain
A is the cross sectional area of the structure member

3 Case study - Lowering of E45

The road E45 is part of the international E-road network, and stretches from Norway to Italy, passing through Gothenburg. In order to be provide space to the large-scale developments of infrastructure in Gothenburg, it was decided that part of E45 had to be lowered in order to accommodate a road-traffic tunnel (Peab AB, 2023). The tunnel is located between the central station and Lilla Bommen in central Gothenburg, shown in figure 3.0.1.

Figure 3.0.1: Aerial view of the site location in Gothenburg (CNES, 2023).

The tunnel will also serve as a foundation for four new city blocks, that are planned on top of the tunnel. The lowering was performed on some 900 meters of the E45, of which half has been covered with a concrete deck, in order to serve as foundation for the prospective city blocks. Peab Anläggning AB, who carried out the construction works of the tunnel, had a turnkey contract with The Swedish Transport Administration as client. The construction process started in 2016 and ended with final inspections in 2021. Due to deep deposits of natural soft clay present, a deep piled foundation was necessary to carry the loads from the tunnel, traffic and future city blocks. Some 4 500 piles were driven, most being approximately 65 meters long, resulting in total length of ca 275 kilometres. Figure 3.0.2 shows a view of the com-

pleted lowering and the entrance of the tunnel. The 6-meter-high concrete retaining walls is visible in the right of the figure

Figure 3.0.2: View of the lowering, retaining walls and entrance of the tunnel.

3.1 Geotechnical site description

In this section some important soil properties are described. The site description, geological and geotechnical properties at the site has been summarized in a report by Peab Anläggning AB: *B01 Beräkningsförutsättningar Geoteknik* (Peab AB, 2016).

The stratigraphy in the area is described by Peab Anläggning (2016) and consists of a layer of fill overlying a deep clay deposit, which sits on top of a friction material and bedrock. The fill consists of two layers where the uppermost part consists of coarser material. The lower part of the fill is mainly made up of masses from dredging, containing clay, silt and mud. The clay layer below the fill is of low to medium sensitivity with an increasing undrained shear strength with depth. The clay layer has been divided into four layers based on a report from Trafikverket (2016). The unit weights in the area can be found in table 3.1.1.

Table 3.1.1: Unit weights of soil layers in the area, reported by Trafikverket (2016).

Soil	**Level**	γ_{unsat} **[kN/m^3]**	γ_{sat} **[kN/m^3]**
Fill layer 1	+2 to +1	18	20
Fill layer 2	+1 to -1	18	18
Clay 1	-1 to -7	16.5	16.5
Clay 2	-7 to -25	16	16
Clay 3	-25 to -45	16.5	16.5
Clay 4	<-45	16.5 + 0.033/m	

The undrained shear strength of soil in the area of the lowering and the tunnel construction was derived for the direct shear zone and then validated through additional triaxial tests. In table 3.1.2, the determined values of the clay's undrained shear strength, c_u, can be seen. For the calculations of geotechnical bearing capacity of

the cohesion piles, the undrained shear strength in the direct shear zone was chosen as input.

Table 3.1.2: Determined undrained shear strength of the clay at the location of the lowering and the tunnel (Peab AB, 2016).

	c_u **in direct shear zone (kPa)**
Level (m)	$14 + 1.38z$ to -45, thereafter 1.89z (z from -1 m)
1	14
0	14
-1	14
-4	18.1
-20	40.2
-45	74.7
-90	159.8

The values for the friction angle ϕ', were derived from the recommendations of The Swedish Transport Administration (Peab AB, 2016). The chosen values can be seen in table 3.1.3.

Table 3.1.3: Determined friction angles for different materials present.

Material	**Friction angle,** ϕ' **(°)**
Filling material	34
Clay	30

The preconsolidation pressure is described by Peab AB (2016) to have been evaluated through several lab tests. The testing scheme included drained and undrained triaxial tests, oedometer incremental loading (IL) tests and CRS tests. For a full view of results from all testing, see Appendix A. The testing has mainly been performed on soil samples from the clay, but tests have also been performed on the filling layer consisting of masses from dredging. The preconsolidation pressure used in calculations, reported by Peab AB (2016), can be seen in figure 3.1.1 and table 3.1.4.

Table 3.1.4: Preconsolidation pressure

Level	σ'_c **[kPa]**
0	41.7
-5	67
-35	292
-45	384
-90	799

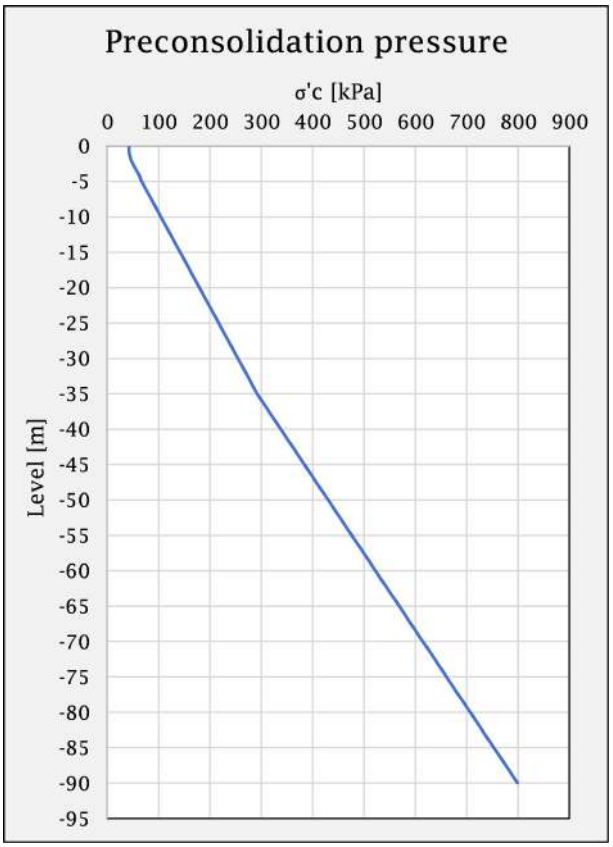

Figure 3.1.1: Evaluated trend of preconsolidation pressure with depth, adopted from a report by Peab Anläggning AB (2016)

In terms of hydrogeology, a fill above the deep clay deposit and a friction layer underneath can be considered as draining layers. The overlying fill was determined to have large spread in hydraulic conductivity, ranging from $k = 10^{-4} - 10^{-7}$ m/s (Peab AB, 2016). The clay layer was determined to have less variability in permeability, but still ranged from $k = 2 \cdot 10^{-10}$ m/s in the deeper part, to $8 \cdot 10^{-10}$ m/s in the upper part of the clay. The in-situ pore water at the location of tunnel was determined to have a slight excess pressure, and thus a hydrostatic distribution of 10.3 kPa/m (= 1.05 mH_2O/m) was determined from a level of +0.3 m.

During the construction period, a large excess pore pressure has developed. The available pore pressure measurements are taken slightly north of the tunnel and E45 and mostly show a linear increasing trend from when the instrumented piles were driven. Compared to in situ pore pressures, a maximum increase of around 80-100 kPa in excess pore pressure has developed. In figure 3.1.3, the change in pore pressure is visualized from the time of driving the instrumented piles, for the depths 12 m, 21 m, 34 m and 50 m. The position for pore pressure measurement is shown in figure 3.1.2.

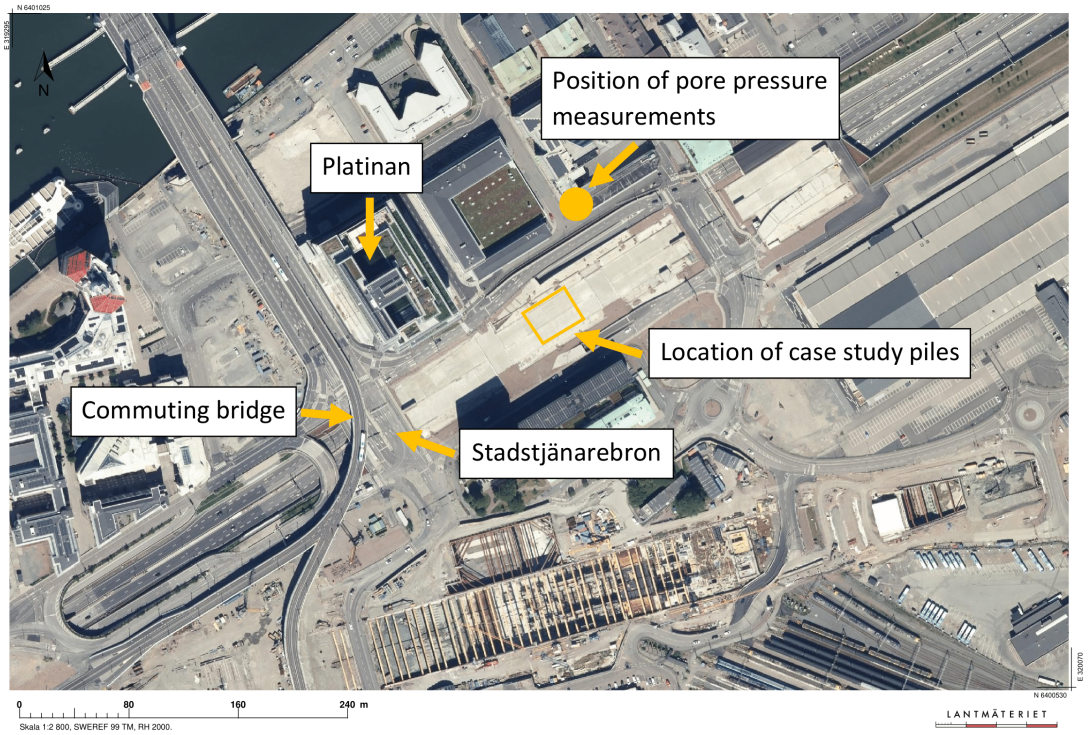

Figure 3.1.2: Position of pore pressure measurements and nearby structures.

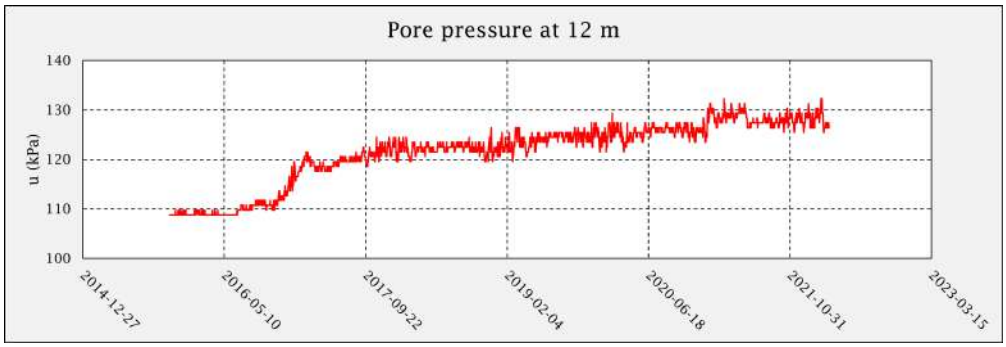

(a) Pore pressure development 12 m depth

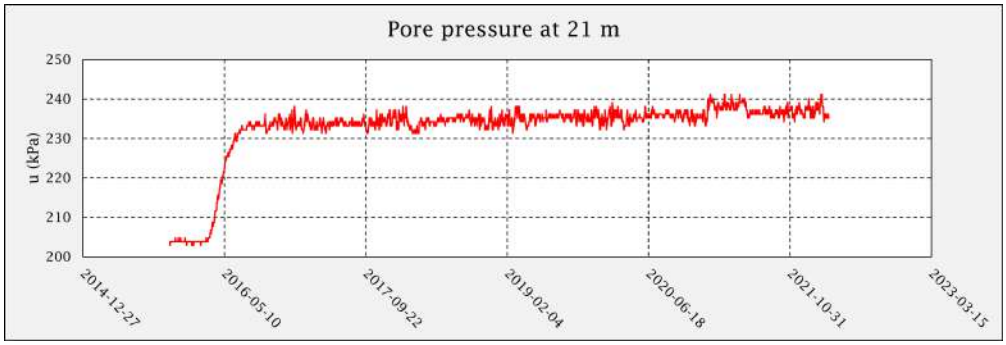

(b) Pore pressure development 21 m depth

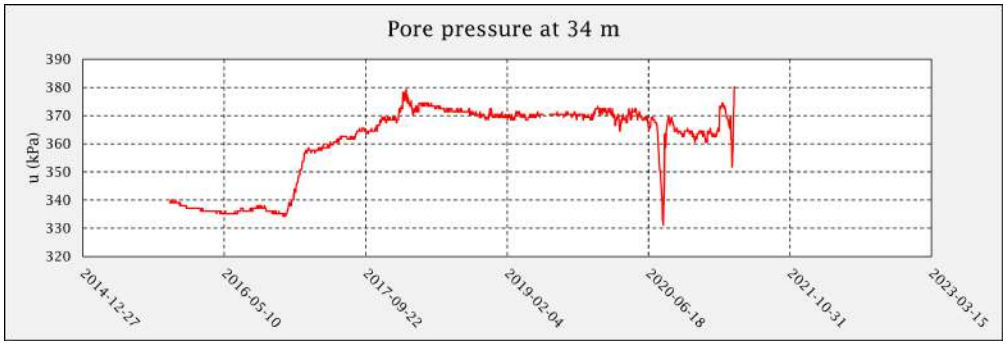

(c) Pore pressure development 34 m depth

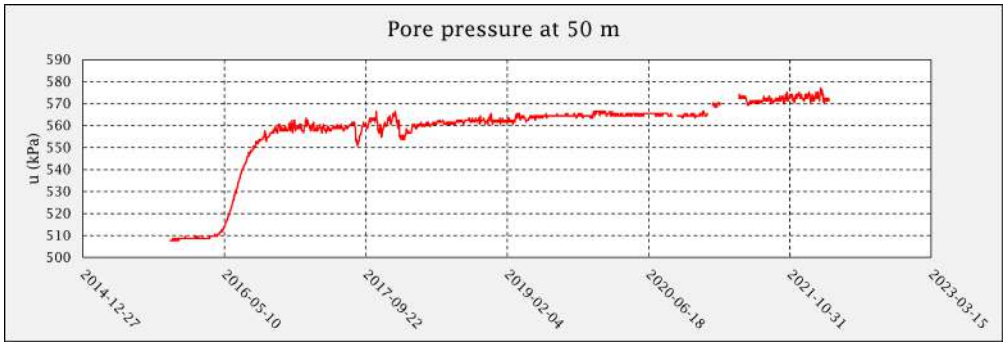

(d) Pore pressure development 50 m depth

Figure 3.1.3: Pore pressure development for different depths. The initial dramatic increase in pore pressure is coinciding when piling for the tunnel started.

The compression modulus M_0 for stresses lower than the preconsolidation pressure has been evaluated from oedometer incremental loading (IL) tests, CRS tests and

triaxial tests. As has the compression modulus M_L. Based on these, is has been shown that the compression modulus M_0 has a good correlation with the undrained shear strength times 400, $M_0 = 400 \cdot c_u$ for the in-situ case. The chosen M_0 is based on one single cycle of unloading-reloading. The adopted profile for the compression moduli M_0 and M_L can be seen in table 3.1.5.

Table 3.1.5: Compression moduli M_0 and M_L adopted from values reported by Peab Anläggning AB (2016).

Level	M_0 **[kPa]**	M_L **[kPa]**
-1	5000	500
-8	-	500
-45	31400	1425
-90	63908	3225

3.2 Tunnel design & foundation plan

A typical cross section of the tunnel is shown in figure 3.2.1. The tunnel is constructed with three main walls that rests on ground concrete beams that in turn are supported by piles.

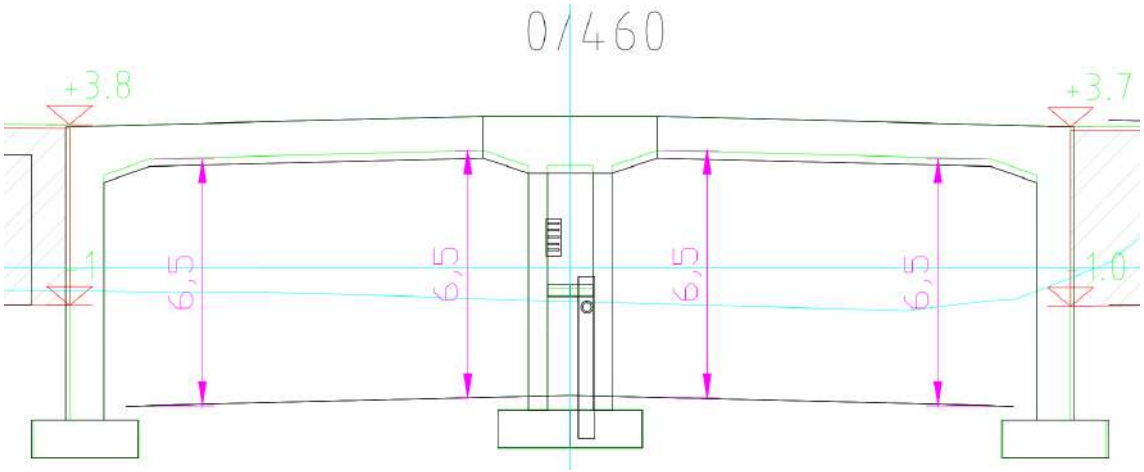

Figure 3.2.1: Typical cross section of the tunnel.

The piles that were driven under the tunnel are primarily divided into eight (8) parts, or monoliths. In figure 3.2.2 a cross section of the tunnel is seen in which the instrumented pile's location and bearing are more apparent. In figure 3.2.3 the monolithic division can be seen together with the location of the three instrumented piles.

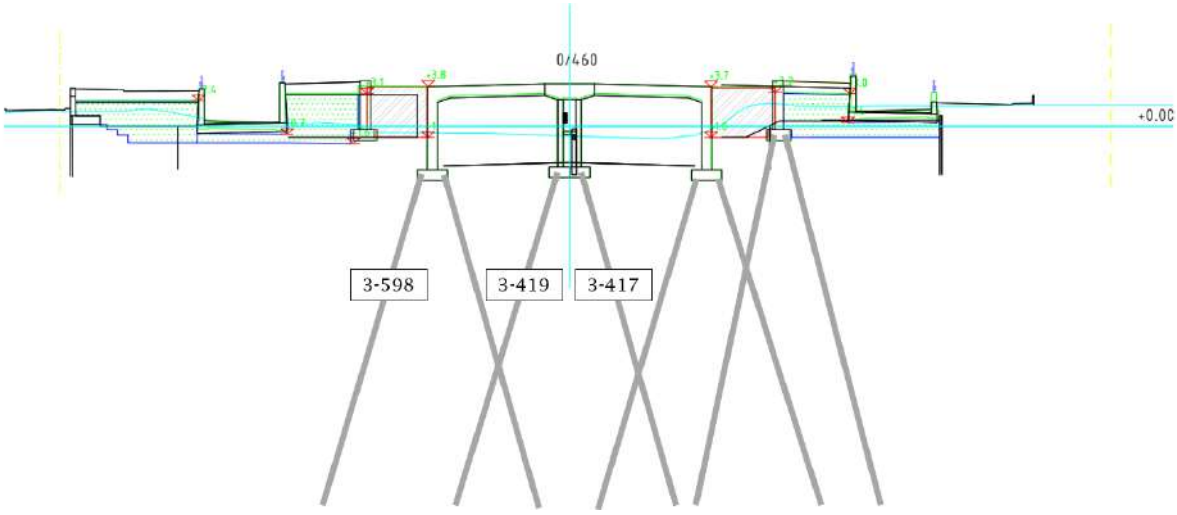

Figure 3.2.2: Location and bearing of the instrumented piles (3-417, 3-419, 3-598) seen in a cross section.

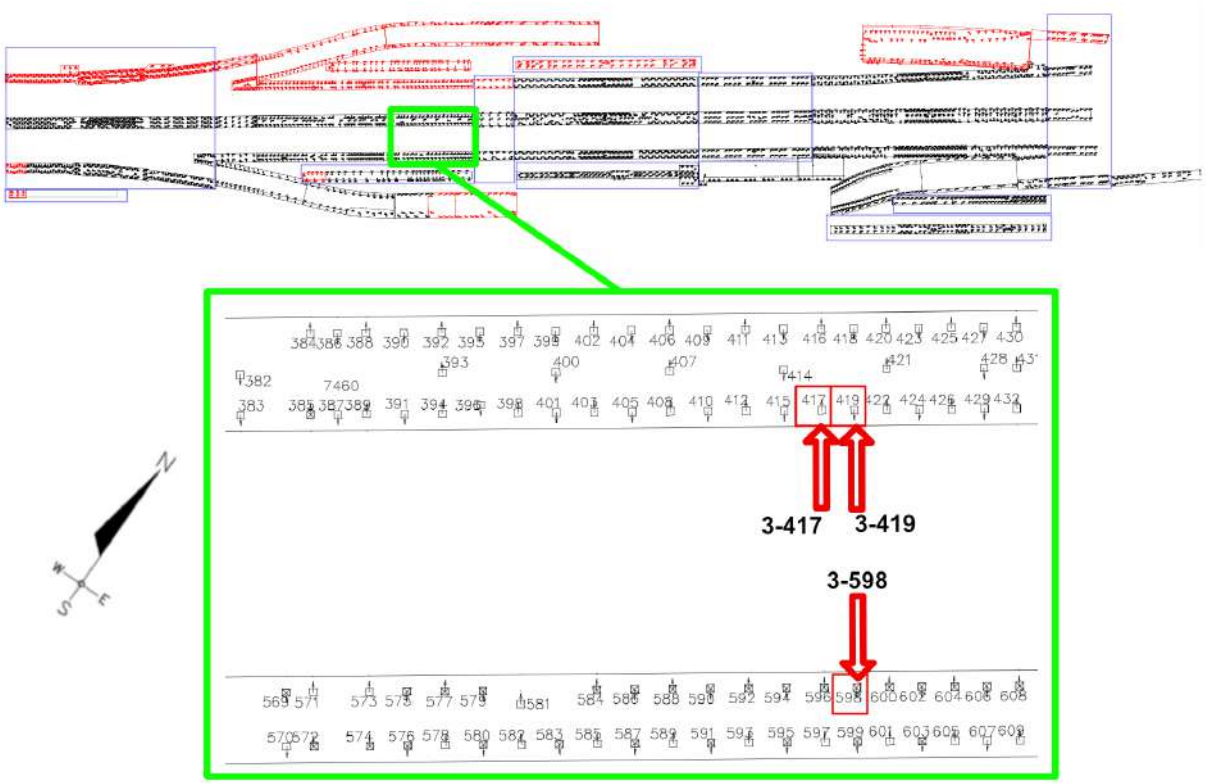

Figure 3.2.3: Location of monolith and the instrumented piles (3-417, 3-419, 3-598) and their respective positions.

As seen in figure 3.2.3 all three instrumented piles are in proximity to each other and located in monolith 3. In figure 3.2.1 and 3.2.2 cross sections of the tunnel can be seen. Below both the north and south tunnel wall, two pile rows with 4:1 inclination supports the tunnel, and under the centre wall there are three pile rows. Both the part of the pile row underneath the centre wall and the south wall where

the case study piles are located have a centre to centre spacing in between piles of 1.2 metres at the pile head. The spacing between the two pile rows supporting the centre and south walls is 2 metres at pile head.

3.3 Pile type and material properties

The instrumented piles are square reinforced concrete piles with a width of 275 mm, shown in figure 3.3.1a. The concrete piles are reinforced with 12 Φ16 mm rebars of type K500C-T and the used concrete grade is C60/75, vct = 0.5. The piles were installed in late August and beginning of September 2017. The cables for the Sister Bars runs along the pile inside a protective steel tube with a diameter of 140 mm on one side of each pile. The piles are driven at an angle of 4:1, and reach a depth of about 65 metres. This in turn means that the total pile length is about 67 metres. The piles consist of 5 elements which are about 13 metres each, as shown in 3.3.1b.

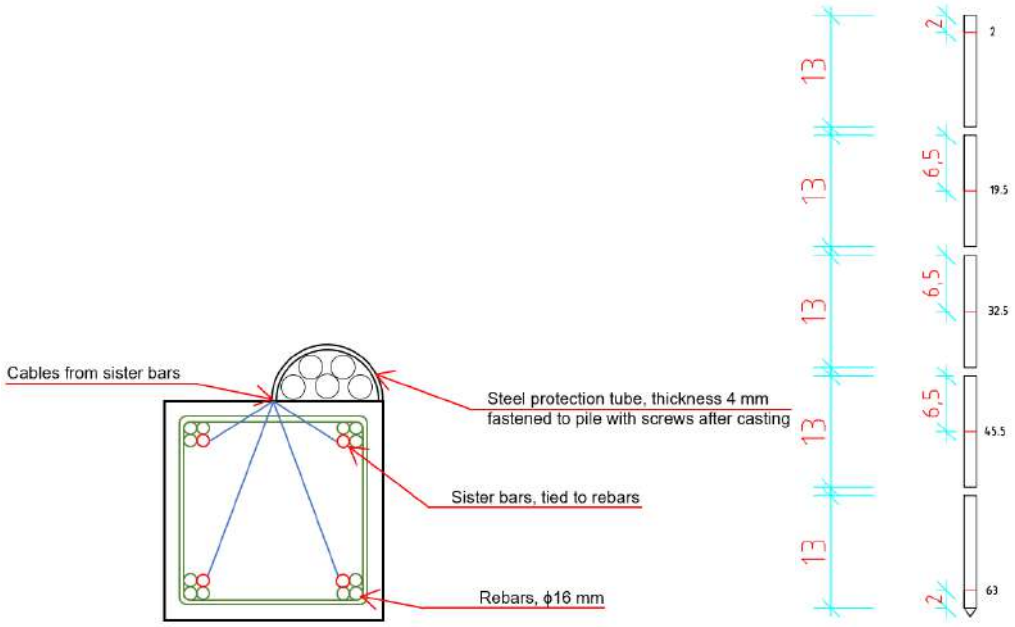

(a) Cross section **(b)** Section

Figure 3.3.1: Sections of instrumented case study piles.

3.4 Additional construction projects in the area

Apart from the lowering of the E45, several other large construction projects have taken place at the case study site that might influence the studied piles. These are important to delineate as they can be a part in explaining the developed load distributions in the instrumented piles. The most relevant nearby construction projects can be seen in figure 3.4.1 below. The yellow group is the case study Gullbergstunneln, the red group are nearby bridge projects by Skanska, the green is the pile driving for Platinan and blue is when the instrumented piles were installed. The

pink section represents the concrete casting for Monolith 3. The location of these projects can be seen in figure 3.1.2.

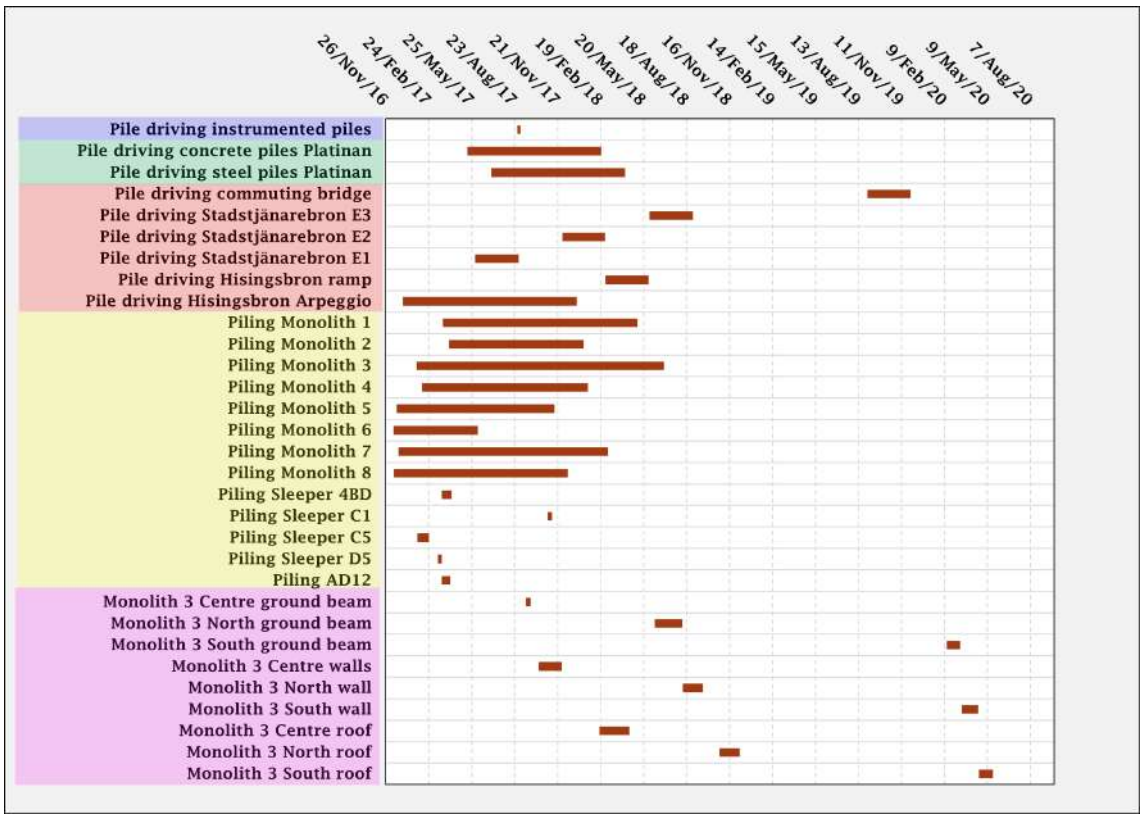

Figure 3.4.1: Timeline of construction projects in the area surrounding Gullbergsvass.

4 Data analysis of strain measurements

The measured data from the instrumented piles was analysed using the methodology presented in the following section. This chapter also includes the results from the data analysis.

4.1 Method

The original format of the measurements was frequencies and temperatures from each of the four strain gauges for each depth of instalment. The evaluation of strains in the piles is based on a benchmark measurement of the frequency and temperature in the strain gauge. All following evaluation of strains and forces are thus based on said benchmark values. The magnitude and direction of the calculated forces are reliant on what benchmark is used for the calculations. In this project, four different dates were used as benchmark:

1. In a lab before pile casting
2. Pile in storage
3. During installation
4. After installation of piles

From the list above, only the results of the first benchmark will be presented in the results section of this report. This is due to the assumption that a benchmark from before casting would yield the most accurate results, as the pile is not influenced by concrete shrinkage or any other induced forces. In addition to the load distribution calculation, the change in load between measurements was calculated, i.e., ΔL as the size and direction is not influenced by any benchmark. The four data points for each depth were combined into an average load in order to remove any discrepancies in forces induced by bending moment, see example provided in figure 4.1.1.

Serial number	Placement	F [kN]	$F_{average}$
1709774	B	426.946	123.42
1709775	D	-215.841	
1709773	C	-109.636	
1709772	A	392.196	

Figure 4.1.1: Example of evaluated loads in pile 3-419 at 32,5 metres depth on the 19^{th} of May 2022.

The average load for each depth is presented in section 4.2. The results for benchmarks 2-4 can be studied in Appendix B.

4.1.1 Strain measurements

The information gathered by the Sister Bar strain gauges was collected via a cabinet constructed with several measuring terminals, which is situated in section 0/460 of the tunnel. Five cables from each Sister Bar strain gauge are connected to the cabinet of which four are used for measurements. See figure 4.1.2 for a view of the setup for data gathering. Readings were gathered by connecting a readout box, model GK 404 from Geokon (Geokon, 2020) to each measuring terminal, see figures 4.1.3a. The four cables from each strain gauge are the positive and negative strain gauge leads and the positive and negative thermistor leads. Both the frequency of the vibrating wires as well as the temperature reported by the thermistor were recorded and extracted, see figure 4.1.3b.

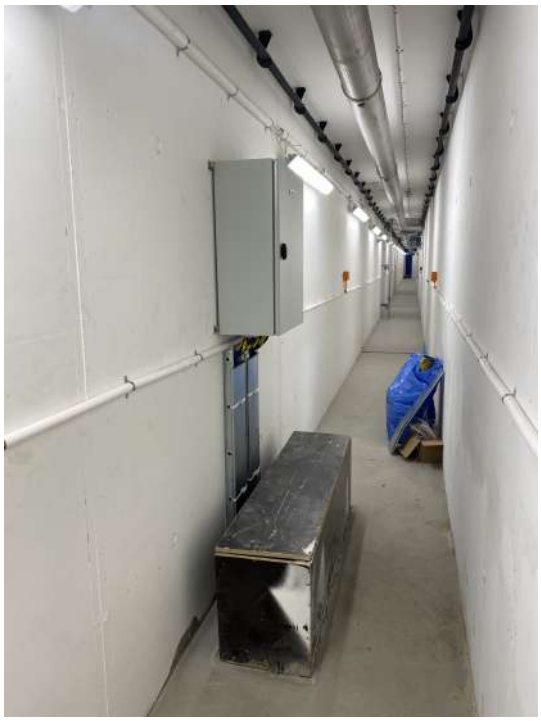

(a) Location of electrical cabinet.

(b) View of cable management inside cabinet.

Figure 4.1.2: Setup for measuring the sister bar strain gauges.

(a) Connecting the readout box to measuring terminals.

(b) GK404-Readout box.

Figure 4.1.3: Taking a reading.

The Sister Bar strain gauges are equipped with vibrating wire transducers that continuously measures the strain and temperature in the piles. However, as the electrical cabinet does not have the ability to store data, readings can only be obtained by physically extracting them from the logger placed in the middle wall of the tunnel, see figure 4.1.2a. This means that the conducted data analysis is based on point values from specific dates and not continuous readings. During the project, data was gathered on two occasions. The first data collection was performed in late February, on the 27^{th}. The second data collection was performed in April, on the 11^{th}.

4.1.2 Identification of outliers

The recorded data was sorted by date and depth of measurements. Preferably a statistical method for outlier identification would be used, but a statistical method for the entire data set would likely not adequately allow for large variations in frequencies and temperatures due to ambient construction processes and seasonal variations in climate that the instrumented case study piles experiences. Instead, a visual method to identify outliers was used, where the entire dataset is sorted and plotted. Values that did not follow the trend were then identified and checked against the remaining recordings for the particular date and depth. If e.g., the temperature recording for a strain gauge strongly disagreed with the other three strain gauges for a particular date and depth, the reading obtained by the disagreeing strain gauge was removed from the dataset and replaced with interpolated values. Analysed plots

for obtained data can be found in figure 4.1.4 for the case study piles.

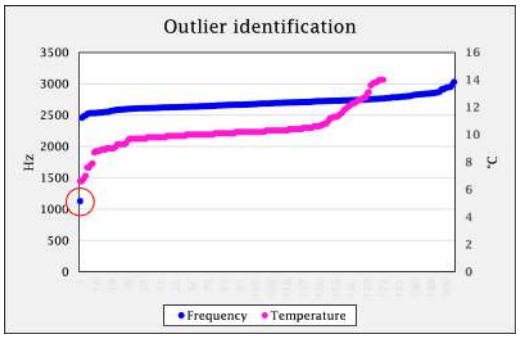

(a) Strain gauge readings from case study pile 3-419.

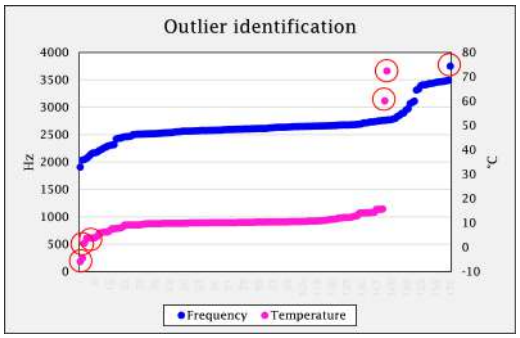

(b) Strain gauge readings from case study pile 3-598.

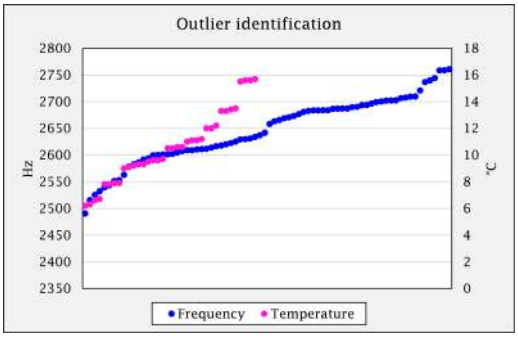

(c) Strain gauge readings from case study pile 3-417.

Figure 4.1.4: Circled data points represent readings determined as false. Points in the graphs represent each frequency and temperature sorted by size.

Note that if a temperature was deemed an outlier, the associated frequency was not necessarily removed. If a strain gauge gave a reading marked as false (regardless of frequency or temperature), that reading was handled as described in section 4.1.3.

4.1.3 Method of interpolation

The dataset of frequencies and temperature readings from the Sister Bars contained several missing values. The dataset for one of the case study piles, pile 3-417, only contained readings from the top level of strain gauges, at 2 metres depth. This is most likely due to that the cables transferring the frequency of the vibrating wire strain gauges were damaged during pile driving.

Regarding the other two case study piles, 3-419 and 3-598, some dates and depths had one or two strain or temperature readings missing or deemed as false. If only the remaining readings had been interpreted and used as a result, this could give a false indication of load distribution, load change or bending moments experienced by the pile. Therefore, missing or false readings from case study piles 3-419 and 3-598 were interpolated. In general, pile 3-598 required exceedingly more interpolation (76/400 = 19% data points) while pile 3-419 only had 11/440 = 2.5% data points

that needed interpolation. Consequently, pile 3-419 should be regarded as the more reliable of the two instrumented piles.

The method for interpolation varied. For the false temperature readings visualized in figure 4.1.4b, these values were all reported by one strain gauge on one depth. These values were replaced with an average temperature reported by the remaining three strain gauges on that level.

For missing or false strain gauge readings the method was based on establishing a relationship between previous readings within a strain gauge level. No relation between levels were considered, but only the relation between strain gauges within the same level. If only one value was missing for a certain strain gauge level, the assumption of a constant relationship between two gauges experiencing tension and/or compression was made. The calculated relationship factor was then used to estimate the missing value. For example, if gauge A and B are experiencing tension, and gauge A is missing in the following measurement, a ratio A/B was established and used to evaluate the missing value in the series. An example is provided below.

2019-04-04		2020-03-03	
A	B	A	B
4248	4752	4592	?

In this example the missing value for gauge B on the 3^{rd} of march would be estimated by assuming a constant ratio between gauge A and B. The ratio would then be $\frac{A}{B} = \frac{4248}{4752} = 0.89$, which could then be used as $\frac{1}{0{,}89} \cdot 4592$ to obtain the missing value for B.

If two values were missing for a certain strain gauge level, the method assumed a constant relationship between the missing value and the average of the remaining readings on that same strain gauge level. The established ratios were then used in the same manner as previously described for one missing value to obtain an interpolated value to represent the missing readings.

4.1.4 Determination of pile modulus

The Young's modulus of the piles was assumed to be 35 MPa after discussion with Peab AB. This modulus was chosen for the entire pile as this thesis is not focused on studying how and if the modulus of concrete piles changes after they are driven. As the pile modulus is used to determine the calculated load experienced by the pile through equation 2.2.5, an increase or decrease in pile modulus affects the calculated load linearly, i.e.

$$F \propto E \tag{4.1.1}$$

It should be emphasized that the modulus of 35 GPa is somewhat arbitrary, and research with FEA have shown that concrete piles in Gothenburg clay can have a modulus as low as 18 GPa (Wood and Karstunen, 2022).

4.1.5 Sensitivity analysis

To study the uncertainty in the output of the calculations a sensitivity analysis of pile properties and data was performed. The Young's modulus was allowed to vary, in order to study how the magnitude and shape of the load distribution was affected. The Young's modulus was also allowed to vary depending on the average strain direction on each level of strain gauges, in order to study how it affected the estimated load distribution. In tension the strain (ε_{actual}) was used together with cross-sectional area and modulus ($E = 210GPa$) for the reinforcement, while for compression the entire piles' area, modulus and strain ($\varepsilon_{load-related}$) was used. This was achieved by an if-function in the calculations, i.e., if the output force showed tension, the load was recalculated with the properties for the reinforcement instead.

Additionally, a sensitivity analysis of temperature and chosen benchmark was performed. Similar to the Young's modulus, the sensitivity due to temperature uncertainty was performed by varying the assumed temperature for calculations.

4.2 Results

The estimated load distribution based on a benchmark frequency from the calibration of the strain gauges can be seen in figure 4.2.1. As evident from the graphs, the piles are mostly experiencing tension during the studied period, but with a trend towards compressive forces over time. The maximum force for both pile 3-419 and 3-598 has a rather constant location. The resolution is however quite poor due to only five levels of strain gauges.

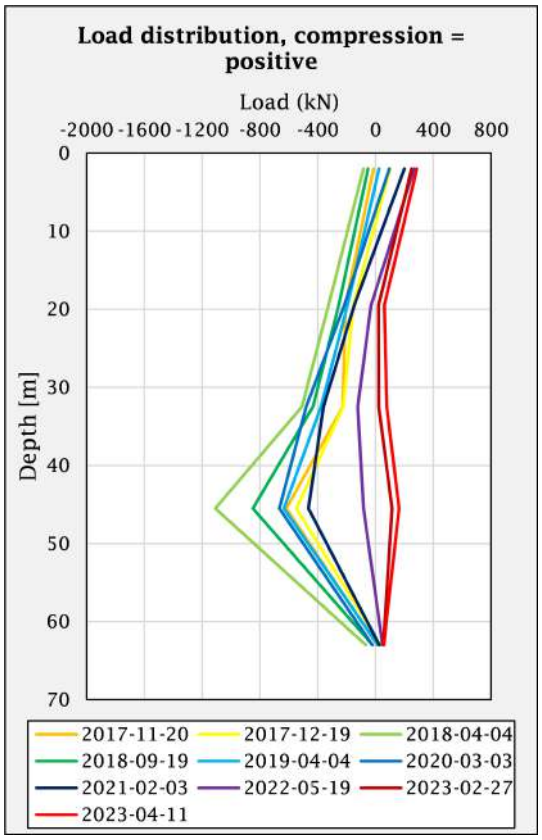

(a) Load distribution of pile 3-419, located in the center wall.

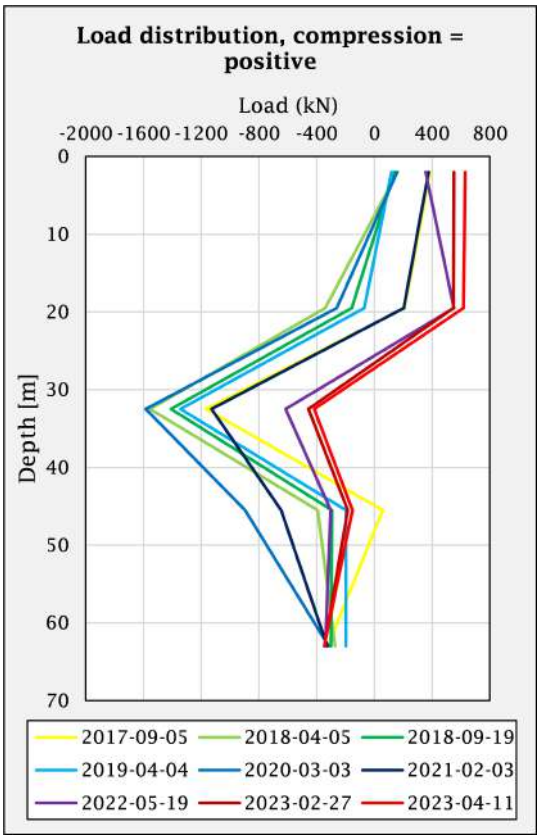

(b) Load distribution of pile 3-598, located in the south wall.

Figure 4.2.1: Estimated load distribution of instrumented piles. Benchmark frequency is based on the calibration of the strain gauges at the factory.

The trend towards increasing compressive forces in pile 3-419 (located beneath the centre wall) can be observed in figure 4.2.2. After pile installation, which takes place on the 28^{th} of August 2017, pile 3-419 experiences a high increase in tensile forces. After that, the pile is subject to large changes in internal forces during the first year and a half after the pile has been installed. Following this period, during the latter half of 2018, the sudden load changes come to a halt. During the beginning of 2020, the pile is subject to unloading as the strain gauges report a negative load change.

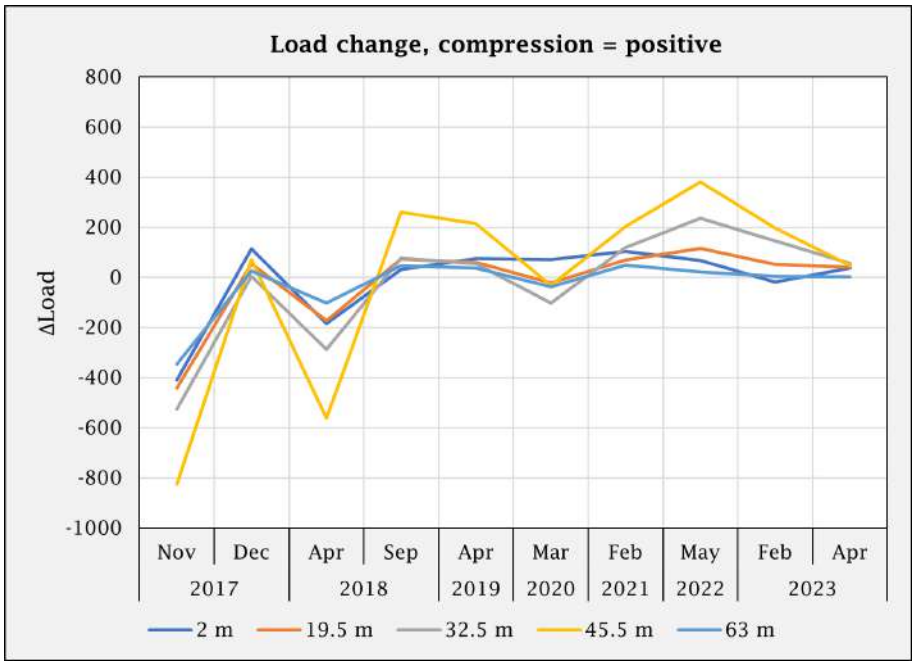

Figure 4.2.2: Load change of pile 3-419, located in the center wall.

For pile 3-598 (located beneath the south wall), the load change with time has less of a clear trend in comparison to pile 3-419, as can be seen in figure 4.2.3. Like pile 3-419, pile 3-598 experiences an unloading, or increasing tension forces after its installation on the 4^{th} of September during 2017. In addition, pile 3-598 also experience increasing tensile forces during both the beginning of 2018 and during the beginning of 2020, as does pile 3-419. The change in load is however of larger magnitude for pile 3-598 than for pile 3-419 during early 2020.

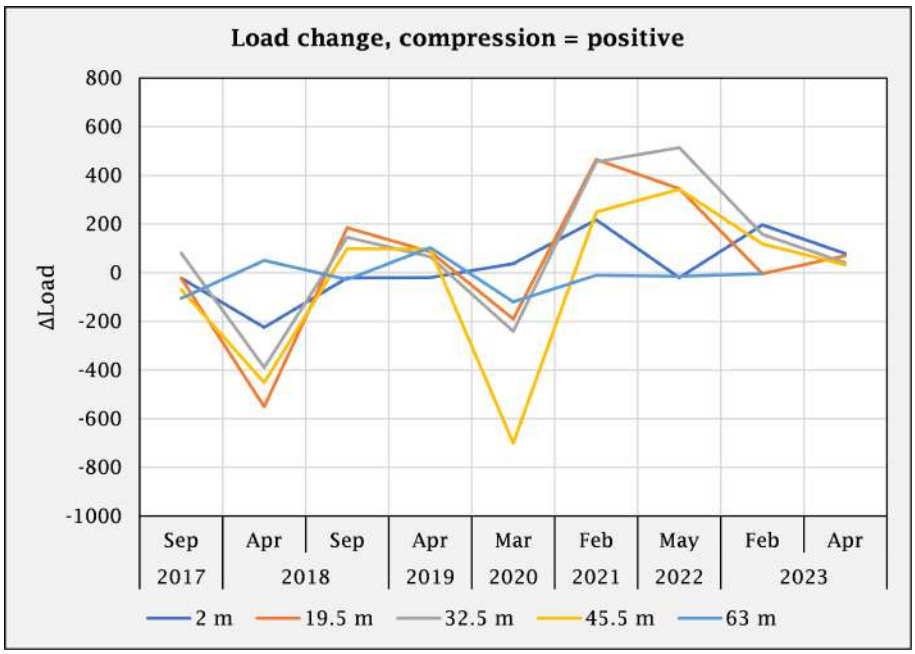

Figure 4.2.3: Load change of pile 3-598, located in the south wall.

Regarding the third case study pile (3-417, located in the centre wall), results are only available for the upper level of strain gauges, at a level of 2 metres from the pile head. This makes useful interpretation of the results for pile 3-417 difficult. The limited results that could be extracted for pile 3-417 can therefore be seen in Appendix E in figures E.0.1 (load over time) and E.0.2 (load change over time). Like piles 3-419 & 3-598 the results are based on a benchmark frequency from the calibration of the strain gauges.

In contradiction to the other case study piles, pile 3-417 seems to experience mainly tensile forces during the study period. Pile 3-417 does however show an unloading during early 2018, and increase in tensile forces during 2020, see figure E.0.2, which reflects what the results show for the other two case study piles. Since only one level of Sister Bars is operational for pile 3-417, the results should be interpreted with caution.

In addition to the graphs showing load distribution (figures 4.2.1a & 4.2.1b) the strain distribution, expressed as microstrains ($\mu\varepsilon$), was plotted as seen in figures 4.2.4a & 4.2.4b. This is using the strain $\varepsilon_{load-related}$, i.e., the strain that the concrete experiences and the strain used to calculate the load distribution seen in figure 4.2.1. This removes any uncertainties regarding choice of Young's modulus for accurate load estimation, and thus only shows the absolute extensions or compressions experienced by the piles.

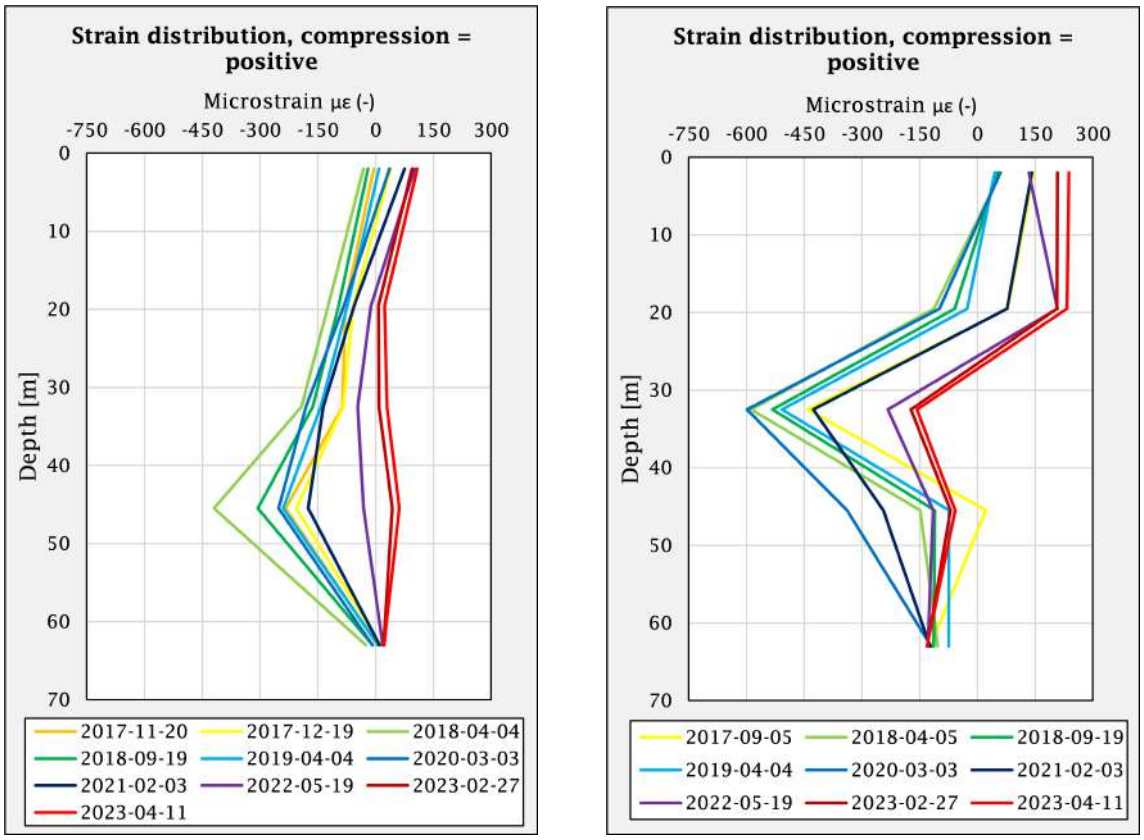

(a) Strain distribution of pile 3-419.

(b) Strain distribution of pile 3-598.

Figure 4.2.4: Estimated strain distribution of instrumented piles. Benchmark frequency is based on the calibration at the factory and strain used is $\varepsilon_{load-related}$.

4.2.1 Sensitivity analysis

Uncertainty in results due to variations in choice of benchmark reading was studied by changing the benchmark used for calculation of forces. It could be seen that while this did not affect the load change, it did influence the magnitude of forces estimated to act on the case study piles. It also influenced whether the piles were interpreted as being subject to tensile or compressive forces in some instances. The conducted sensitivity analysis focused on two inputs: temperature and elastic modulus. These parameters were chosen as they are based on assumptions. The differences in load distribution due to change of benchmark reading can be observed in Appendix B.

Regarding influence of temperature variations and variations in Young's modulus, the two have different impacts on the result. As can be seen in figure 4.2.5b a change in assumed temperature displaces the graph in parallel, the temperature has an arithmetic relationship with the interpreted load. The Young's modulus on the other hand has a geometric proportionality to the interpreted load, as can be observed in figure 4.2.5a. The interpretation of load is therefore more sensitive towards changes in Young's modulus than for changes in temperature.

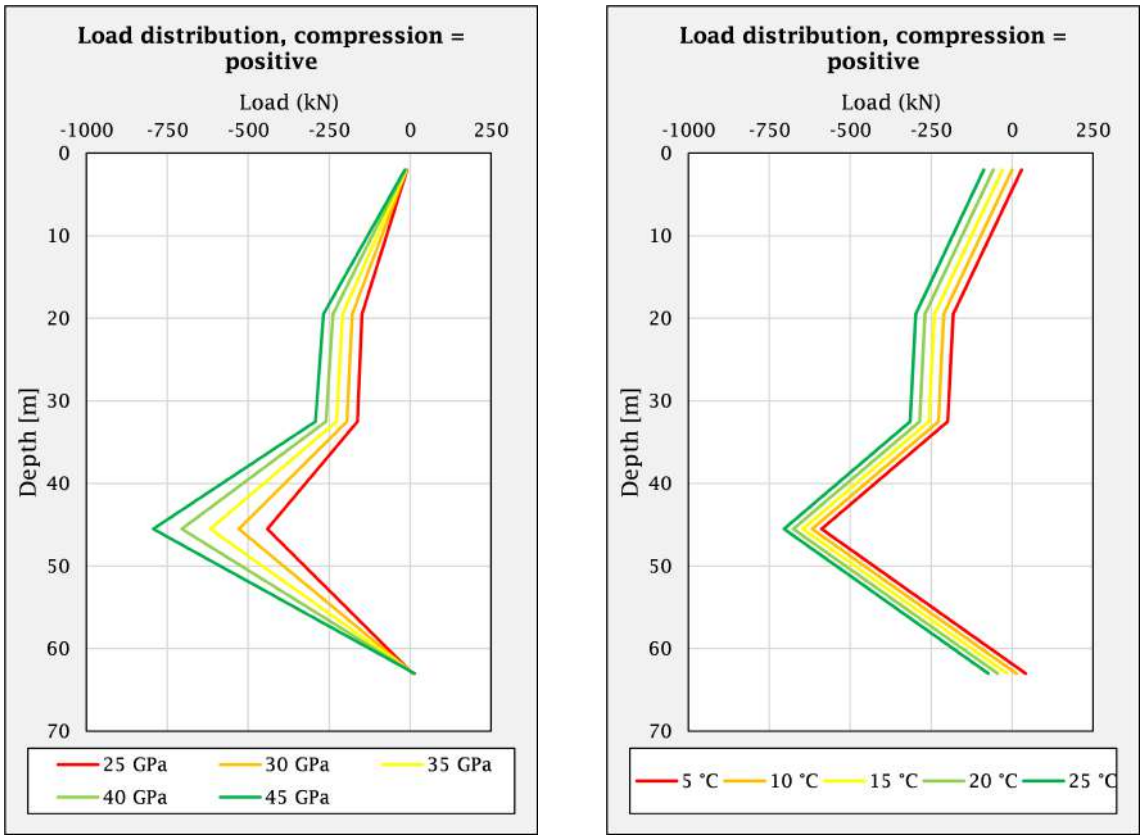

(a) Change in E-modulus of concrete. **(b)** Change in temperature.

Figure 4.2.5: Sensitivity analysis for pile 3-419 on the 20^{th} of November 2017.

In addition, the calculated load decreases greatly if it is assumed that the reinforcement carried all load in tension and that the concrete carries all load in compression. In figure 4.2.6 the load distribution for pile 3-419 and 3-598 can be seen, with varying E-modulus and cross-section area depending on the direction of the strain. For tension, a modulus of 210 GPa and area of 0.002 m^2 was used, while for compression 35 GPa and 0.076 m^2. This yields a similar shape of the load distribution compared to figure 4.2.4, but with lower load magnitudes.

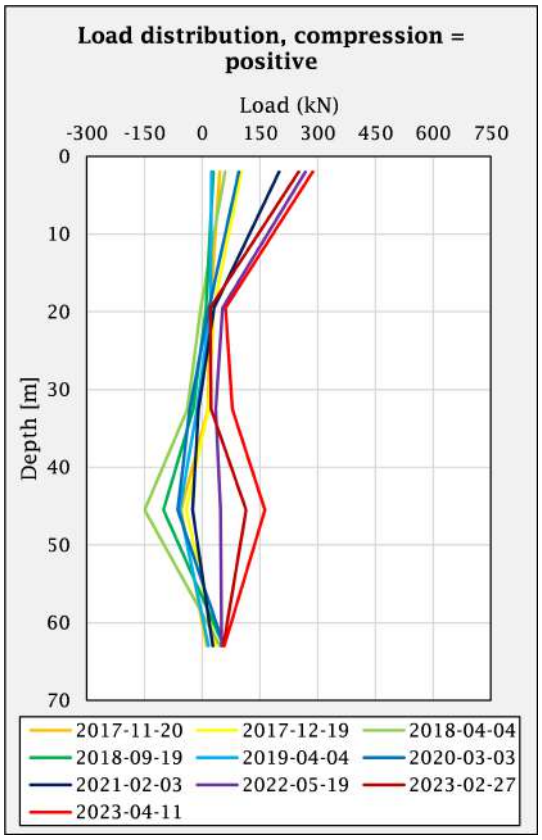

(a) Load distribution of pile 3-419, located in the centre wall.

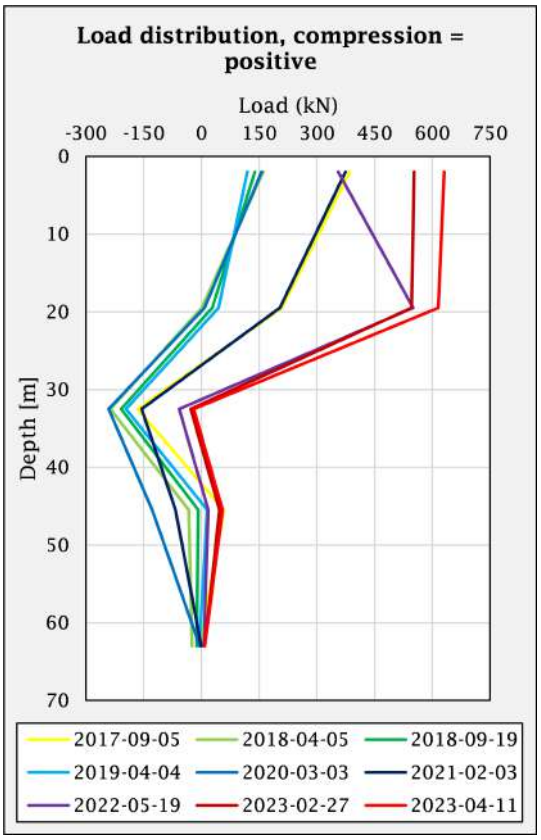

(b) Load distribution of pile 3-598, located in the south wall.

Figure 4.2.6: Estimated load distribution of instrumented piles with varying E-modulus and cross-sectional area depending on strain direction. Benchmark frequency is based on the calibration of the strain gauges at the factory.

5 Analytical analysis of pile behaviour

The analytical analysis was performed as a series of hand calculations using both a total stress method and an effective stress method. The analytical analysis includes both a study of how the load is distributed in a pile assuming that the entire soil profile is heaving or settling. This chapter includes a presentation of the methodology and the results.

5.1 Method

An analytical analysis of the load distribution was performed using both the α- and β-methods, described in sections 2.1.3 and 2.1.4 assuming both settlement and heaving of the entire soil profile. The analytical analysis was based on the assumption that **a single pile** is driven vertically and in the middle of the excavation, as opposed to the case study piles that were driven at an angle, and in close proximity to each other. Additionally, the 6-meter excavation was taken into account in the β-method by decreasing the total stress with an unloading of an assumed 2:1 distribution starting from the excavation bottom. The bottom of the excavation was assumed to be 30 meter wide, and the assumed length of the excavation was 400 metres, see in table 5.1.2. In the α-method the excess pore pressure and new stresses after unloading was considered by decreasing the undrained shear strength as:

$$c_u = c_{u,0} \cdot OCR^{-0.2} \tag{5.1.1}$$

as recommended by Larsson, 2008. The in-situ undrained shear strength is decreased with a function of the new OCR, i.e., the OCR distribution after unloading is utilized.

Due to the presence of a large excess pore water pressure, the focus relied on the β-method as this is based on effective stresses (see section 2.1.4). The excess pore water pressure was taken into account when calculating the effective stress used in the β-method. The excess pore pressure used is however from a measurement located outside the excavation area, so the results from the β-method are associated with uncertainty. In order to determine the β-factor, previous research by Peab AB, 2020 on a nearby 50-meter pile was utilized. In the report, pile failure is described to

be reached in a static loading test at 1820 kN. This result was then used to calculate an appropriate β-factor to be used in the analytical analysis of the case study piles in this report. The α-factor was estimated based on figure 2.1.2 with $\frac{L}{d} = 236$ and $\frac{\overline{c_u}}{\overline{\sigma'_0}} = 0.33$. Used alpha and beta-factors can be observed in table 5.1.1.

Table 5.1.1: Used α- and β-factors for analytical analyses.

α	0.7
β	0.3

The pile head load for the analytical calculation was chosen through an estimation of the tunnel mass distributed on the total amount of piles, as can be seen in table 5.1.2. The unit weight of the tunnel's concrete was overestimated in order to account for the large amount of reinforcement used. The cross-sectional area, the tunnel length, number of pile rows and centre to centre distance was adopted from blueprints shared by Peab AB.

Table 5.1.2: Input for estimation of pile head load

Pile head load estimation		
Cross section area	51	m^2
Tunnel length	400	m
Tunnel mass volume	21600	m^3
Density of tunnel	2750	kg/m^3
Mass tunnel	59400000	kg
Total load	583308	kN
Number of piles	1000	$-$
Pile head load	**550**	kN

The stratigraphy, associated unit weights, hydrostatic pore pressure distribution and undrained shear strength used in the calculation were all based on the site description that can be studied in chapter 3. The excess pore pressure distribution and magnitude was adopted from Peab AB (2020), and used for the β-method.

The hand calculations also include an estimation of load distribution assuming heaving of the soil profile, utilizing the α- & β-methods, in accordance with report 100 by Pålkommissionen (2004), but with reversed signs so that:

$$E = Q_\infty - \int_0^z f_m dA \tag{5.1.2}$$

$$R = R_{toe} - \int_z^L f_m dA \tag{5.1.3}$$

with $R_{toe} = 0$ due to cohesion piles in soft clay. There is an argument to be made that the pile toe resistance is in fact not negligible for long cohesion piles. Still, this was assumed for reasons of simplification.

5.2 Results

The hand calculations were performed by using the $\alpha-$ & $\beta-$methods as described in section 2.1.3 and 2.1.4. As a basis for the following calculations the stresses in the soil were calculated for the in-situ case (σ_0, σ'_0) and the case after unloading (σ_{UL}, σ'_{UL}) and plotted together with the relevant pore pressures, and pre consolidation pressure (see figure 5.2.1). In figure 5.2.1 Δu represents the measured excess pore pressures from pile driving in the area, measured in December 2020.

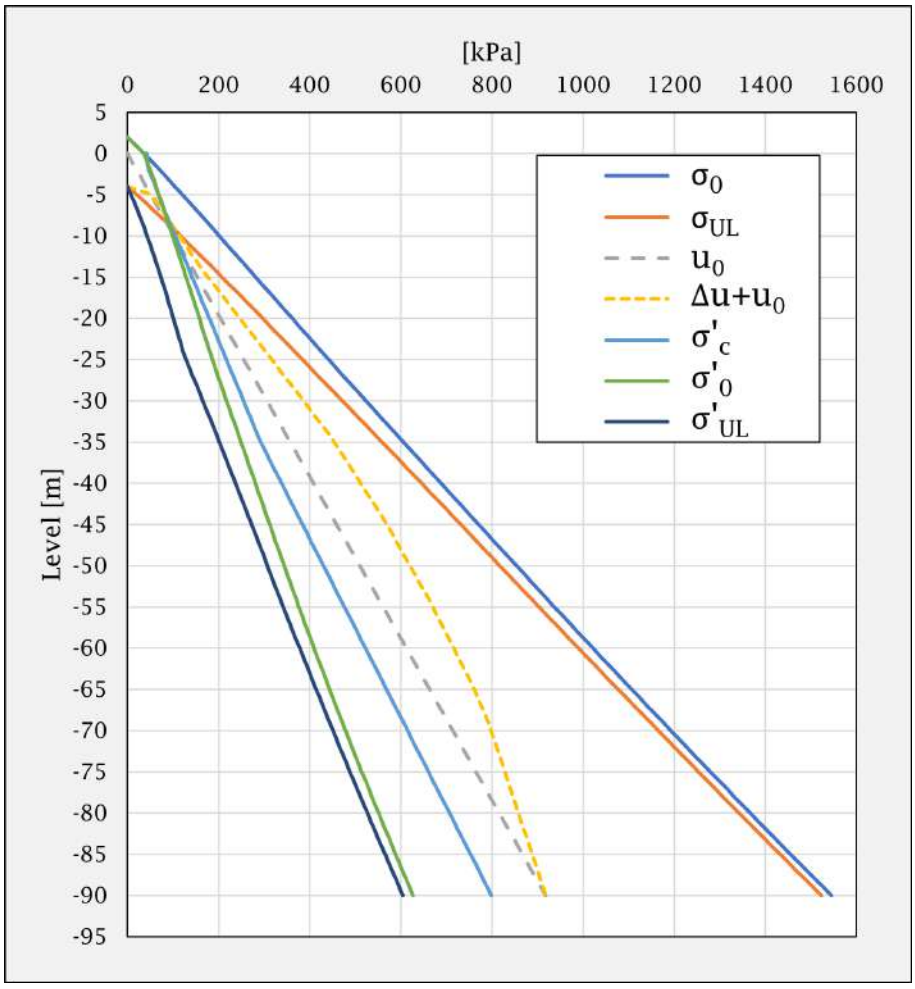

Figure 5.2.1: Stresses in the soil as a function of depth. Δu represents measured excess pore pressures from pile driving.

In figure 5.2.2 the OCR as a function of depth can be seen. This was used as a basis of calculation for the α-method, by using the OCR to estimate a decreased undrained shear strength after unloading (see equation 5.1.1).

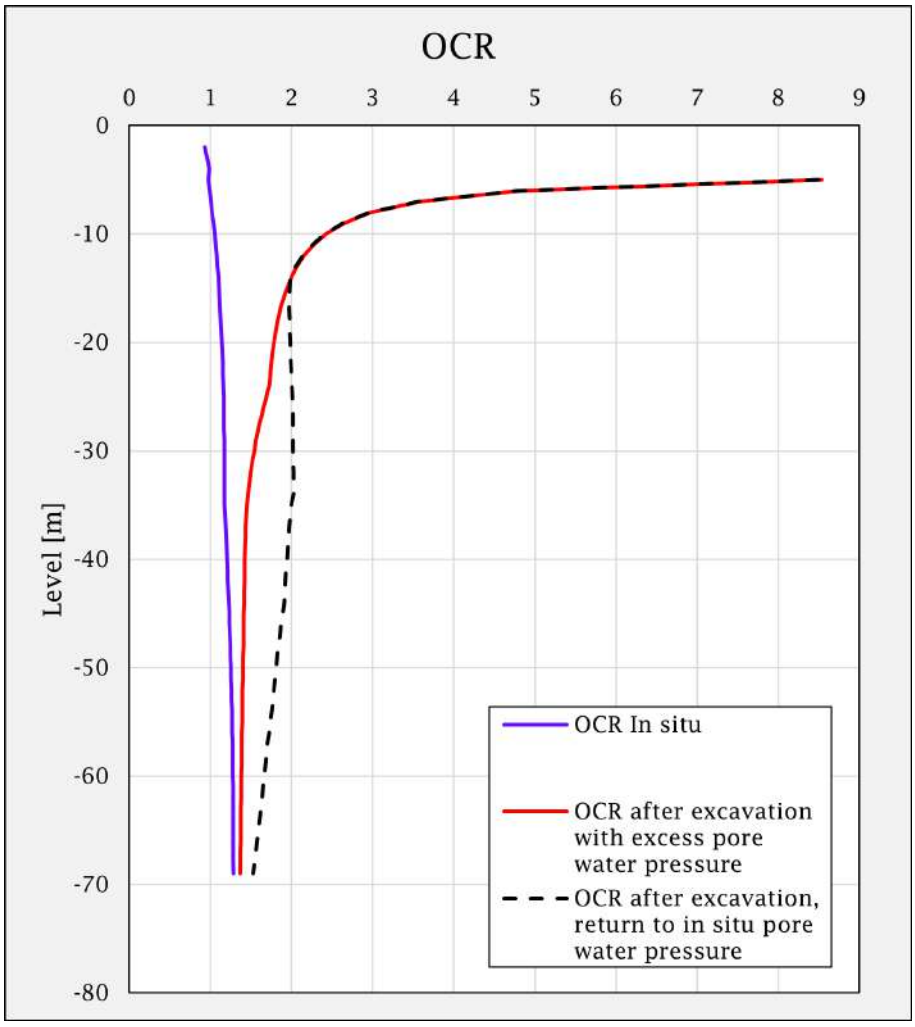

Figure 5.2.2: OCR as a function of depth for different cases. Red curve was used as input for equation 5.1.1.

In figure 5.2.3 the load distribution for both the assumption of heaving and subsiding soil throughout the whole soil profile can be seen in the same graphs. Since the α-method is based on total stresses, it is not able to directly capture any effects on estimated drag load and geotechnical bearing capacity due to the excess pore water pressure, but indirectly by decreasing the undrained shear strength. In table 5.2.1 it can be seen that the calculated magnitude of the geotechnical bearing capacity decreases considerably when the large excess pore water pressure is taken into account.

The estimated drag load is lower when using the α-method compared to the β-method, both for the β-method with excess pore water pressure and without. The estimated maximum compressive forces in the piles also vary depending on chosen method of calculation. The highest estimation is found when using the β-method, followed by the β-method with excess pore water pressure and the α-method, see table 5.2.1.

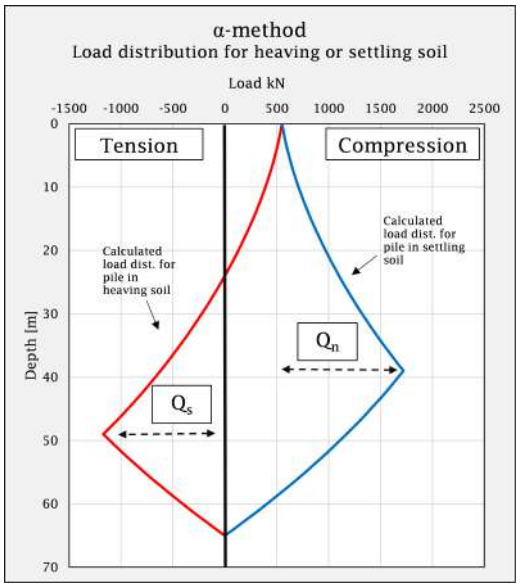

(a) Calculated load distribution with the α-method for both a heaving soil and subsiding soil.

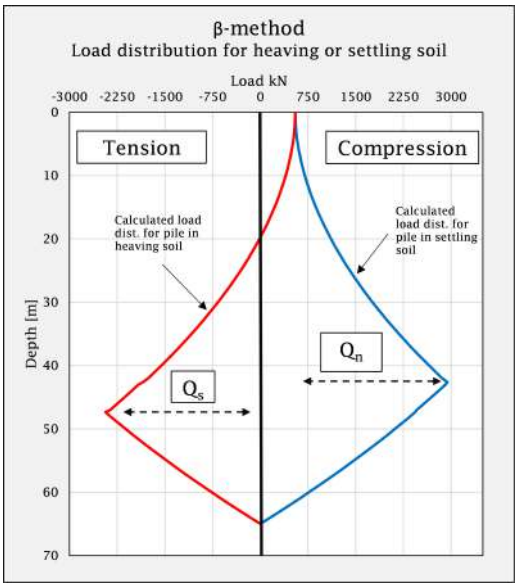

(b) Calculated load distribution with the β-method for both a heaving soil and subsiding soil.

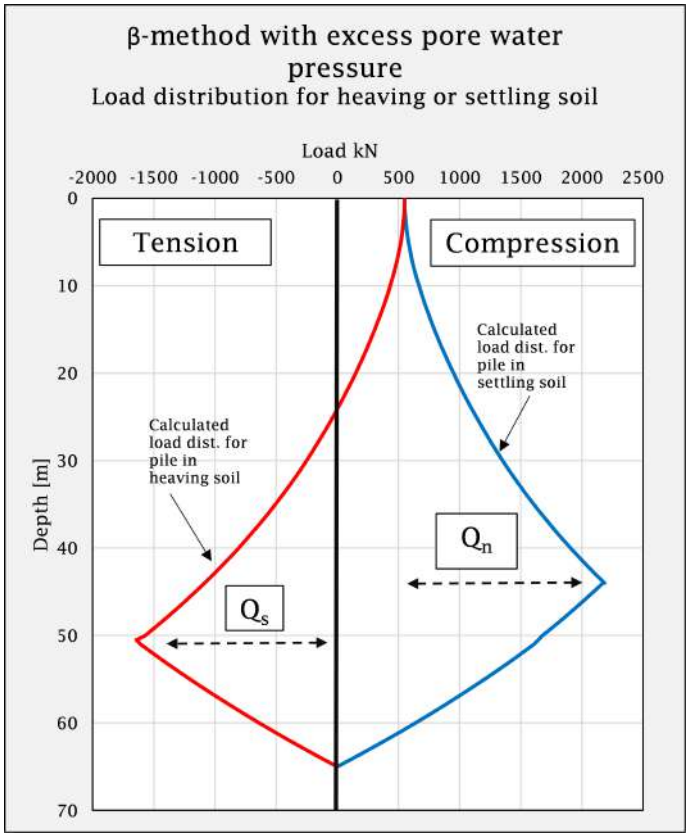

(c) Calculated load distribution with the β-method for both a heaving soil and subsiding soil, with consideration to excess pore water pressure distribution.

Figure 5.2.3: Calculated load distribution of a single vertical pile, considering both the case of heaving and settling soil.

The position of the estimated neutral plane varies slightly depending on what method is used. When comparing the load distribution assuming the whole soil profile settles, it is evident that the α-method predicts the highest location of around 39 meters below the pile head, followed by the β-methods of around 43 meters. It should be noted that the analytical calculations assume a single pile in the middle of the excavation. Comparing the two sides of each graph it can be concluded that a heaving soil profile results in a lowering of the neutral plane.

Table 5.2.1: Geotechnical capacity, load effects and positions of the neutral planes.

	α-method	β-method	β-method with Δu
R_{GEO} (kN)	2900	5400	3900
Q_n (kN)	1200	2400	1600
Q_s (kN)	1200	2400	1600
F_{max} (kN)	1700	2900	2200

6 Numerical analysis of pile behaviour

To study possible explanations of the measured load distribution, a finite element analysis was conducted using PLAXIS2D. The FE model is a simplification of the actual site and aimed capture how a deep excavation in combination with nearby mass displacement piling affects a single pile at the bottom of an excavation similar to the case study. This chapter first presents the methodology for FE modelling, followed by the obtained results.

6.1 Method

The simulations were carried out using a Plane strain model with 15-noded elements. To model the clay layers of the case study site, Soft Soil Creep (SSC) was chosen as the soil model. The Soft Soil Creep model can be used to analyse time-dependant behaviour of soft soils and includes both primary and unloading/reloading compression. To model the topmost fill layer and the drainage layer at the bottom, Mohr-Coloumb (MC) was chosen as the soil model. For a more in-depth description of used material models and so forth see the Materials Model Manual (Bentley, 2022a) and the Reference Manual (Bentley, 2022b). The properties for each soil layer were adopted from Peab AB, 2016 and can be seen in tables 6.1.1 and 6.1.2 below. The interface strength reduction factor, R_{inter}, for all soil layers was set to the default value of 1. The earth pressure coefficient at rest, K_0, was set to *Automatic* for all soil layers.

Table 6.1.1: Soil parameters used in PLAXIS2D.

Material		**Gravel (Fill at exc. bottom)**	**Fill 1**	**Fill 2**	**Clay 1**	**Clay 2**	**Clay 3**	**Clay 4**
Level (m)		-3.5 to -4	+2 to +1	+1 to -1	-1 to -3	-3 to -7.5	-7.5 to -15	-15 to -25
Soil model		MC	MC	SSC	SSC	SSC	SSC	SSC
Drainage type		Drained	Drained	Drained	Undr. A	Undr. A	Undr. A	Undr. A
Saturated unit weight (kN/m^3)	γ_{sat}	18	20	18	16.5	16.5	16	16
Unsaturated unit weight (kN/m^3)	γ_{unsat}	18	18	18	16.5	16.5	16	16
Void ratio	e	Default	Default	1.3	1.9	1.9	1.9	1.8
Stiffness (kPa)	E'_{ref}	120E+03	7.00E+04	N/A	N/A	N/A	N/A	N/A
Poissons ratio	ν	0.3	0.2	0.2	0.2	0.2	0.2	0.2
Modified compr. Index	λ^*	N/A	N/A	0.2	0.165	0.17	0.2	0.29
Modified swell. Index	κ^*	N/A	N/A	8.30E-03	8.30E-03	8.30E-03	9.00E-03	1.10E-02
Modified creep index	μ^*	N/A	N/A	8.30E-03	4.50E-03	4.50E-03	4.60E-03	7.81E-03
Shear strength (kPa)	c'_{ref}	5	2	2	2.85	2.85	2.85	6.3
Friction angle (°)	ϕ	35	34	30	30	30	30	30
Diletancy angle (°)	ψ	0	0	0	0	0	0	0
Permeability (m/d)	$k_h = k_v$	5	0.1206	6.91E-05	6.91E-05	6.91E-05	6.90E-05	6.90E-05
Pre overburden pressure (kPa)	POP	N/A	N/A	15	11	10.5	0	0
Overconsolidation ratio	OCR	N/A	N/A	1	1	1	1.12	1.15

Table 6.1.2: Continuation of soil parameters used for modelling in PLAXIS2D.

Material		**Clay 5**	**Clay 6**	**Clay 7**	**Clay 8**	**Clay 9**	**Clay 10**	**Bottom**
Level (m)		-25 to -35	-35 to -45	-45 to -55	-55 to -65	-65 to -75	-75 to -95	-95 to -97
Soil model		SSC	SSC	SSC	SSC	SSC	SSC	MC
Drainage type		Undr. A	Undr. A	Undr. A	Undr. A	Undr. A	Undr. A	Drained
Saturated unit weight (kN/m^3)	γ_{sat}	16.5	16.5	16.67	17	17.33	18	18
Unsaturated unit weight (kN/m^3)	γ_{unsat}	16.5	16.5	16.67	17	17.33	18	18
Void ratio	e	1.8	1.7	1.59	1.56	1.56	1.43	0.8
Stiffness (kPa)	E'_{ref}	N/A	N/A	N/A	N/A	N/A	N/A	200000
Poissons ratio	ν	0.2	0.2	0.2	0.2	0.2	0.2	0.2
Modified compr. Index	λ^*	0.29	0.31	0.31	0.3	0.3	0.3	N/A
Modified swell. Index	κ^*	0.0115	0.0118	0.0119	0.0115	0.0115	0.0111	N/A
Modified creep index	μ^*	0.0074	0.00676	0.00609	0.00544	0.00482	0.00365	N/A
Shear strength (kPa)	c'_{ref}	8.1	9.6	13.5	15.6	24.5	24	5
Friction angle (°)	ϕ	30	30	30	30	30	30	30
Diletancy angle (°)	ψ	0	0	0	0	0	0	0
Permeability (m/d)	$k_h = k_v$	6.92E-05	3.45E-05	3.46E-05	1.73E-05	1.73E-05	1.73E-05	0.1206
Pre overburden pressure (kPa)	POP	0	0	0	0	0	0	N/A
Overconsolidation ratio	OCR	1.2	1.2	1.2	1.2	1.2	1.2	N/A

The single pile, for which the response was studied in PLAXIS2D, was modelled as an embedded beam. The parameters chosen for the embedded beam can be seen in table 6.1.3 below. The shear resistance of the interface between the embedded beam and the soil in the axial direction was set through defining the axial skin resistance of the pile. This was set to multi-linear, with 0.9:1 relationship between the undrained shear strength of the soil and the axial skin resistance of the pile, i.e., the axial skin resistance was set to 90% of the undrained shear strength of the clay. This relationship can be compared with the description of the α-factor and total stress method in section 2.1.3. The resistance of the interface between the embedded beam and the soil in the lateral direction was set to the default value, i.e., unlimited.

Table 6.1.3: Parameters used to model a case study pile as an embedded beam in PLAXIS2D.

Material type	Unit weight (kN/m^3)	Pile spacing (m)	Cross section type	Width (m)	Stiffness (GPa)	Axial skin resitance
Elastic	25	1.2	Predefined, solid square beam	0.275	35	Multi-linear $0.9 \cdot c_u$

Before the model geometry was created, a validation of the soil properties was performed by simulating an IL Oedometer and CRS using the SoilTest tool in

PLAXIS2D. This was performed for the levels 19.5 meters and 57 meters. In figure 6.1.1 the results from these simulations are plotted together with the Oedometer & CRS results from the lab (Peab AB, 2016).

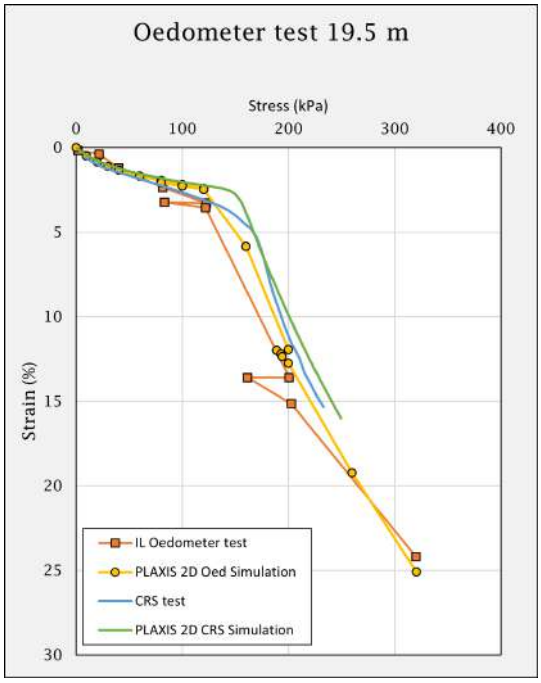

(a) Oedometer & CRS simulation and lab results for level 19.5 meter.

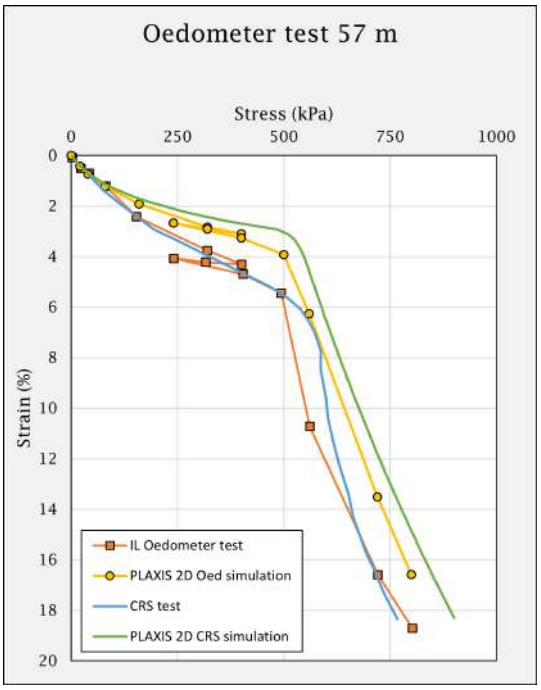

(b) Oedometer & CRS simulation and lab results for level 57 meter.

Figure 6.1.1: Validation of soil properties through a IL oedometer & CRS simulation in PLAXIS2D.

A validation of the modified creep index μ^* was performed by studying the distribution and magnitude of settlements for the soil layers. The area of the case study is known to have approximately 3-4 mm of creep per year (Peab AB, 2016). Therefore, a consolidation phase of 100 years was calculated to see the magnitudes of the creep settlements. As shown in figure 6.1.2 the creep in the model show agreement with empiricism.

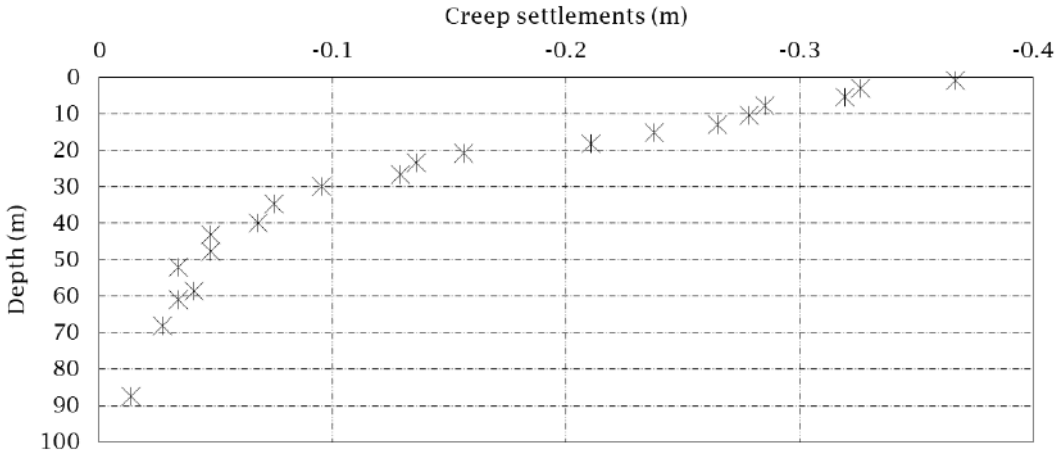

Figure 6.1.2: Magnitude and distribution of creep settlements calculated with PLAXIS2D.

When creating the FE model, the location of the building Platinan was included. A width of the modelled geometry was chosen in order to minimize the risk of adverse boundary effects on the result. The ground water table was set to +0.3 m before construction began and was during construction of the excavation lowered in two stages, 3 metres during each stage. Vertical boundaries were set to be normally fixed in terms of deformations and to be closed for groundwater flow. The lower horizontal boundary was set to be fully fixed and open to groundwater flow. The upper horizontal boundary was set to be free to deform and open to groundwater flow.

Three cases were analysed. The first being a base case, with a single loaded pile, and no excavation or surrounding influences. The weight from the tunnel was modelled as a point load of 550 kN/m, in line with what is presented in section 5.1 in table 5.1.2. The base case was analysed in order to establish the interaction between soil and pile with no effects from unloading or nearby piling considered. The second case is a model of the excavation and a single loaded pile in appropriate calculation phases. This was done in order to study the effect of unloading on forces developing in the single pile. The third case added potential effects from nearby piling (an approximation of project Platinan).

6.1.1 Base case - single vertical loaded pile

Before any effects from unloading of the clay deposit or nearby piling was studied, a base case was established. This model is simply a loaded vertical pile installed in a soil that was allowed to consolidate. This was done in order to see how the load was distributed along the pile, without any external influences. In figure 6.1.3 the geometry used for the base case can be seen. The calculation phases were an initial phase (K_0-procedure) followed by a 1-day Plastic phase wherein the embedded beam is activated. In the next phase the load was activated over a 30-day period. Following this, the calculations included 8 consolidation phases ranging from 1 year

to 120 years. All calculation phases were carried out as staged construction with phreatic pore pressure.

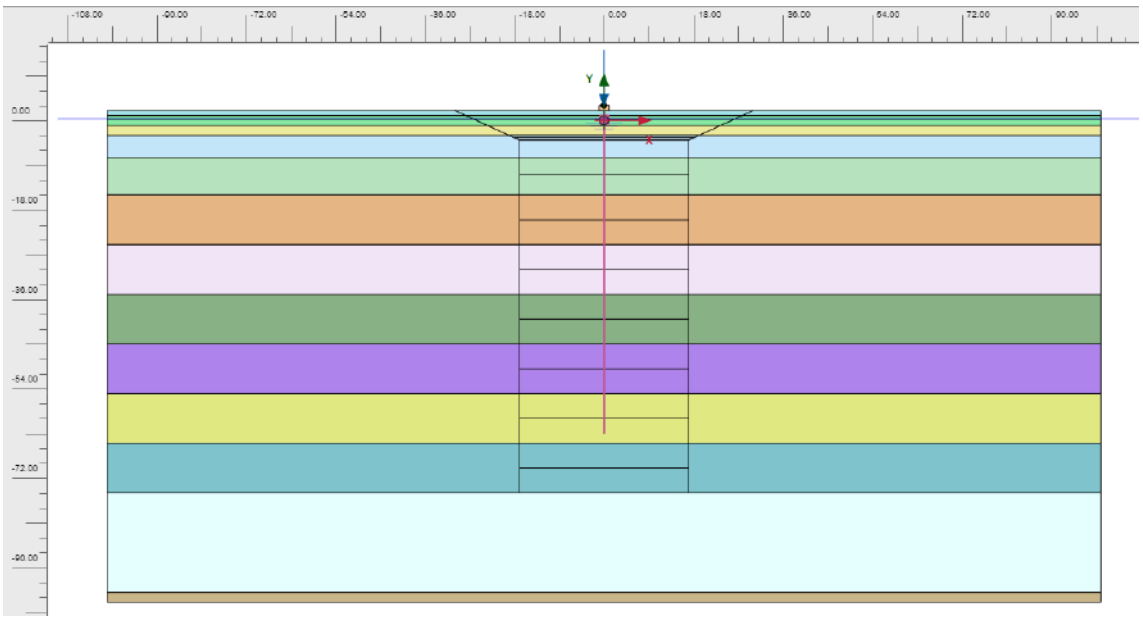

Figure 6.1.3: Geometry used to model effects on load distribution from the base case.

6.1.2 Unloading due to excavation

To isolate the effects on load distribution in a single straight pile from an excavation, a PLAXIS2D model where an excavation of 6 metres was executed in 2 steps, each 3 metres, was analysed. As the excavation was executed, the groundwater table was assumed to be lowered in the same manner as the excavation bottom, starting at around 10 metres from the excavation and ending at the bottom of the excavation. The used geometry can be seen in figure 6.1.4 below.

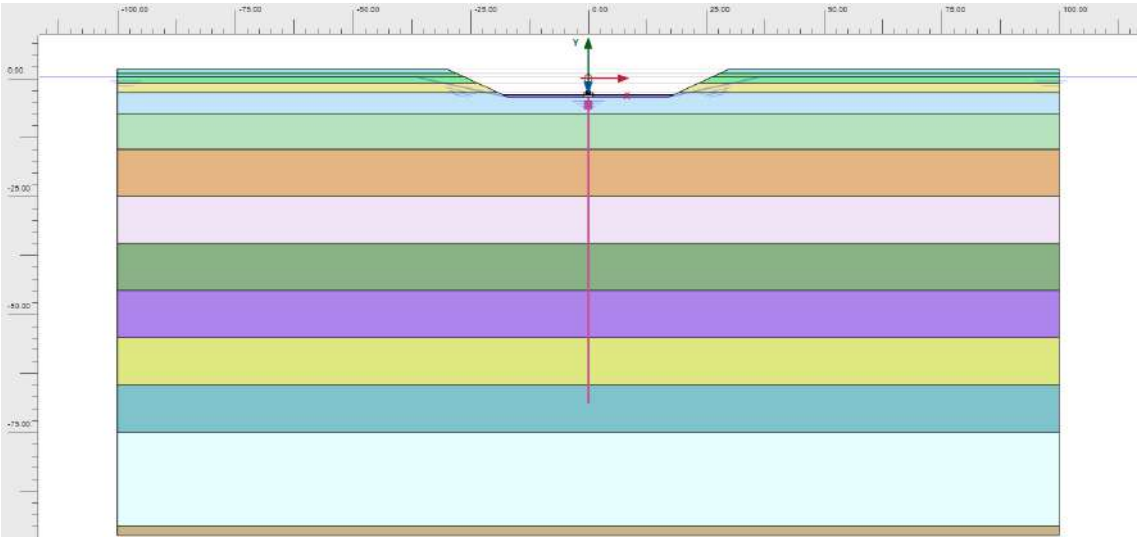

Figure 6.1.4: Geometry used to model effects on load distribution from just an excavation.

To see the effects of mesh fineness, a mesh sensitivity analysis was carried out by looking at how the deformations at a point in the middle of the excavation bottom changed with varied number of elements. Based on this analysis, which can be seen in Appendix C, the mesh generation setting was set to Medium which resulted in 2312 number of elements. The final mesh can be seen in Appendix C in figure C.0.2. Additionally, the chosen construction stages for calculation and their respective time frame can be seen on table 6.1.4 below. All calculation phases were carried out as staged construction with phreatic pore pressure. For other settings the default settings were used.

Table 6.1.4: Chosen staged construction phases in PLAXIS2D.

Stage	Duration	Calculation type	Comments
Initial phase	-	K_0-procedure	
Excavation phase 1	90 days	Consolidation	Excavation from +2 to -1 and lowering of groundwater table
Consolidation	30 days	Consolidation	
Excavation phase 2	90 days	Consolidation	Excavation from -1 to -4 and lowering of groundwater table
Pile driving	1 day	Plastic	Embedded beam is activated
Consolidation	60 days	Consolidation	
Backfill	60 days	Consolidation	Gravel backfill (0.5 m) is added
Loading	60 days	Consolidation	Point load of 550 kN is activated
Consolidation 1 year	365 days	Consolidation	
Consolidation 2 years	365 days	Consolidation	
Consolidation 3 years	365 days	Consolidation	
Consolidation 4 years	365 days	Consolidation	
Consolidation 5 years	365 days	Consolidation	
Consolidation phases, 10, 50 & 120 years	N/A	Consolidation	

6.1.3 Unloading due to excavation plus effects from nearby piling

To model the piling in the Platinan construction project, the soil within the foundation of Platinan was given a volume expansion. The excavation process was kept from the previous model presented in section 6.1.2. The used geometry can be seen in figure 6.1.5 below.

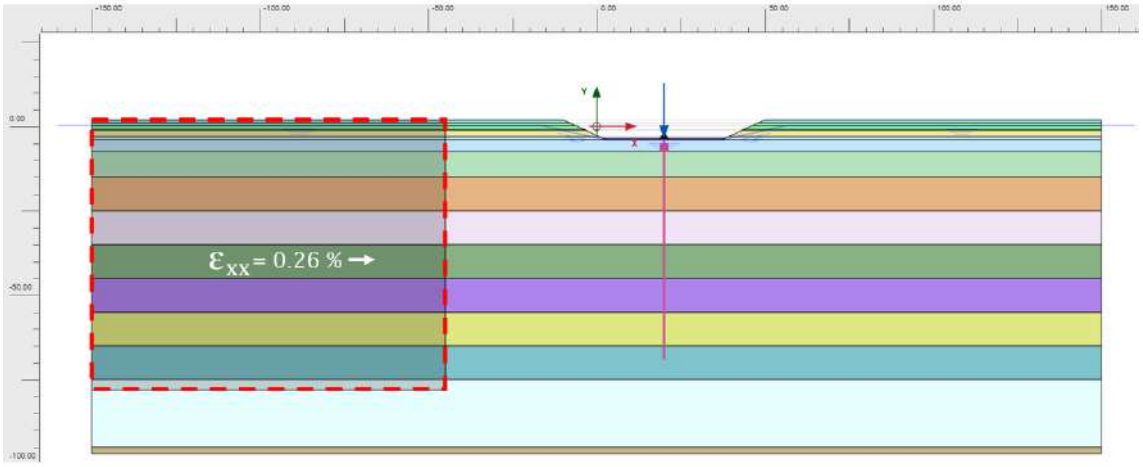

Figure 6.1.5: Geometry used to model effects on load distribution from an excavation and piling of nearby Platinan. Red region indicates the soil area that was allowed to expand in the positive x-direction.

Based on reports filed during the piling as well as plans and drawings for the piling, an assumed volume expansion of a soil block below Platinan was calculated. The volume occupied by the piles divided by the volume of soil was used as a volume expansion factor. Data for piling in Platinan can be seen in table 6.1.5

Table 6.1.5: Properties of pile foundation for Platinan.

(a) Hollow steel piles

Number of	348	
Length	78	m
Diameter	323.9	mm
Thickness	12.5	mm
Degree of plugging	1/3	

(b) Concrete piles

Number of	756	
Length	78.1	m
Diameter	275	mm
Clay core	8	m

For all concrete piles, clay cores were extracted before pile driving. The clay cores were assumed to be 8 metres deep, and for this depth the concrete piles were assumed to not contribute to any volume expansion. This meant that only 70 metres of the 78 metres long concrete piles were assumed to give a volume expansion. For the steel piles, 52 metres of the 78 metres long piles were assumed to give a mass displacement. The piles were assumed to be driven at 60 meters from the excavation. Since a plain strain model was used, the calculated volume expansion factor was divided by 4 to emulate the assumption that the displacement occurs in all four

points of the compass. Furthermore, the displacement and the modelled volume displacement was assumed to only occur in the horizontal direction (ε_{xx}).

To see the effects of mesh fineness, a mesh sensitivity analysis was carried out by looking at how the deformations at a point in the middle of the excavation bottom changes with varied number of elements. Based on this analysis, which can be seen in Appendix D, the mesh generation setting was set to Medium with local refinement which resulted in 4470 number of elements. The final mesh can be seen in Appendix D in figure D.0.2. Additionally, the chosen construction stages for calculation and their respective time frame can be seen on table 6.1.6 below. As can be observed in the table, after the time step that simulated piling in the Platinan project, all volume expansion was deactivated and ε_{xx} set to zero. All calculation phases were carried out as staged construction with phreatic pore pressure.

Table 6.1.6: Chosen staged construction phases in PLAXIS2D.

Stage	Duration	Calculation type	Comments
Initial phase	-	K_0-procedure	
Excavation phase 1	90 days	Consolidation	Excavation from +2 to -1 and lowering of groundwater table
Consolidation	90 days	Consolidation	
Excavation phase 2	90 days	Consolidation	Excavation from -1 to -4 and lowering of groundwater table
Pile driving	1 day	Plastic	Embedded beam is activated
Consolidation	60 days	Consolidation	
Backfill	60 days	Consolidation	Gravel backfill (0.5 m) is added
Loading	60 days	Consolidation	Point load of 550 kN is activated
Platinan piling	280 days	Consolidation	Volume strain of $\varepsilon_{xx} = 0.26\%$ in the area marked in figure 6.1.5 activated
Consolidation 1 year	365 days	Consolidation	Volume strain inactivated
Consolidation 2 years	365 days	Consolidation	Volume strain inactivated
Consolidation 3 years	365 days	Consolidation	Volume strain inactivated
Consolidation 4 years	365 days	Consolidation	Volume strain inactivated
Consolidation 5 years	365 days	Consolidation	Volume strain inactivated
Consolidation phases, 10, 50 & 120 years	N/A	Consolidation	

6.1.4 Sensitivity of PLAXIS2D model

For the numerical models, apart from a mesh-convergence study, a simple sensitivity analysis studying the following inputs was performed

- Axial skin resistance of the embedded beam was varied between $0.7c_u$ and $1.1c_u$
- Volume expansion factor (simulation of nearby piling) was varied between 0.13% to 0.52%
- Dead load was varied between 350 kN and 750 kN

The result sensitivity for the above inputs was estimated by evaluating how much the maximum force in the embedded pile, as well as displacements at excavation bottom, changed when varying the respective inputs.

6.2 Results

This section includes results from numerical analyses performed using PLAXIS2D for a base case, a case simulating only effects from unloading due to excavation and a case simulating the effects of both unloading and nearby soil displacements due to piling

6.2.1 Base case

The load distribution over time for the base case can be seen in figure 6.2.1. As the loaded pile is situated in a subsiding soil, there is a clear trend towards drag loads developing, but it takes a considerable time for large drag loads to develop (more than 10 years).

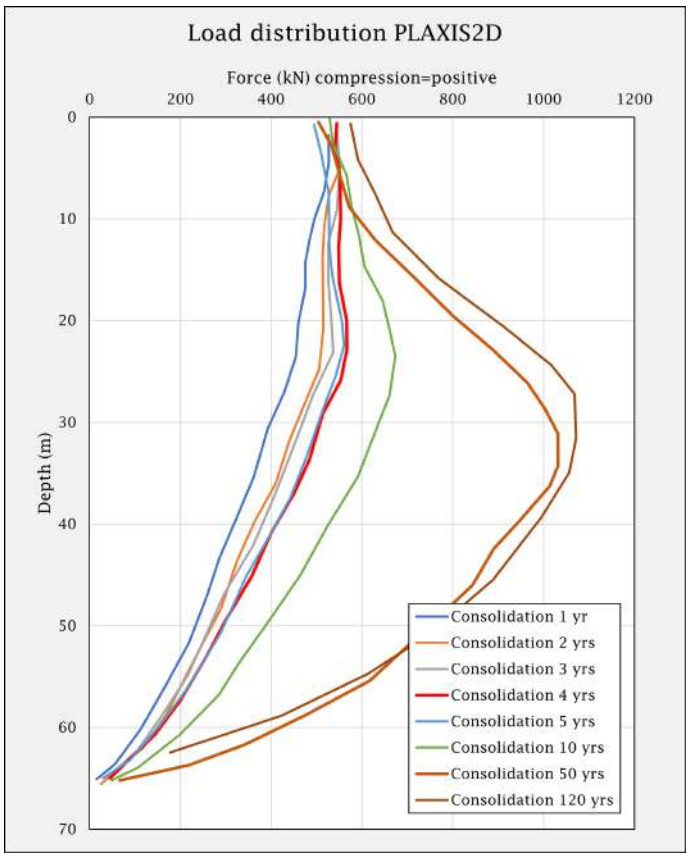

Figure 6.2.1: Load distribution in pile calculated by PLAXIS2D for the base case.

For the base case the neutral plane is situated around 30 meters in the long term, whereas the neutral plane is situated close to the pile head until after 3 years of consolidation. From 4 years of consolidation, the neutral plane has started to move downwards along the pile. During the final calculation steps of the numerical modelling, a neutral plane has formed at around half the pile length.

6.2.2 Unloading due to excavation

The modelled load distribution in a pile installed in a soil that experiences an excavation of 6 meters can be observed in figure 6.2.2. As can be seen in figure 6.2.2a, the excavation alone can generate enough heaving of the soil body to generate tensile loads within the pile. However, the tension forces are effectively neutralised as backfill is added at the excavation bottom. When the pile head load, representing the weight of the tunnel, is activated in the next phase, the entire pile is in compression (figure 6.2.2b). After this step, the neutral plane of the pile seems to form at the pile head. In the long term (50-120 years consolidation), there are significant drag loads developing, which can be studied in more detailed in figure F.0.1 in Appendix F.

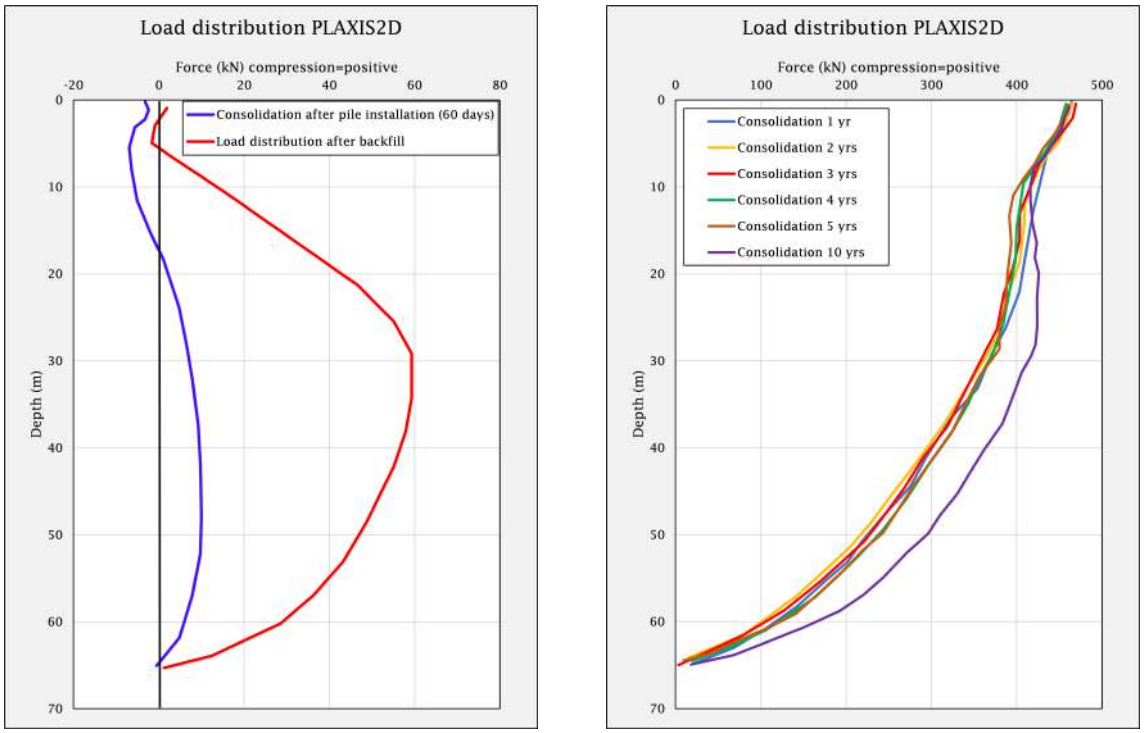

(a) Strain distribution of pile 3-419.

(b) Strain distribution of pile 3-598.

Figure 6.2.2: Load distribution in pile calculated by PLAXIS2D for the excavation only.

Displacements at pile head in the excavation bottom can be seen in figure 6.2.3 below.

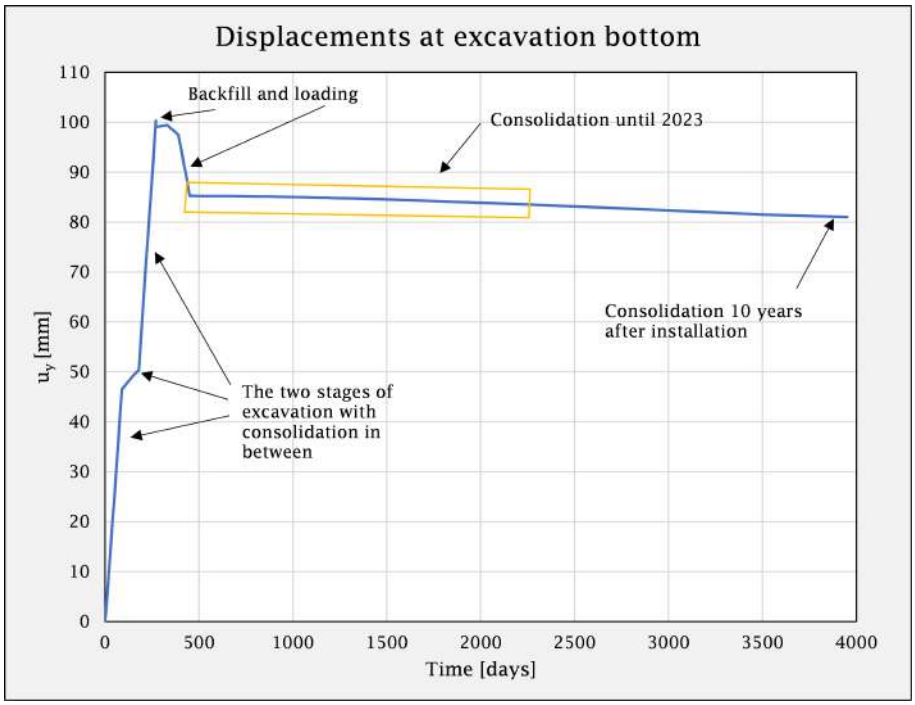

Figure 6.2.3: Displacements at excavation bottom calculated by PLAXIS2D for the excavation.

As can be seen, in figure 6.2.3 there is a heaving effect between the two stages of excavation, but the backfill and loading results in settlements. The consolidation phase shows a slow trend towards settlements over time.

6.2.3 Unloading due to excavation plus effects from nearby piling

The modelled load distribution in a pile installed in a soil that has both been excavated and subject to nearby piling can be observed in figure 6.2.4 below. The result from numerical modelling shows that piling, at a similar distance as Platinan, has the potential to induce tension forces within a pile. When also analysing a consolidation period of 50 and 120 years after pile installation, a significant drag load develops in the pile, see Appendix F and figure F.0.2.

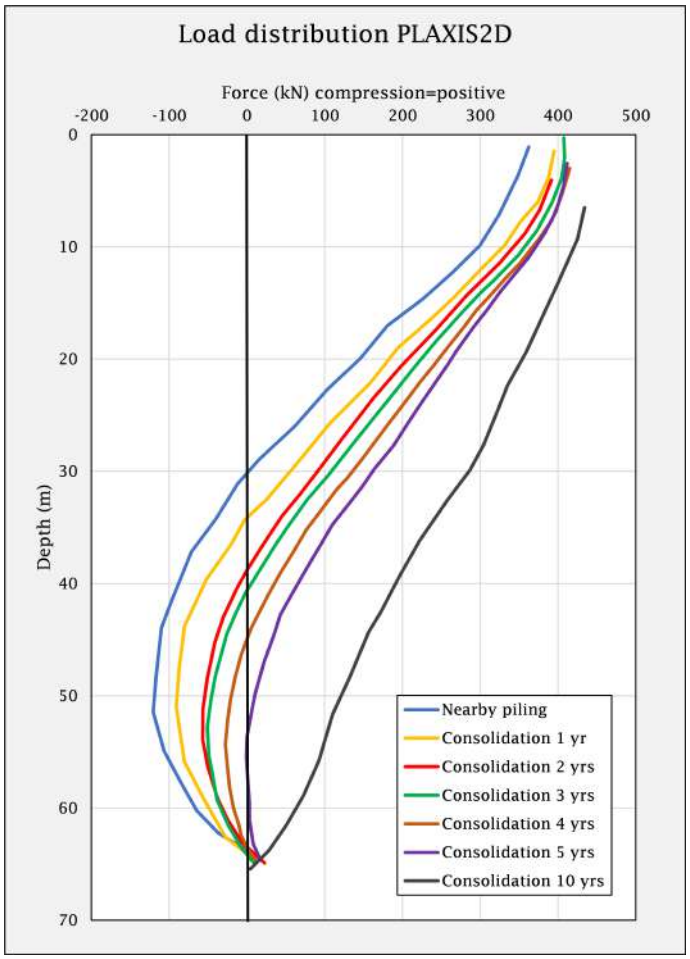

Figure 6.2.4: Load distribution in pile calculated by PLAXIS2D for the excavation in combination with nearby piling.

Displacements at pile head in the excavation bottom can be seen in figure 6.2.5 below. There is heaving between the excavation phases, but considerably more upward movement when piling for Platinan is simulated. After this, the consolidation shows a slow trend towards settlements.

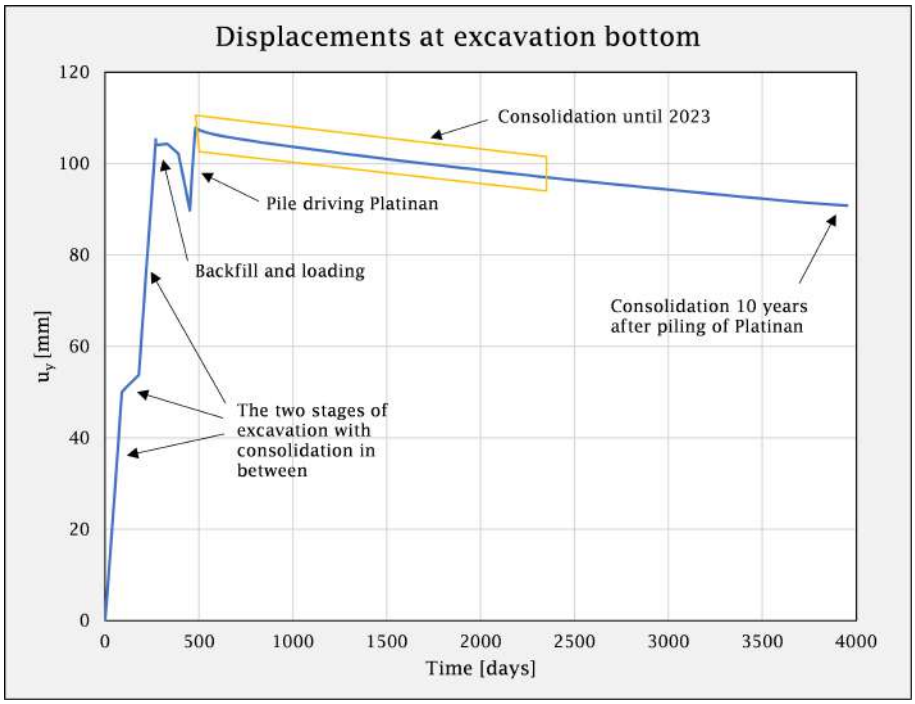

Figure 6.2.5: Displacements at excavation bottom calculated by PLAXIS2D for the excavation in combination with nearby piling.

6.2.4 Sensitivity of PLAXIS2D model

In table 6.2.1 & 6.2.2 the results of the sensitivity analysis for the combined case of nearby piling plus excavation, and excavation only are shown. The varied input was the axial skin resistance (ASR), the volume expansion due to nearby piling and the dead load (Q_d). The percentages represent the relative change in results with regards to the chosen inputs for the original model: $ASR = 0.9 \cdot c_u$, $\varepsilon_{xx} = 0.26\%$ and $Q_d = 550$ kN.

Table 6.2.1: Results from sensitivity analysis in model of effects from excavation and nearby piling in PLAXIS2D. Comparison is with original PLAXIS2D model.

	Maximum tension load during nearby piling	Only compressive forces in pile	Maximum developed compressive force	Maximum movement at pile head
Axial skin resistance $0.7 \cdot c_u$	-3.0%	10 years after installation	-3.7%	-0.3%
Axial skin resistance $1.1 \cdot c_u$	+1.0%	10 years after installation	+1.3%	+0.1%
Volume expansion $\varepsilon_{xx} = 0.13\%$	No tension load induced However, relative unloading	-	-3.7%	-2.3%
Volume expansion $\varepsilon_{xx} = 0.52\%$	+262%	55 years after installation	+8.7%	15%
Dead load 350 kN	+53%	10 years after installation	-12%	+4.4%
Dead load 750 kN	-45%	4 years after installation	+12%	-2.3%

Table 6.2.2: Results from sensitivity analysis in model of effects from excavation in PLAXIS2D. Comparison is with original PLAXIS2D model.

	Maximum developed compressive force	**Final settlement at pile head**
Axial skin resistance $0.7 \cdot c_u$	-2.6%	+1.3%
Axial skin resistance $1.1 \cdot c_u$	+0.8%	-0.5%
Dead load 350 kN	-13%	-14%
Dead load 750 kN	+13%	+15%

7 Discussion

The results show that the case study piles are subject to large changes in experienced internal forces. With time, both case study piles 3-419 and 3-598 show a trend towards compressive forces, see figures 4.2.2 and 4.2.3. The results from case study pile 3-417 are not considered as useful due to that only one level of strain gauges is functioning.

The piles have been experiencing tensile loads during a majority of the study period. Following this, the axial load has changed towards compressive forces. Even though pile 3-419 and pile 3-598 do not show identical load distribution over time, the trends in change of internal forces is similar. It should be emphasized that pile 3-419 and 3-598 are situated in different places, one under the centre wall of the tunnel and one beneath the south wall. Additionally, the data obtained from pile 3-598 contains more outliers and needed more interpolation than that of pile 3-419, so an exact agreement should not be expected.

Comparing the load distributions in figures 4.2.1a and 4.2.1b with figure 5.2.3 it can be said that although the results points toward a settling of the surrounding soil with time, maximum negative skin friction has not yet been mobilized along the case study piles. The analytical analysis presented in figure 5.2.3 represents two extreme cases but can be useful for comparison of the shape of the load distribution to the empirical results, rather than comparing the actual magnitude of forces. To reiterate, the analytical results are based on a single vertical pile, whereas the instrumented piles are located in groups and have an inclination, so a direct comparison is not entirely valid. The single vertical pile in the analytical and numerical examples are not members of any pile rows or groups, whereas the instrumented piles are, and are therefore subject to group effects.

7.1 Tension loads in case study piles

The results from the data evaluation raises questions about the apparent tension loads in the piles. The trend to recognize in figures 4.2.1a and 4.2.1b is a shifting from tension forces towards relative compression. Although the instrumented piles represent a very small sample of the somewhat 4 500 piles in the foundation, the result can be tested against several hypotheses to identify more or less likely reasons for the load distribution in the piles. Comparing the empirical results for pile 3-419 in figure 7.1.1a to the analytical and numerical results in figures 7.1.1b and 7.1.1c

the resemblance is striking. The magnitude of the maximum tension force in the analytical and numerical results do not conform with the measured forces. This is however expected since the measured load distribution is very sensitive to chosen Young's modulus, and chosen frequency benchmark, see Appendix B. Therefore, the magnitude of the calculated forces can be deemed uncertain. What is more interesting is the shape of the load distribution, which shows conformity between the analytically calculated results, the numerical simulation and the measured results, see figure 7.1.1.

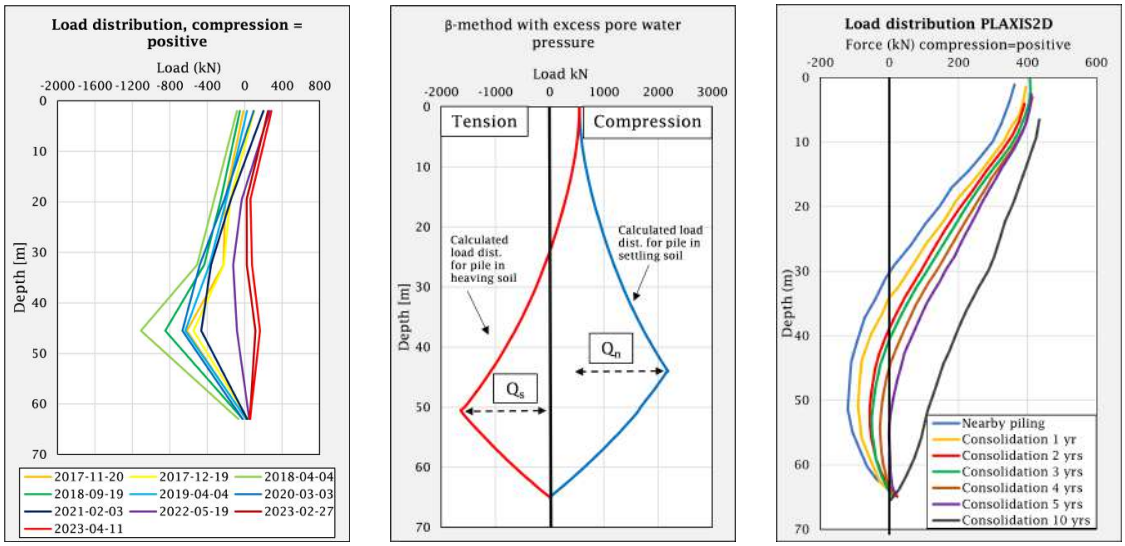

(a) Calculated forces in the instrumented pile 3-419, for various dates.

(b) Analytical calculation of load distribution in a single vertical pile.

(c) Load distribution estimated with PLAXIS2D for a single vertical pile.

Figure 7.1.1: Comparison of results.

7.1.1 Unloading effects due to excavation

Before pile driving for the foundation of the tunnel, 6 meters of soil was excavated, which resulted in a significant unloading of the deep clay deposit. The unloading induced a stress relaxation and heave of the excavation bottom. Heaving of soil below the excavation bottom could induce positive skin friction along parts of the pile shaft, and could subsequently be an explanation as to why the case study piles are subject to tension. In addition, it can be argued that the topmost strain gauges do not show a load as high as the applied dead load due to a possible heaving pressure on the cast concrete ground beam relieving some of the load of the tunnel.

As explained by Tornborg, 2017 the issue of induced tension forces due to heaving of excavation bottoms might be particularly problematic when the excavation is performed after the piles are installed. This is partly the case for the instrumented piles at E45, since they are installed in an excavation of around 5 meters, whereafter the last metre is excavated.

It could be argued that heave due to unloading would yield a measurable displacement of the tunnel. However, very little relative displacement of pile and soil is needed to develop maximum friction. The relative displacements can therefore be very small, but still sufficient to induce the positive skin friction needed for tension forces to emerge.

The numerical model shows contradicting results to the results from the data analysis. Tension forces are induced due to unloading only, although very small and they are situated close to the pile head (in contrast, the data analysis show large tension loads in the lower part of the pile). The numerical model shows that the heaving phase due to unloading is abruptly cancelled by adding half a metre of backfill at the excavation bottom. Therefore, the model indicates that the tensile loads apparent in the strain data analysis is not due to unloading alone.

7.1.2 Soil heave due to nearby pile driving

The instrumented case study piles were driven several months after nearby piles within that monolith (see figure 3.2.3). Thus, the tensile forces that the results show cannot be due to adjacent piling. However, piling was still conducted within the case study project, for example in nearby monoliths 2 and 4, but also in monoliths further from the case study piles. As long pile lengths cause soil heave in a larger circumferential area than a short pile, this effect could be an explanation to the tension forces within the piles. At the time of the last measurement, the data displays that the case study piles have transitioned towards experiencing compressive forces. This can be an indication that the heave due to nearby piling is transitioning into settlements. However, the time between heaving and subsiding of soils due to driving of displacement piles is still open for debate.

Following the discussion on piling of other monoliths, multiple other large construction projects have taken place within the nearby area, see figures 3.4.1 and 3.1.2. Many of these larger construction projects, similarly to the one studied in this thesis, are founded on long driven piles, both displacement concrete piles and hollow steel piles. What indicates that the tension is an effect from nearby piling is that the load change curves for both pile 3-419 and 3-598 show a large increase in tensile forces during late 2017/beginning of 2018, at the same time pile driving at Platinan and other monoliths took place (figure 3.4.1).

The results from the numerical model show that tension forces present in the piles can be induced from nearby piling. The shape of the load distribution presented in figure 7.1.1 show conformity between the PLAXIS2D model and the calculated loads. The similarity in load distribution between the numerical model and the data analysis suggests that it is likely that the measured tension forces are in fact an effect from nearby piling.

The changes in loads over time can be explained by different events. As seen in figure 7.1.2 the spike towards tension during 2018 coincides well with the comple-

tion of the pile driving for both nearby Platinan and other monoliths in the case study, giving support to the argument that the tension formed is an effect from driving of displacement piles. The dismantling of the formwork for monolith 3 during 2020 also coincides well with a trend towards compression in the pile. This suggests that the loads previously carried by the scaffolding is being transferred to the pile head.

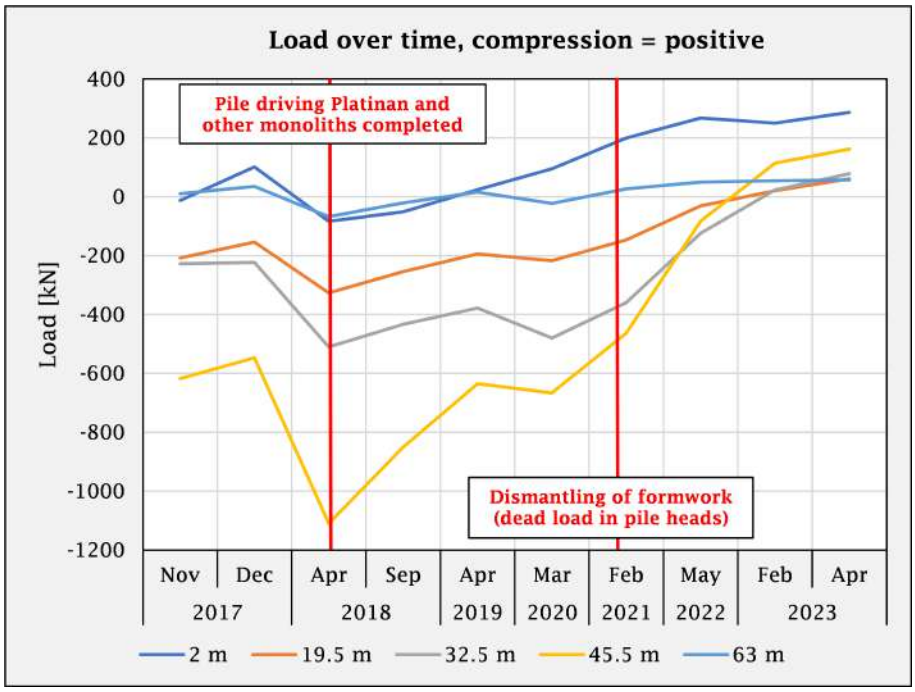

Figure 7.1.2: Load over time for pile 3-419 with time stamps for completion of nearby pile driving and dismantling of formwork.

7.2 Sensitivity analyses

In this section the results from the sensitivity analyses are discussed. First the sensitivity regarding the data analyses, e.g., benchmarks, temperature and Young's modulus is discussed, followed by a discussion on the uncertainty of output from the PLAXIS2D models.

7.2.1 Data analysis

By changing the benchmark reading used to evaluate internal forces in the instrumented piles, it could be observed that the result is sensitive regarding the chosen benchmark. From Appendix B it is evident that chosen benchmark does not only affect the magnitude of forces, but also the direction of resultant internal pile loads. Following this, studying the load change between different data points removes the influence of chosen benchmark. Ultimately, the benchmark from before casting of the piles was chosen as the most representative to use for estimating the load distribution within the pile. By choosing this benchmark, the whole evolution of pile

forces can be studied.

The output is more sensitive towards a change in modulus rather than temperature. For a given relative change in temperature or Young's modulus, the latter affects the magnitude of estimated forces more substantially. As can be seen from the results in figure 4.2.5a the variance in results increase with the magnitude of the force. The magnitude of the maximum force can vary up to $\Delta \approx 450$ kN. This suggest that determination of an accurate Young's modulus is of most importance if reliable magnitudes of loads should be determined. However, there is also uncertainty regarding how the modulus of cohesion piles evolves over time. For instance, creep can reduce the modulus of concrete (Gambali and Shanagam, 2014) and by extension, the pile. At small strains in a concrete cohesion pile the modulus has been shown to have a non-linear behaviour (Yannie and Alén, 2015), meaning the modulus changes depending on the stresses in the pile. High tensile forces can also reduce the pile modulus (Yannie and Alén, 2015). As concrete does not have a high tensile strength, the case study piles could have cracks, which in turn would decrease the Young's modulus.

7.2.2 Numerical modelling

The results presented in tables 6.2.1 and 6.2.2 show that varying axial skin resistance does not affect the maximum tension loads significantly. The magnitude of dead load however does have a somewhat linear proportionality to the magnitude of the developed tension forces in the pile. The volume expansion used to simulate nearby piling has a very significant impact on the maximum tension loads in the pile. In the sensitivity analysis, a doubling of the volume expansion yields more than triple the size of tension loads. Since there are many uncertainties involved when estimating an accurate volume expansion, the results show that nearby piling can very much induce large tension forces in piles. Furthermore, the constructed models do not include mass displacement from the piling within the case study itself, which would likely yield additional tensile loads.

7.3 Potential errors

Potential errors in the results relate to assumptions made, representation and uncertainties in methods used. There are obvious questions about how representative the instrumented piles are for the foundation, as they represent a very small selection of the total number of piles. Related to this, there is an uncertainty associated with the distribution of dead load i.e., if the tunnel is sufficiently stiff to cause an evenly distributed load. The excess pore pressure used in the hand calculations were based of measurements taken at some distance from the excavation area. These measurements do not necessarily reflect the pore pressure distribution under the excavation, which could influence estimated load distributions. The method of data processing through interpolation also results in a risk of bias to the results.

Perhaps the largest potential error lies in assumed mechanical properties of the

instrumented piles. The results presented are assuming that the whole cross section of the pile contributes in tension. However, when subject to tensile forces, concrete is known to yield and cracks can form, making the reinforcement carry most of the applied load. Assuming the entire pile cross section contributes to load carrying when the pile is in tension results in calculated loads of a higher magnitude compared to if the reinforcement was assumed to act as the sole load carrier. However only assuming that it is the reinforcement that carries load, regardless of direction, is not correct either as the concrete is the main load carrier in compression. It can be argued that for segments and readings where the pile is in tension it would be more appropriate to evaluate forces within the reinforcement only, i.e., base the calculation on the cross-sectional area, Young's modulus and strain for the reinforcement only. This results in a significant decrease in magnitude of forces, as shown in figure4.2.6 from the sensitivity analysis for the data evaluation.

8 Conclusion

The data analysis of the strain measurements indicates that the instrumented case study piles in the lowering of the E45 in Gothenburg have experienced axial tension forces for some period after they were driven. The results from FE modelling indicate that these axial tension forces are an effect from nearby displacement piling. In addition, relative increase in tension loads coincide fairly well with piling for nearby projects such as Platinan and pile driving for other monoliths. Although unloading is known to cause heave and positive skin friction, numerical analysis indicates that unloading would yield a load distribution unlike what the data analysis shows. The shape of the measured load distribution instead shows agreement with hand calculations and the numerical model including influence from nearby piling. This suggests that these piling works are a probable explanation of the tension in the piles. In summary this report concludes that:

- The instrumented piles have transitioned from experiencing axial tension to axial compression, indicating emergence of drag loads due to settlements.
- The pile's Young's modulus heavily influences the magnitude of the calculated load in the pile.
- The chosen benchmark frequency heavily influences the magnitude and direction of the calculated load in the pile.
- The installation of a large number of displacement piles has the potential to generate tension in neighboring deep foundations.

8.1 Future studies

Since buildings are planned on top of the tunnel, the most important recommendation is to continue to gather data from the instrumented piles in the future. This is important for continuous insight into the development of forces within the piles.

Regarding other further studies, a most relevant recommendation is to properly investigate the Young's modulus for prefabricated piles as this greatly affect the magnitude of loads calculated with Sister Bar strain gauges. Tests investigating the non-linearity between stress-strain in concrete piles would be beneficial for determining varying tangent-moduli relating to the strain in the pile. This could be used to calculate loads more accurately in the pile. In addition, it is known that the Young's modulus for concrete piles tend to decrease with time, but further studies on the rate at which this occurs, and what the lower bound is, would be beneficial.

Another suggestion for further studies is to investigate how heaving or subsiding soils affect inclined piles, as the positive or negative skin friction is not parallel to the piles driven direction. Related to this, more research on the time factor in heaving would be of interest, i.e., at what rate heave due to unloading occurs for given geotechnical properties.

Bibliography

Alén, C. (2012). *Pile foundations - short handbook* (tech. rep. No. 1.1). Architecture and Civil Engineering. Sven Hultins gata 8.

Altahrany, A., & Elshehawy, E. (2022). Negative skin friction development on single pile and pile group embedded in soft clay. *MEJ. Mansoura Engineering Journal*, *47*, 1–9. https://doi.org/10.21608/bfemu.2022.254981

Bentley. (2022a). *Material Models Manual* (User manual). Bentley. https://communities.bentley.com/cfs-file/__key/communityserver-wikis-components-files/00-00-00-05-58/5315.2D_2D00_3_2D00_Material_2D00_Models.pdf

Bentley. (2022b). *PLAXIS 2D - Reference Manual* (User manual). Bentley. https://communities.bentley.com/cfs-file/__key/communityserver-wikis-components-files/00-00-00-05-58/1212.2D_2D00_2_2D00_Reference.pdf

Brown, M. J., & Hyde, A. F. L. (2008). Rate effects from pile shaft resistance measurements. *CANADIAN GEOTECHNICAL JOURNAL*, *45*(3), 425–431. https://doi.org/10.1139/T07-115

Chen, Q., Haque, N., Abu-Farsakh, M., & Fernandez, B. A. (2014). Field investigation of pile setup in mixed soil. *Geotechnical Testing Journal*, *37*(2). https://doi.org/10.1520/GTJ20120222

CNES. (2023). Aerodata international surveys [Retrieved from Google Maps].

Dugan, J. P. J., & Freed, D. L. (1984). Ground heave due to pile driving. *28*. https://scholarsmine.mst.edu/icchge/1icchge/1icchge-theme1/28

Edstam, T. (2011). *Massundanträngning i samband med pålslagning i lera* (tech. rep.). SBUF.

Fellenius, B. (2023). *Basics of foundation design*. www.fellenius.net.

Fellenius, B. H. (1971). *Negative skin friction on long piles driven in clay* (tech. rep. SGI Proceedings, 25). Statens geotekniska institut.

Fellenius, B. H. Negative skin friction and settlement of piles. In: 1984.

Fellenius, B. H. (1997). Discussion on "piles subjected to negative friction: A procedure for design" authored by h. g. poulos published in geotechnical engineering, vol. 28, no. 1, pp. 23 - 44. *Geotechnical Engineering*, *28*(2), 277–281.

Fellenius, B. H. (1999). Discussion on bitumen selection for reduction of downdrag on piles (j-l. briaud, 1997 asce journal of geotechnical engineering, vol. 123, no. 12, pp. 1127-1132). *Geotechnical Engineering*, *125*(4), 341–344.

Fellenius, B. H. Piled foundation design - clarification of a confusion. In: 2006.

Fellenius, B. H. (2006b). Results from long-term measurement in piles of drag load and downdrag. *Canadian Geotechnical Journal*, *43*(4), 409–430. https://doi.org/10.1139/t06-009

Flemming, K., Weltman, A., Randolph, M., & Elson, K. (2008). *Piling engineering* (3rd ed.). Taylor; Francis.

Gambali, A. K., & Shanagam, N. K. (2014). Creep of concrete. *International Journal of Engineering Development and Research*, *2*(4), 3800–3802. https://www.ijedr.org/papers/IJEDR1404068.pdf

Geokon. (2011). *Rebar strainmeters (sister bars)* (E.1). Geokon, Incorporated. 48 Spencer Street, Lebanon, NH, 03766.

Geokon. (2013). *Installation manual - models 4911a/4911 vw rebar strain meters* (O). Geokon, Incorporated. 48 Spencer Street, Lebanon, NH, 03766.

Geokon. (2020). *Model gk-404 vibrating wire readout* (O). Geokon, Incorporated. 48 Spencer Street, Lebanon, NH, 03766.

Haque, M. N., Abu-Farsakh, M. Y., Tsai, C., & Zhang, Z. (2017). Load-testing program to evaluate pile-setup behavior for individual soil layers and correlation of setup with soil properties [Cited by: 19]. *Journal of Geotechnical and Geoenvironmental Engineering*, *143*(4). https://doi.org/10.1061/(ASCE)GT.1943-5606.0001617

Huang, T., Zheng, J., & Gong, W. (2015). The group effect on negative skin friction on piles [8th International Conference on Asian and Pacific Coasts (APAC 2015)]. *Procedia Engineering*, *116*, 802–808. https://doi.org/https://doi.org/10.1016/j.proeng.2015.08.367

Kania, J., & Sorensen, K. (2018). A Static Pile Load Test on a Bored Pile Instrumented with Distributed Fibre Optic Sensors.

Kania, J., Sorensen, K., & Fellenius, B. (2020). Application of Distributed Fibre Optic Sensing in Piles. *Geotechnical Engineering Journal of the SEAGS & AGSSEA*, *51*(1).

Klohn, E. J. (1963). Pile heave and redriving. *Transactions of the American Society of Civil Engineers*, *128*(1), 557–577. https://doi.org/10.1061/TACEAT.0008694

Knappett, J., & Craig, R. F. (2012). *Craig's soil mechanics* (8th ed.). Spon Press.

Konkol, J., & Balachowski, L. (2017). Influence of installation effects on pile bearing capacity in cohesive soils - large deformation analysis via finite element method. *Studia Geotechnica et Mechanica*, *39*, 27–38. https://doi.org/10.1515/sgem-2017-0003

Lam, C., & Jefferis, S. (2011). Critical assessment of pile modulus determination methods. *Canadian Geotechnical Journal*, *48*, 1433–1448. https://doi.org/10.1139/t11-050

Larsson, R. (2008). *Jords egenskaper* (tech. rep.). SWEDISH GEOTECHNICAL INSTITUTE.

O'Reilly, M., & Al-Tabbaa, A. (1990). Heave induced pile tension: A simple one dimensional analysis. *Ground Engineering*, 28–33. https://cdn.ca.emap.com/wp-content/uploads/sites/13/1990/06/Ground-Engineering-June-1990-Heave-induced-pile-tension-a-simple-one-dimensional-analysis.pdf

Pålkommissionen. (2004). *Kohesionspålar* (tech. rep. No. 100).

Pålkommissionen. (2022). *Pålstatistik för Sverige 2021* (tech. rep. 2022:1).

Peab AB. (2016). *E45 Lilla Bommen-Marieholm Tunnel, nedsänkning, Falutorget samt Gullbergsmotet - B01 Beräkningsförutsättningar Geoteknik* (tech. rep.). Peab Anläggning AB.

Peab AB. (2020). *Teknisk Rapport provbelastning* (tech. rep. No. 4001).

Peab AB. (2023). *E45 Lilla Bommen – Marieholm*. Retrieved January 30, 2023, from https://peab.se/projekt/e45-lilla-bommen--marieholm/

Peleveiledningen. (1987). *Norwegian pile guideline (in Norwegian)* (tech. rep.). Norges byggstandardiseringsråd.

Sagaseta, C., Whittle, A. J., & Santagata, M. (1997). Deformation analysis of shallow penetration in clay. *International Journal for Numerical and Analytical Methods in Geomechanics*, *21*(10), 687–719. https://doi.org/https://doi.org/10.1002/(SICI)1096-9853(199710)21:10<687::AID-NAG897>3.0.CO;2-3

Sinnreich, J. (2020). Optimizing the Arrangement of Strain Gauges in Pile Load Testing. *Geotechnical Testing Journal*, *44*. https://doi.org/10.1520/GTJ20200033

Terzaghi, K. (1943). *Theoretical soil mechanics*. John Wiley & Sons, Ltd. https://doi.org/https://doi.org/10.1002/9780470172766.fmatter

Tornborg, J. (2017). *Svälltryck på grund av avlastning i lös lera* (tech. rep. No. 13303). SBUF.

Trafikkontoret. (2021). *Erfarenhetsrapport projektsamarbete och teknik vid arbeten i anslutning till götaälvbron* (tech. rep.). Göteborgs Stad.

Trafikverket. (2016). *Förfrågningsunderlag E45 Sänkning, inkl. ändrings PM03* (tech. rep. No. 6.8.1). Trafikverket.

Wersäll, C., & Massarsch, K. R. (2013). Soil heave due to pile driving in clay, 480–498. https://doi.org/10.1061/9780784412770.032

Wood, T., & Karstunen, M. (2022). Modelling the creep of deep foundations in soft gothenburg clays. *European Journal of Environmental and Civil Engineering*, *26*(7), 2581–2599. https://doi.org/10.1080/19648189.2017.1344146

Wrana, B. (2015). Pile load capacity – calculation methods. *Studia Geotechnica et Mechanica*, *37*. https://doi.org/10.1515/sgem-2015-0048

Yannie, J., & Alén, C. (2015). *Field test of tension piles - on long term behavior* (tech. rep.). Chalmers University of Technology.

A Appendix 1

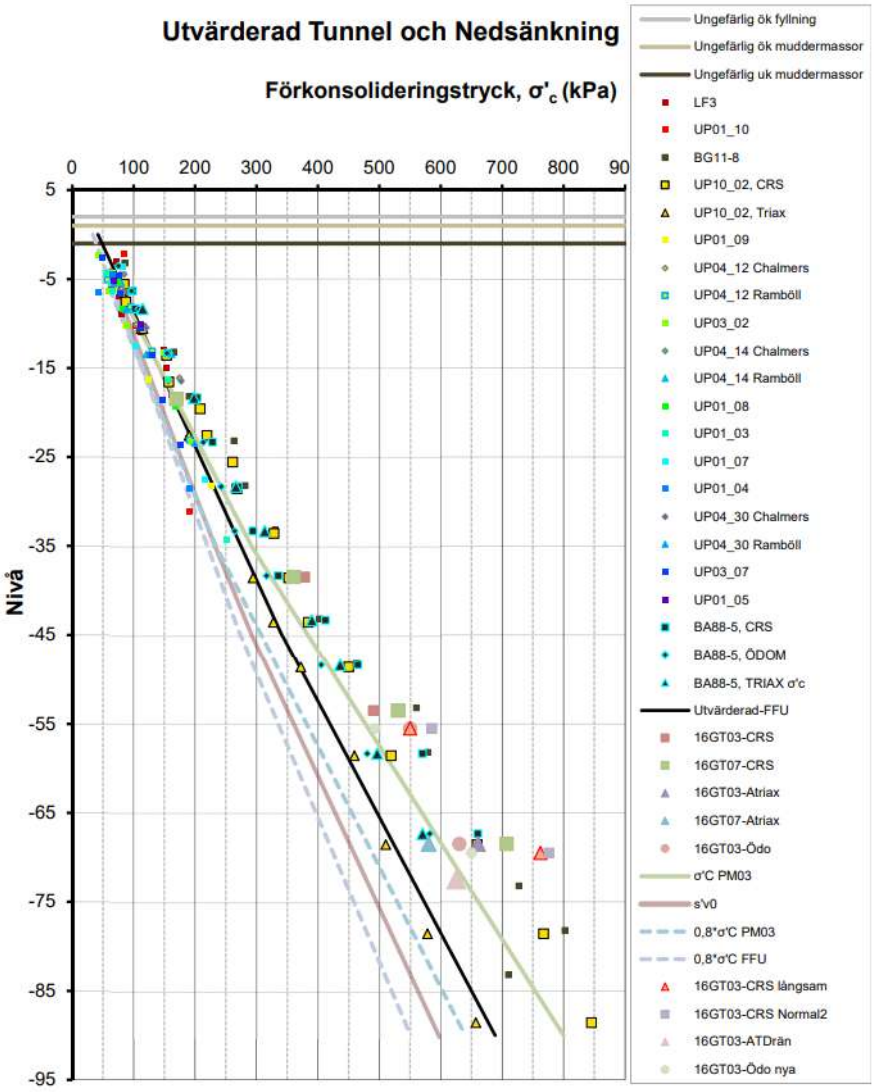

Figure A.0.1: Preconsolidation pressure and chosen profile, obtained from Peab AB, 2016.

B Appendix 2

B.1 Benchmark from installation

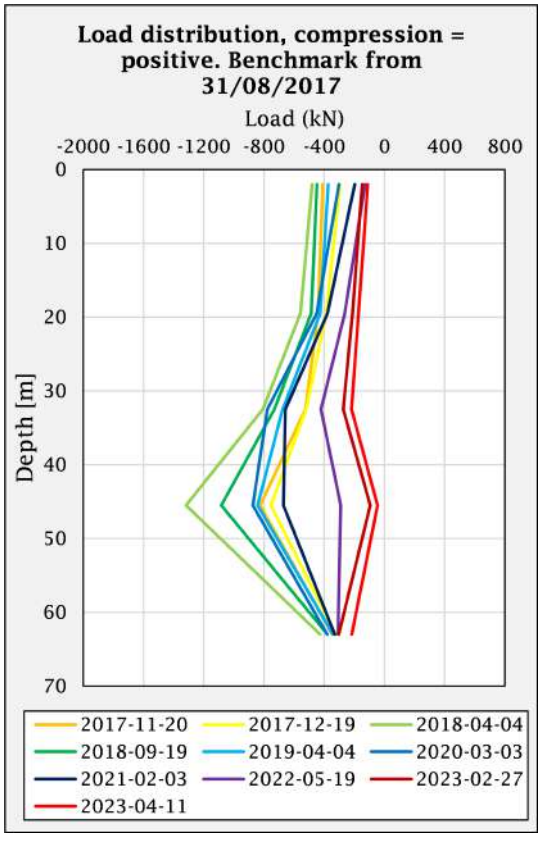

(a) Load distribution of pile 3-419, located in the center wall.

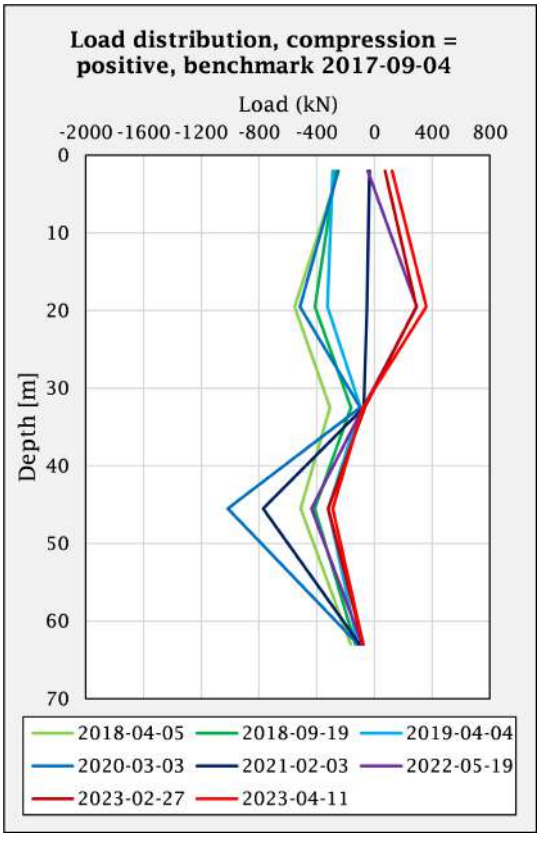

(b) Load distribution of pile 3-598, located in the south wall.

Figure B.1.1: Estimated load distribution of instrumented piles. Benchmark frequency from installation of the pile.

B.2 Benchmark from storage

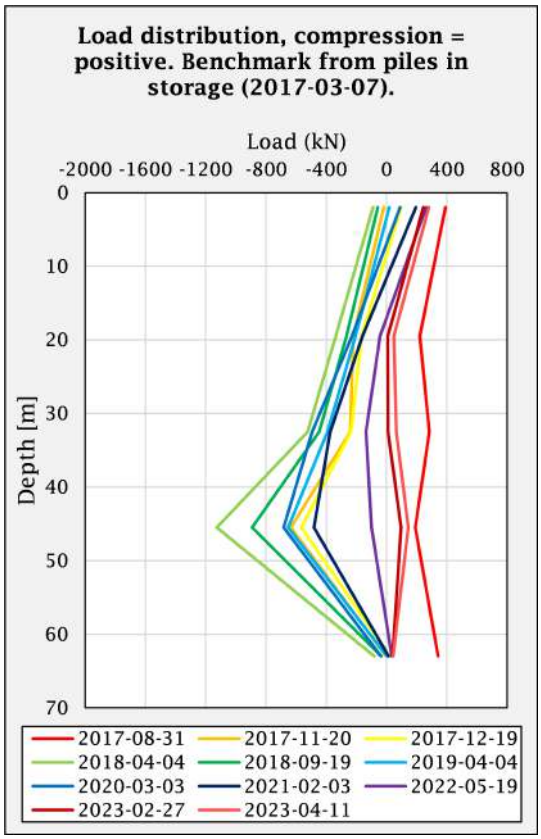

(a) Load distribution of pile 3-419, located in the center wall.

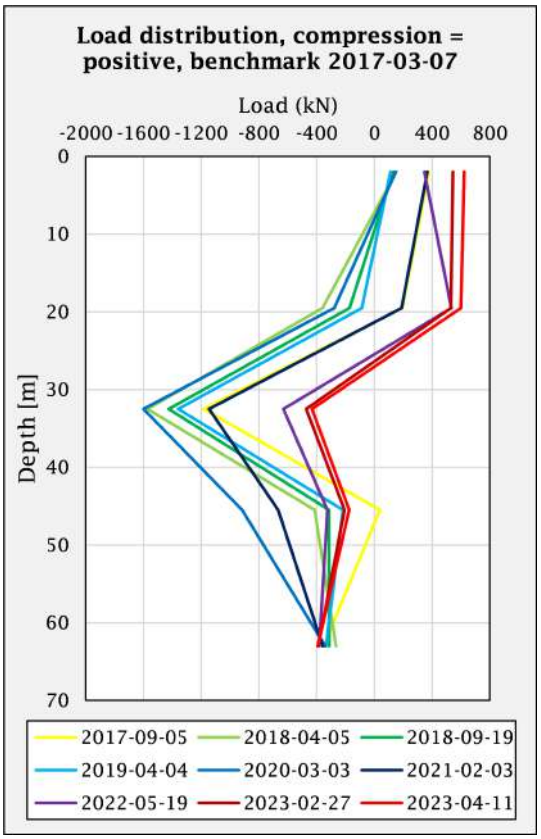

(b) Load distribution of pile 3-598, located in the south wall.

Figure B.2.1: Estimated load distribution of instrumented piles. Benchmark frequency from storage.

B.3 Benchmark from a few days after pile driving

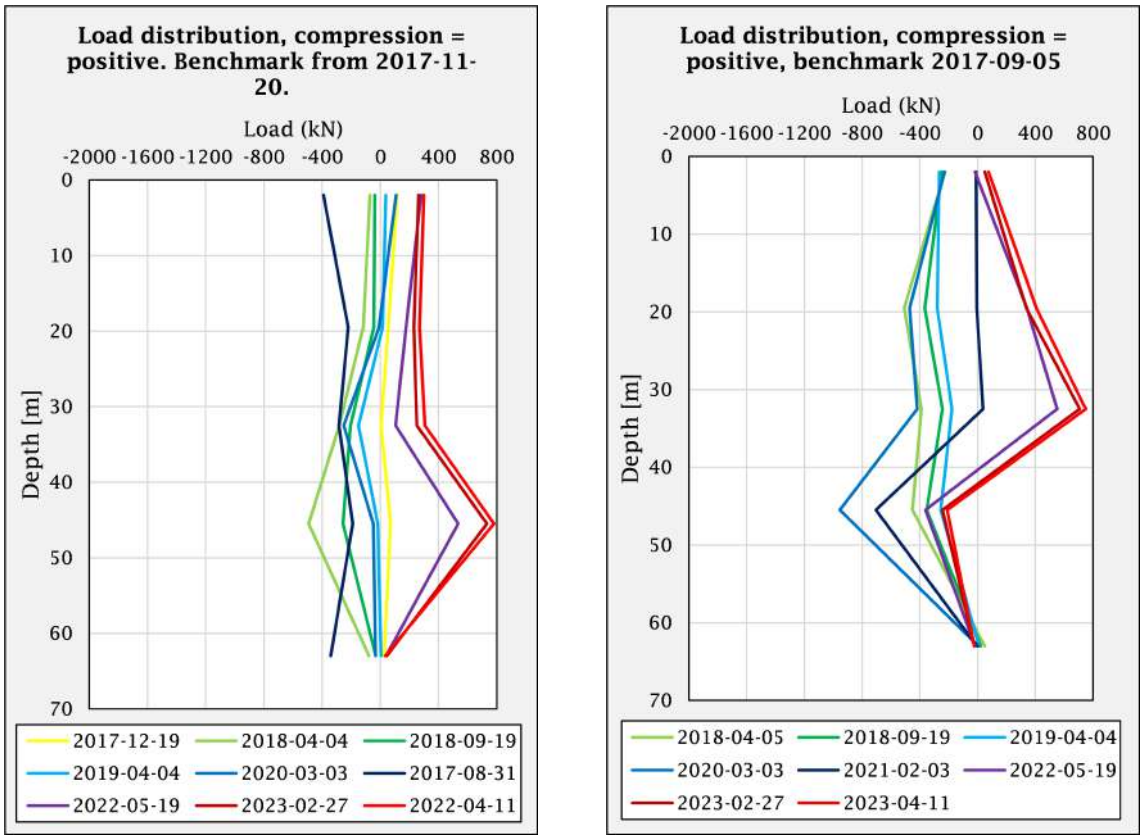

(a) Load distribution of pile 3-419, located in the center wall.

(b) Load distribution of pile 3-598, located in the south wall.

Figure B.3.1: Estimated load distribution of instrumented piles. Benchmark frequency from after pile driving.

C Appendix 3

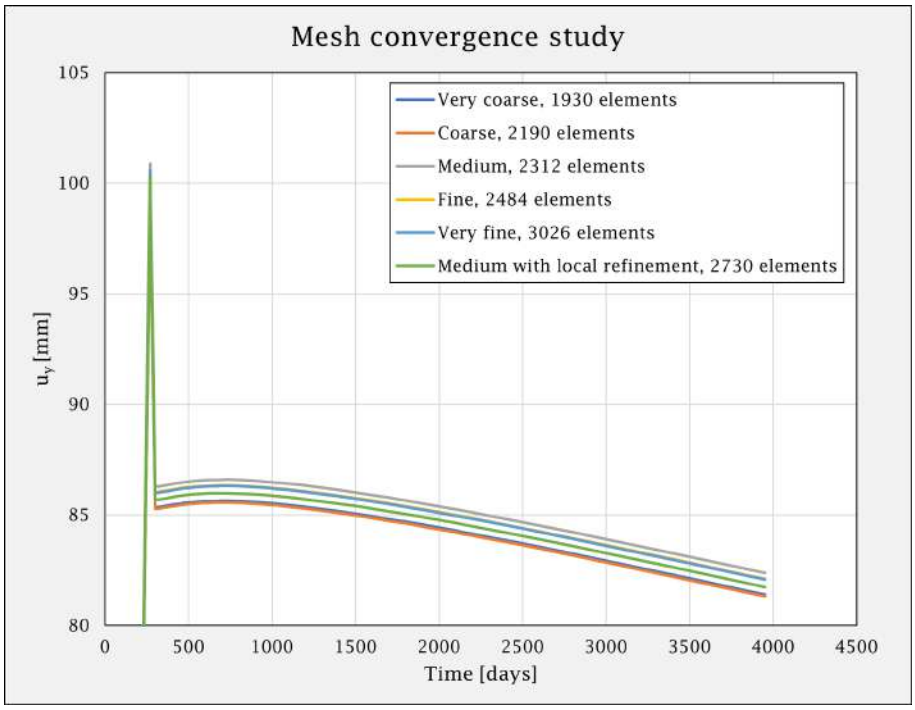

Figure C.0.1: Mesh convergence analysis for the excavation numerical model in PLAXIS2D.

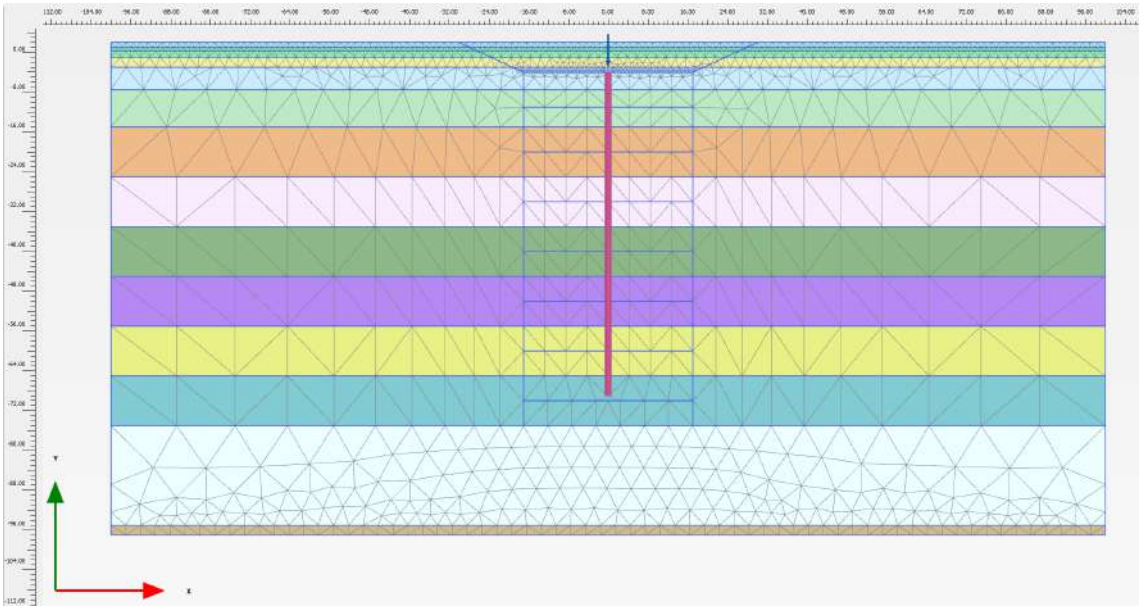

Figure C.0.2: Final mesh used in PLAXIS2D calculations, Medium 2132 elements.

D Appendix 4

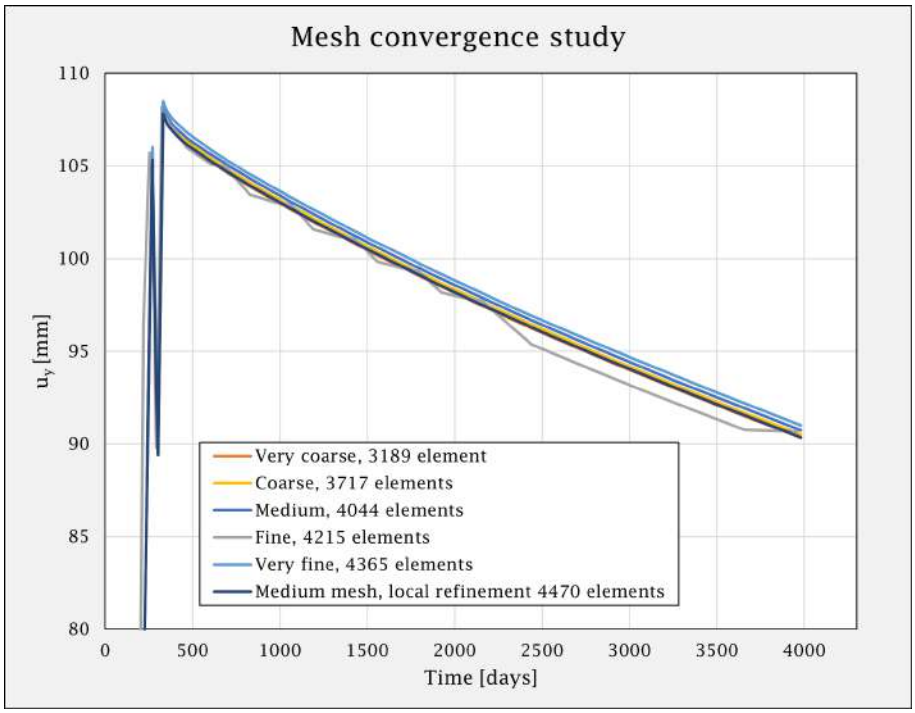

Figure D.0.1: Mesh convergence analysis for the excavation and volume expansion numerical model in PLAXIS2D.

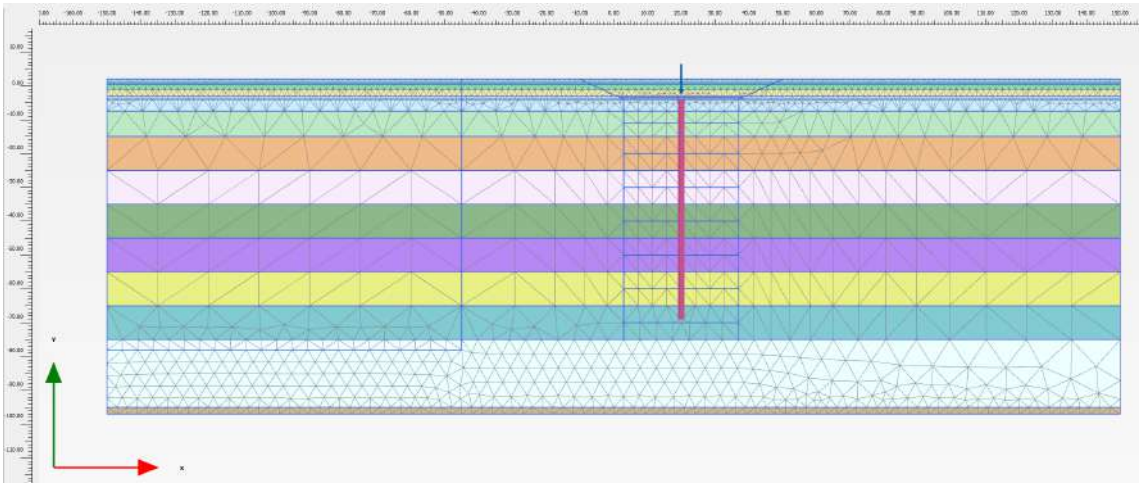

Figure D.0.2: Final mesh used in PLAXIS2D calculations, Medium 4470 elements.

E Appendix 5

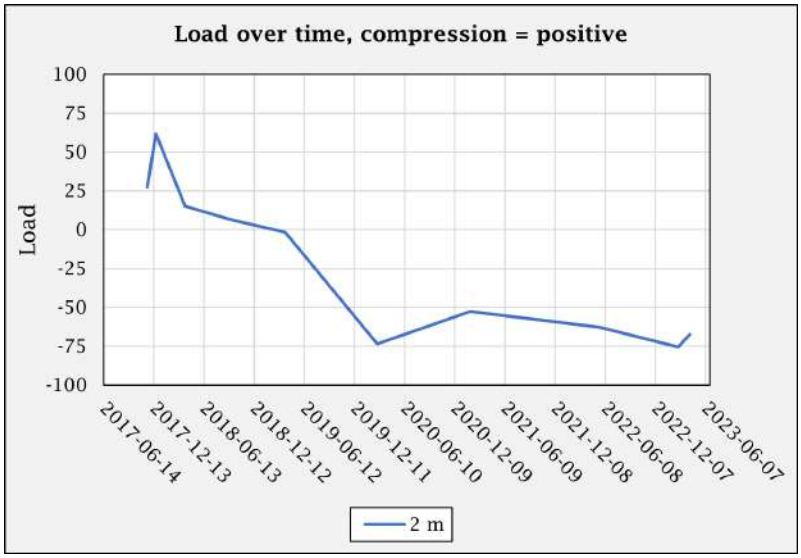

Figure E.0.1: Evaluated load 2 metres from the top of pile 3-417, located in the center wall.

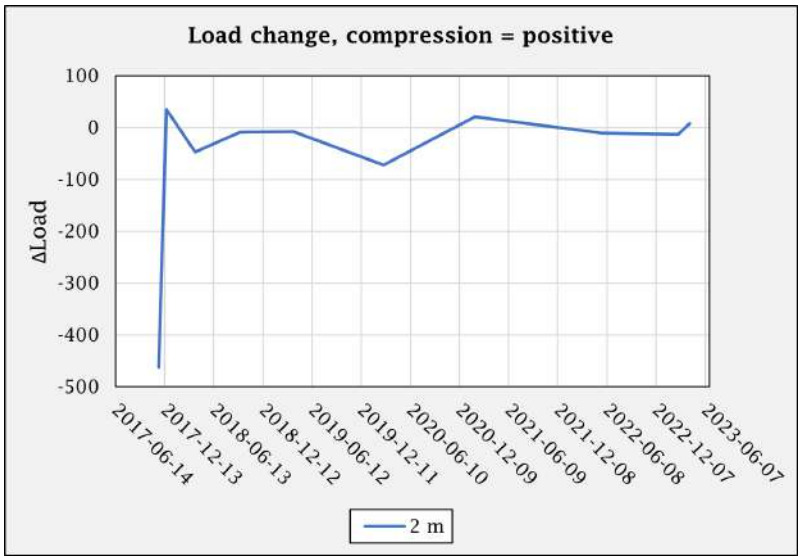

Figure E.0.2: Load change 2 metres from the top of pile 3-417, located in the center wall.

F Appendix 6

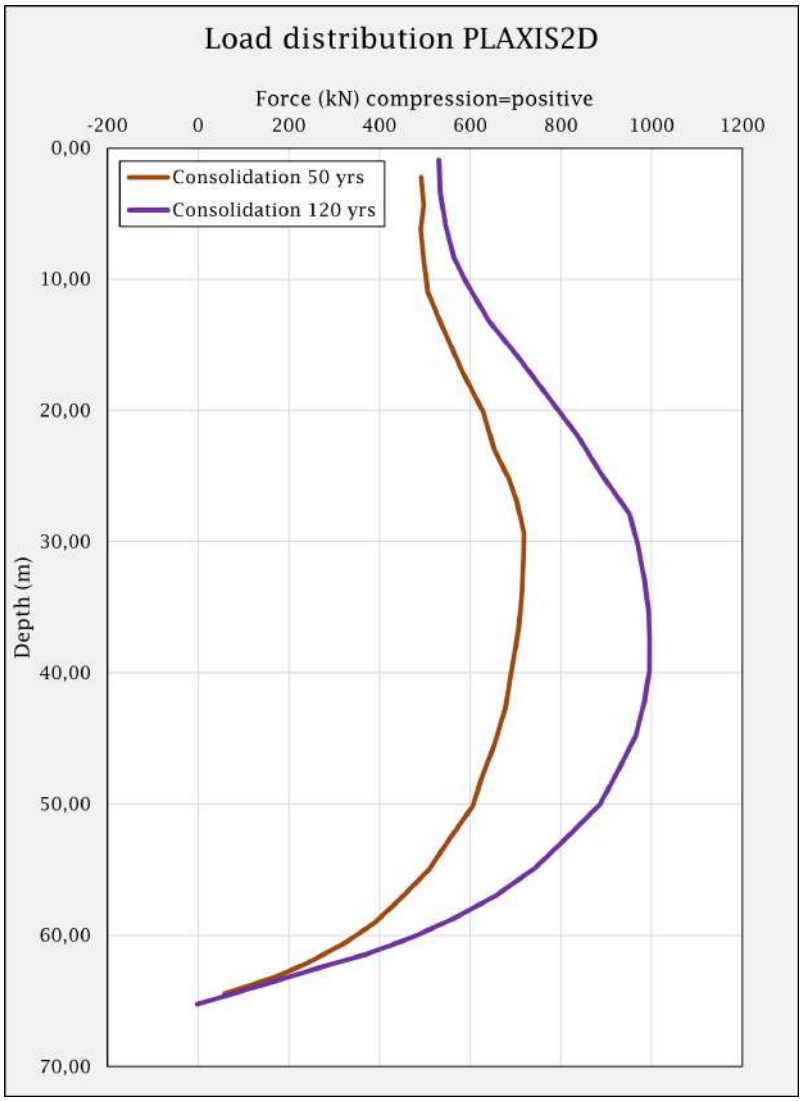

Figure F.0.1: Long term load distribution in pile calculated by PLAXIS2D for the excavation only.

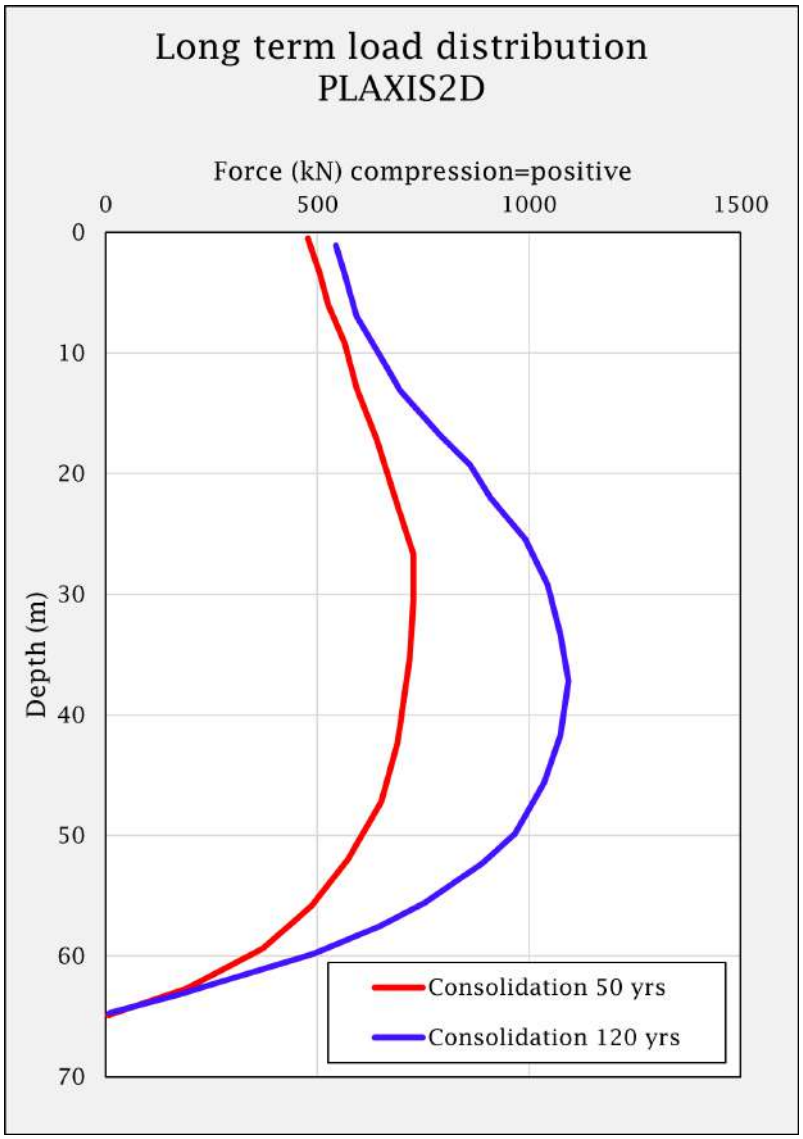

Figure F.0.2: Long term load distribution in pile calculated by PLAXIS2D for the excavation in combination with nearby piling.

G Appendix 7

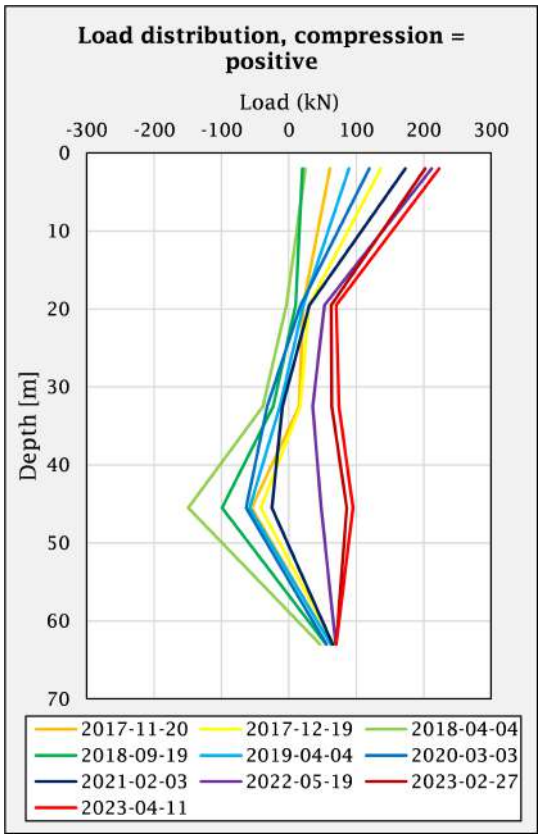

(a) Load distribution of pile 3-419, located in the center wall.

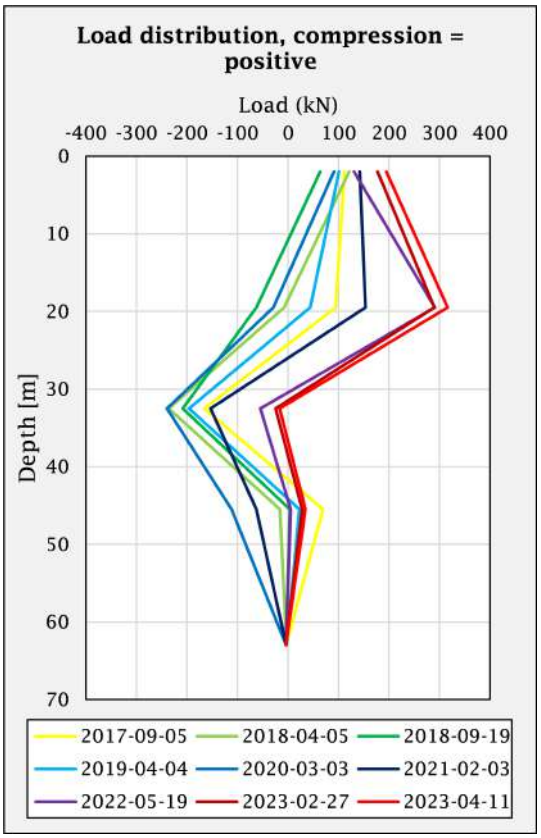

(b) Load distribution of pile 3-598, located in the south wall.

Figure G.0.1: Load distribution for pile 3-419 & 3-598, with reinforcement carrying all the load.